Modelling interaction of DNA with carbon nanostructures

Mansoor Hassan S Alshehri

Thesis submitted for the degree of

Doctor of Philosophy

in

Applied Mathematics

at

The University of Adelaide

(Faculty of Engineering, Computer and Mathematical Sciences)

School of Mathematical Sciences



July 2014

Contents

Abstract **x**

Signed Statement **xii**

Acknowledgements **xiii**

Author's publications **xiv**

1 Introduction **1**

1.1 Overview 1

1.1.1 Interaction of DNA with carbon nanotubes 4

1.1.2 Adsorption of DNA on graphite 7

1.1.3 The binding of C_{60} fullerene to DNA 10

1.1.4 Continuum approximation and Lennard-Jones potential 11

1.1.5 Thesis structure 14

1.1.6 Nomenclature 15

2 Interaction of double-strand DNA inside single-walled carbon nanotubes **16**

2.1 Abstract 16

2.2 Introduction 17

2.3 Atomic interaction potentials 20

2.3.1 Lennard-Jones potential 20
2.3.2 DNA and CNT geometry 21
2.3.3 General case 23
2.4 Interaction of carbon nanotube with DNA 24
2.4.1 Special case $\phi = \pi$ 26
2.5 Conclusions 29
2.5.1 Nomenclature 31

3 Determination of the optimal nanotube radius for single-strand DNA encapsulation 32
3.1 Abstract 32
3.2 Introduction 33
3.3 Energy between ssDNA molecule and carbon nanotube 35
3.3.1 Suction energy ssDNA entering carbon nanotube 37
3.3.2 Preferred single-walled carbon nanotube to enclose ssDNA . . 40
3.4 Conclusions 44
3.4.1 Nomenclature 46

4 Offset configurations for single and double strand DNA inside single-walled carbon nanotubes 47
4.1 Abstract 47
4.2 Introduction 48
4.3 Continuum approximation and Lennard-Jones potential 50
4.4 Offset ssDNA molecule inside SWCNT 51
4.5 Offset dsDNA molecule inside SWCNT 55
4.5.1 Offset dsDNA molecule inside SWCNT for $\phi = \pi$ 57
4.5.2 Offset dsDNA molecule inside SWCNT for $\phi = 12\pi/17$ 59
4.6 Conclusions 60

4.6.1 Nomenclature 61

5 DNA adsorption on graphene **62**

5.1 Abstract 62

5.2 Introduction 63

5.3 Method 65

5.4 Interaction of ssDNA and dsDNA molecules with graphene sheet when helix axis is perpendicular to sheet 67

5.4.1 Interaction of dsDNA molecule and graphene sheet 68

5.4.2 Interaction of ssDNA molecule and graphene sheet 69

5.5 Interaction of ssDNA and dsDNA molecules with graphene sheet when helix axis is parallel to sheet 71

5.5.1 Interaction of dsDNA molecule and graphene sheet 72

5.5.2 Interaction of ssDNA molecule and graphene sheet 72

5.6 Interaction of ssDNA and dsDNA molecules with graphene sheet for different helix axis orientations 75

5.7 Conclusions 77

5.7.1 Nomenclature 81

6 C_{60} fullerene binding to DNA **82**

6.1 Abstract 82

6.2 Introduction 83

6.3 Mathematical modelling 85

6.4 Interaction between C_{60} and dsDNA 85

6.4.1 Interaction of C_{60} and dsDNA for $\phi = \pi$ 88

6.4.2 Interaction of C_{60} and dsDNA for $\phi = 12\pi/17$ 89

6.5 Interaction of C_{60} and ssDNA 92

6.5.1 Binding energy of C_{60} fullerene to ssDNA 92

6.5.2 Interaction of fullerenes assuming helical configuration to axis of ssDNA . . . 96
6.6 Conclusions . . . 100
6.6.1 Nomenclature . . . 102

7 Summary **103**

A **108**
A.1 **Analytical evaluation of (2.3.1)** . . . 108
A.2 **Analytical evaluation of (2.4.1)** . . . 110

B **112**
B.1 **Analytical evaluation of (3.3.1)** . . . 112

C **117**
C.1 **Analytical evaluation of (4.4.2)** . . . 117
C.2 **Analytical evaluation of J_n appeared in (4.5.4)** . . . 119

D **123**
D.1 **Analytical evaluation of I_n^* appeared in (5.5.1)** . . . 123
D.2 **Analytical evaluation of Y_n appeared in (5.6.2)** . . . 125

E **127**
E.1 **Analytical evaluation of (6.4.1)** . . . 127

Bibliography **132**

List of Tables

1.1.1 Lennard-Jones parameters [1] 13

2.3.1 Numerical values of constants used in this chapter. 22

3.3.1 Numerical values of constants used in this chapter. 38

4.3.1 Numerical values of constants used in this chapter (* denotes data from [2] and ** denotes data from [3]). 52

5.3.1 Numerical values of constants used in this chapter (* denotes data from [2] and ** denotes data from [3]). 67

5.6.1 Interaction energy for different values of the rotational angle Ω. . . 77

6.3.1 Numerical values of constants used in this chapter (* denotes data from [2], ** denotes data from [3] and *** denotes data from [4]). . 86

6.5.1 Angular spacing Φ and energy of system $E_{cc}/N - 1$ (eV) for a pair of C_{60} fullerenes in helical configuration comprising N C_{60} molecules. 100

List of Figures

1.1.1 Assumed geometry for one turn of helix (34 Å) in double helix of B-DNA 2
1.1.2 Graphene-based nanostructures [5] 8

2.3.1 Assumed geometry of double helix B-DNA for one turn of helix (34 Å) 22
2.3.2 Double-strand DNA molecule inside a single-walled carbon nanotube 25
2.4.1 Total interaction potential between DNA molecule inside (18, 18)-(21, 21) CNTs as function of DNA radius r for $\phi = 12\pi/17$ 26
2.4.2 Total interaction potential between DNA molecule and CNT as function of tube radius a for $\phi = 12\pi/17$ 27
2.4.3 Total interaction potential between DNA molecule inside (18, 18)-(21, 21) CNTs as function of DNA radius r for the special case $\phi = \pi$ 28
2.4.4 Total interaction potential between DNA molecule and CNT as function of tube radius a for the special case $\phi = \pi$ 29

3.3.1 Assumed geometric profile of ssDNA molecule 36
3.3.2 ssDNA molecule at entrance to single-walled carbon nanotube . . . 39

3.3.3 Interaction potential between ssDNA molecule and (10, 10)-(16, 16) carbon nanotubes 41
3.3.4 Single-strand DNA molecule inside single-walled carbon nanotube . 43
3.3.5 Interaction potential between ssDNA molecule inside (8, 8)-(13, 13) CNTs as function of ssDNA radius r 43
3.3.6 Interaction potential between ssDNA molecule and CNT as function of tube radius a 44

4.3.1 Geometry for (a) double and (b) single helicoid of B-DNA for one complete rotation of helix (34 Å) 52
4.4.1 Schematic for offset ssDNA molecule inside single-walled carbon nanotube 55
4.4.2 Total potential energy for offset ssDNA molecule inside (13, 13), (16, 16) and (20, 20) SWCNTs with respect to the offset distance δ 55
4.5.1 Schematic for offset dsDNA molecule inside a single-walled carbon nanotube 58
4.5.2 Total potential energy for offset dsDNA molecule inside (20, 20), (23, 23) and (26, 26) SWCNTs with respect to the offset distance Δ for $\phi = \pi$ 58
4.6.1 Total potential energy for offset dsDNA molecule inside (20, 20), (23, 23) and (26, 26) SWCNTs with respect to the offset distance Δ for $\phi = 12\pi/17$ 60

5.4.1 Interaction between ssDNA and dsDNA molecules with helix axis for the perpendicular to sheet 70
5.4.2 Total potential energy when axis of DNA helix is perpendicular to graphene sheet 71
5.5.1 Interaction between ssDNA and dsDNA molecules with helix axis parallel to sheet 74

5.5.2 Total potential energy of DNA molecule when helix axis is parallel to graphene sheet 74
5.6.1 Interaction between ssDNA and dsDNA molecules with graphene sheet for arbitrary helix axis inclination. 78
5.6.2 Total potential energy of the DNA molecule with graphene sheet for different values of the rotational angle Ω. 78
5.6.3 Interaction between the DNA molecule for helix axis (a) perpendicular (b) parallel to graphene sheet for different lengths of DNA. . . 79

6.4.1 C_{60} fullerene binding to dsDNA molecule 88
6.4.2 Energy profile of C_{60} binding to dsDNA with respect to distance Δ for $\phi = \pi$ 90
6.4.3 Energy profile of C_{60} binding to dsDNA molecule with respect to rotational angle Ω for $\phi = \pi$ 91
6.4.4 3D plot of C_{60} binding to dsDNA at $\Omega = \pi/2, 3\pi/2$ and $\Delta = 7.7$ Å for $\phi = \pi$ 91
6.4.5 Energy profile of C_{60} binding to dsDNA with respect to distance Δ for $\phi = 12\pi/17$ 93
6.4.6 Energy profile of C_{60} binding to dsDNA with respect to rotational angle Ω for $\phi = 12\pi/17$ 94
6.4.7 3D plot of C_{60} binding to dsDNA at $\Omega = 2.1, 5.4$ rad and $\Delta = 2.4, 14.5$ Å for $\phi = 12\pi/17$ 94
6.5.1 C_{60} fullerene binding to ssDNA molecule. 95
6.5.2 Energy profile of C_{60} binding to ssDNA with respect to distance δ . 97
6.5.3 (a) energy profile for C_{60} binding to ssDNA with respect to rotational angle Ω, (b) relation between distances δ and tilting angle Ω 98
6.5.4 3D plot of C_{60} binding to ssDNA at $\Omega = \pi/2, 3\pi/2$ rad and $\delta = 6.5$ Å 98

6.5.5 Helical configuration for N C_{60} fullerenes binding to ssDNA for $\delta = 6.5$ Å 100
6.5.6 3D plot of several C_{60} binding to ssDNA at $\Phi = 1.23$ rad and $\delta = 6.5$ Å. 101

Abstract

This thesis focuses on the development of mathematical models for the interaction between deoxyribonucleic acid molecules (DNA) and certain carbon nanostructures. We model such atomic interactions by adopting the 6-12 Lennard-Jones potential and the continuum approach. The latter assumes that a discrete atomic structure can be replaced with an average constant atomic surface density of atoms that is assumed to be smeared over each molecule, in our case a DNA molecule and a carbon nanostructure. First, we develop a mathematical model for the interaction between a deoxyribonucleic acid molecule and a carbon nanotube, and we examine the storage of DNA molecules in carbon nanotubes. Following earlier authors, the carbon nanotube is modelled as a right circular cylinder, while the helical structure of the DNA molecule is modelled as a continuously twisted ribbon. We next determine the binding energies between DNA molecules interacting with a graphene sheet, and finally, we determine the binding energies of a C_{60} fullerene interacting with a DNA molecule.

Experiments in nanotechnology are often expensive and time consuming, and mathematical models and numerical simulations are necessary to complement the efforts of experimentalists and to confirm observed experimental outcomes. Despite recent improvements in the rapidity of numerical simulations, they can be more time consuming than the direct evaluation of an analytical expression arising from a mathematical model, because of the large numbers of atoms and force-field cal-

culations that may be involved. Although a mathematical model will necessarily include many assumptions and approximations, nevertheless often the main physical parameters and optimal configurations can be accurately predicted. The model calculations presented here for ideal systems, represent average outcomes, and generally there is good agreement with any existing numerical results that are obtained from more intensive computational schemes.

Here, we model the mechanics of the encapsulation of DNA molecules in carbon nanotubes to determine the optimal carbon nanotube that encloses the DNA molecule. The total interaction energy is calculated from the continuum approximation, where the atoms in each structure are assumed to be smeared over the surfaces of an ideal cylinder and a twisted ribbon, and the optimal carbon nanotube to enclose the DNA molecule is derived as the minimum energy configuration. Moreover, the binding energies between the DNA molecule adsorbing onto a graphene surface are derived by minimizing the binding energies to determine the preferred locations of the DNA molecules with respect to the graphene sheet. Finally, the binding of C_{60} to a DNA molecule is investigated, again by adopting the continuum approximation for modelling nanostructures.

In summary, the original contribution of this thesis is the development of ideal mathematical models and new analytical formulae for the interaction energy between deoxyribonucleic acid molecules and various types of carbon nanostructures, including carbon nanotubes, graphite, and C_{60} fullerene. The interaction energies between the DNA molecules and the nanostructures are determined analytically from the mathematical models and thus can be readily evaluated using standard computer algebra packages such as MAPLE and MATLAB. Hence, the interaction mechanisms and equilibrium configurations for a wide variety of systems might be fully and quickly investigated.

Signed Statement

I certify that this work contains no material which has been accepted for the award of any other degree or diploma in any university or other tertiary institution and, to the best of my knowledge and belief, contains no other material previously published or written by another person, except where due reference has been made in the text. In addition, I certify that no part of this work will, in the future, be used in a submission for any other degree or diploma in any university or other tertiary institution without the prior approval of the University of Adelaide. I give consent to this copy of my thesis when deposited in the University Library, being made available for loan and photocopying, subject to the provisions of the Copyright Act 1968. The author acknowledges that copyright of the published works contained within this thesis resides with the copyright holder(s) of those works.

I also give permission for the digital version of my thesis to be made available on the web, via the University's digital research repository, the Library catalogue and also through the web search engines, unless permission has been granted by the University to restrict access for a period of time.

SIGNED: ..... DATE: .....

Acknowledgements

I gratefully acknowledge the people who have made this thesis possible. First of all I would like to thank the tireless assistance of my supervisors Dr. Barry Cox and Prof. Jim Hill. Without their informal approach, unwavering support, never ending advice and countless appointment less meetings, this thesis would never have been possible. I would also like to thank the King Saud University (Saudi Arabia) for the awarding of a PhD Scholarship.

Author's publications

1. M. H. Alshehri, B. J. Cox, and J. M. Hill. Interaction of double-stranded DNA inside single-walled carbon nanotubes. *Journal of Mathematical Chemistry*, 50:2512–2526, 2012.

2. M. H. Alshehri, B. J. Cox, and J. M. Hill. DNA adsorption on graphene. *European Physical Journal D*, 67: 226 (9pp), 2013.

3. M. H. Alshehri, B. J. Cox, and J. M. Hill. Offset configurations for single- and double-strand DNA inside single-walled carbon nanotubes. *European Biophysics Journal*, 43: 25–33, 2014.

4. M. H. Alshehri, B. J. Cox, and J. M. Hill. Determination of the optimal nanotube radius for single-strand DNA encapsulation. *Micro and Nano Letters*, 9: 113–18, 2014.

5. M. H. Alshehri, B. J. Cox, and J. M. Hill. C_{60} fullerene binding to DNA. *Submitted to The European Physical Journal B*, June 2014.

Chapter 1

Introduction

1.1 Overview

Deoxyribonucleic acid (DNA) is a molecule that is the basic hereditary material in humans and almost all other known organisms. The first reports on the DNA molecule were by Friedrich Miescher in 1869 and by Avery, MacLeod, and McCarty in 1944 [6]. The DNA molecule consists of two long polymers with simple units, called nucleotides, that are composed of five elements: carbon (C), oxygen (O), hydrogen (H), nitrogen (N), and phosphorus (P). That is, the DNA molecule comprises two long helical polynucleotide chains that are composed of four nucleotide subunits. Each nucleotide is composed of sugar attached to a single phosphate group with four possible bases: guanine (G), cytosine (C), adenine (A), and thymine (T). The nucleotides are linked together in a chain by sugar-phosphates. With reference to Fig. 1.1.1, we assume the B-DNA form which is the structure commonly found inside cells [3], and we consider a unit cell of length 34 Å within a DNA molecule. The spaces between the DNA strands are called groove sites, and there are two DNA groove sites created by the coiling of the two helices around each other; the wider groove is called the major groove and is 22 Å in length, while the smaller groove is

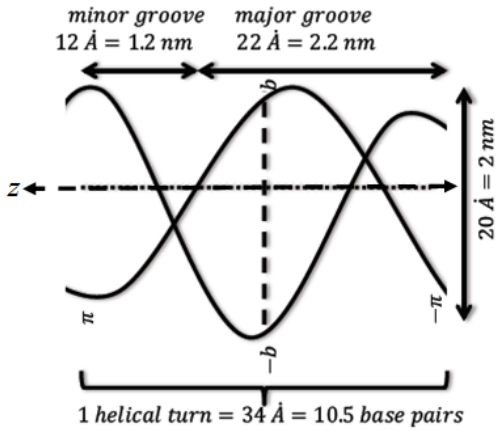


Figure 1.1.1: Assumed geometry for one turn of helix (34 Å) in double helix of B-DNA

called the minor groove and is 12 Å in length [3]. Many different structures at the nanoscale have been created using molecular recognition between complementary strands of double-strand DNA (dsDNA), for example, single-strand DNA (ssDNA) is constructed from a large molecular library [7–11]. Furthermore, DNA has some unique features that make it an excellent fundamental building block for molecular nanotechnology, such as its nanoscale structural geometry, self-recognition structure, and self-assembly [12, 13]. Since the discovery of the double-helix structure of deoxyribonucleic acid (DNA) by Watson and Crick in 1953 [14], the discipline of structural DNA nanotechnology has grown rapidly and has greatly influenced the fields of materials science and micro-engineering [15]. In addition, many studies on the structure and properties of DNA have been performed in the fields of molecular biology and genetic engineering, thus providing many new applications of DNA to almost all areas of science and engineering. A number of stated aims have already been achieved, including the extension of self-assembled crystalline systems from 2D to 3D and the achievement of 2D algorithmic assembly [16]. The large number of studies in the field of structural DNA nanotechnology has generates promise for the coming decade. The functionalization and applications of nanostructures and DNA

molecules have recently emerged as exciting topics in areas such as biomechanics, biochemistry, thermodynamics, electronics, optics, and magnetic properties [17–20]. For example, Niemeyer [21] shows that DNA can be used as a bottom-up building material and provides details for the construction of different DNA-based nanostructures through hybridization. Benenson et al. [22] show that the applications of DNA in medical areas have increased recently, with DNA now being used for diagnosis and drug delivery. Seeman and his group use branched DNA structures to construct Borromean rings (each comprising three mutually interlocked rings), knots, cubes, octahedral objects, and periodic lattices and tiles in 2D and 3D. They also use reciprocal exchange between DNA double helices [7, 23] to construct branched DNA motifs such as Holliday junctions, related structures, and parallelograms in order to create periodic assemblies with complex microstructures such as micron-scale mechanical arrays. We comment that the Holliday junction is a moving junction between four strands of DNA [24], and the related structures are double crossovers (DX), triple crossovers (TX), and paranemic crossovers (PX). According to Shen et al. [25], paranemic crossovers are'four-stranded coaxial DNA complexes containing a central dyad axis that relates two flanking parallel double helices'.

Carbon nanostructures such as graphite, carbon nanotubes, and C_{60} fullerene have fundamentally different geometric structures, and their geometry is one of the most important factors in their special features and potential applications. Thus, combined carbon nanostructures and DNA molecules have many potential uses in several fields owing to the novel structures of carbon nanomaterials and the bioactivity of DNA [26]. Mathematical models play an important role in obtaining an improved comprehension of how DNA molecules interact with other nanostructured materials. A deeper understanding of interactions between DNA molecules and materials at molecular level is critical in order to make possible new applications of DNA molecules and carbon nanostructures. In addition, a modelling approach based

on applied mathematics provides computationally efficient outcomes, identifies important physical parameters, and enables predictions as well as general behaviour. This thesis focuses on the development of mathematical models for the interaction between DNA molecules and carbon nanostructures in order to 1) investigate the encapsulation of DNA molecules in carbon nanotubes, 2) investigate the adsorption of DNA molecules on graphene, and 3) determine the surface binding energies between DNA molecules interacting with C_{60} fullerene.

The following section outlines the interaction of DNA molecules with a carbon nanotube. Ssection 1.1.2 examines the adsorption of DNA molecules on a graphene sheet. Section 1.1.3 provides some discussion of C_{60} fullerene binding to DNA molecules. Section 1.1.4 provides an explanation of the approach employed in this thesis, which is the continuum approximation combined with the Lennard-Jones potential, and a brief summary is provided. Section 1.1.5 presents the structure of this thesis.

1.1.1 Interaction of DNA with carbon nanotubes

Carbon nanotubes are cylindrical macromolecules composed entirely of carbon atoms, with a geometric configuration defined by a pair of integers (n, m), which are known as the chiral vector numbers [27]. Carbon nanotubes are categorized as multi-walled carbon nanotubes (MWCNTs) and single-walled carbon nanotubes (SWCNTs) [28, 29]. With their exceptional properties, carbon nanotubes have attracted the interest of many scientists worldwide. Two decade after the discovery of CNTs, the field of structural CNT technology has grown rapidly, and the number of articles related to nanotube research has increased enormously. The time dependence of the overall number of articles on nanotubes is still indicating a strong increase in research activity in this area [30]. The interaction of CNTs with biomolecules has been a subject of great interest during the last few decades, owing to the wide

range of applications facilitated by the outstanding physical and chemical properties of CNTs. Carbon nanotubes with open ends provide internal cavities (1–2 nm in diameter) that are capable of accommodating small biomolecules [31, 32].

Recently, the functionalization and applications of carbon nanotubes (CNTs) and deoxyribonucleic acid (DNA) have emerged as exciting topics in areas such as biomechanics, biochemistry, thermodynamics, electronics, optics, and magnetic properties [17]. Therefore, the study of the interactions between CNTs and DNA molecules is an active research discipline. CNT/DNA hybrids hold promise for new applications in medical areas. For example, SWCNTs and DNA can be used together as vehicles for drug and gene delivery and DNA transfection [22, 33, 34]. Moreover, the DNA molecule can be used to increase CNT solubility in organic media, further the advancement and applications of nanostructures, and distinguish metallic CNTs from semiconducting CNTs [35].

Many approaches in numerical modelling, such as density functional theory (DFT) and molecular dynamics (MD) simulations, are used to describe the interaction of DNA molecules with carbon nanotubes and study the possibility of encapsulating DNA molecules in carbon nanotubes. Molecular dynamics (MD) simulation, which is a method appropriate for investigating the dynamic properties of gas-solid systems, may provide insights into the fundamental interactions between CNTs and DNA molecules. For example, Xue and Chen [36] employ an MD simulation to study the translocation of a dsDNA molecule through an SWCNT, they assume that the dsDNA molecule simulated are comprised of eight base pairs. They show that the dsDNA molecules can be inserted into (20, 20) CNT with a radius of approximately 13.6 Å within 100 ps *in vacuo*. Lau et al. [37] use an MD simulation to investigate the encapsulation of dsDNA in SWCNTs with diameters of 30 Å and 40 Å. They study the effect of confinement on the structure and dynamics of double-strand DNA molecule in a nanotube, using a nonpolarizable SWCNTs to

model the hydrophobic pore. They find that the structure of the dsDNA molecule is not significantly perturbed if the counterions are included in the nanotube. Xu et al. [38] use a tight-binding method combined with MD simulations to investigate the electrostatic signals generated by DNA segments inside short semiconducting SWCNTs, and they obtain stronger electrical signals for the semiconducting CNTs when DNA bases were present inside the CNTs.

Goa et al. [2] use MD simulations to investigate the dynamics of ssDNA molecules encapsulated in CNTs, and they found that the ssDNA molecule can be encapsulate in a (10, 10) CNT with a radius of 6.8 Å. Pei et al. [39] employ MD simulations to investigate the translocation of ssDNA molecules inside CNTs in water, and they find that the ssDNA is unable to enter an (8, 8) CNT with a radius of approximately 5.4 Å but passes through larger carbon nanotubes with armchair chiralities in the range (10, 10)–(14, 14) and radii of approximately 6.8–9.5 Å. Xue and Chen [36] employ MD simulations to study the translocation of ssDNA molecules through SWCNTs both *in vacuo* and in an aqueous environment. They show that the insertion of the ssDNA molecule into a (10, 10) CNT is spontaneous within 100 ps *in vacuo* but no corresponding spontaneous insertion of the ssDNA into the (10, 10) CNT occurs within 2 ns in an aqueous environment at a temperature of 400 K and pressure of 3 bar.

Shim et al. [40] focus on encapsulating DNA molecules in CNTs, while Cui et al. [41] show that the dsDNA molecule can be encapsulated in MWCNTs in water at 400 K and 3 bar. Ito et al. [32] use fluorescence microscopy to study the transport of the dsDNA molecule through an MWCNT with a diameter of 77 nm. Kamiya and Okada [34] employ DFT to investigate the encapsulation of ssDNA inside SWCNTs, and they find that the encapsulation reaction is exothermic for nanotubes with radii greater than 6.15 Å. D'yachkov et al. [42] use a molecular docking method to study the complex formation of ssDNA molecule with nanotubes as a function of both the

nucleotide composition of the DNA and the diameter of the nanotube. They find that the diameter of a (14, 14) nanotube is too small for an ssDNA molecule to enter.

Nevertheless, very little of the work to date was done by adopting conventional modelling approaches from applied mathematics. Here, by using classical applied mathematical modelling, we derive explicit analytical expressions for the encapsulation of DNA in single-walled carbon nanotubes. The continuum approximation can be utilized to obtain the potential energy of the intermolecular interaction, which can be derived from the classical Lennard-Jones potential function [43]. The approach employed in this thesis is to model the van der Waals interactions using the 6-12 Lennard-Jones potential function together with the continuum approximation. The interacting molecules are replaced by uniform atomic density over ideal surfaces, and the total interaction is determined by integrating the Lennard-Jones function over the surfaces in question.

1.1.2 Adsorption of DNA on graphite

Graphene is a single-layer carbon crystal with a high electrical conductivity through the plane of the material. As shown in Fig. 1.1.2, there are a number of nanostructures, such as carbon nanotubes and fullerenes, that are based on graphene as the fundamental material [5]. The existence of isoloted graphene sheets was first reported in 2004 [44]. Because of its unique physicochemical properties such as high surface area, excellent thermal conductivity, and great mechanical strength, graphene shows considerable promise for many applications in fields such as electronics, energy storage, bioscience, and biotechnologies. It has recently been established that graphene is the strongest material known [44–47].

The DNA molecule and graphene sheet are ideal nanostructures that can be used in different arrangements to fabricate novel hybrid nanobiomaterials and con-

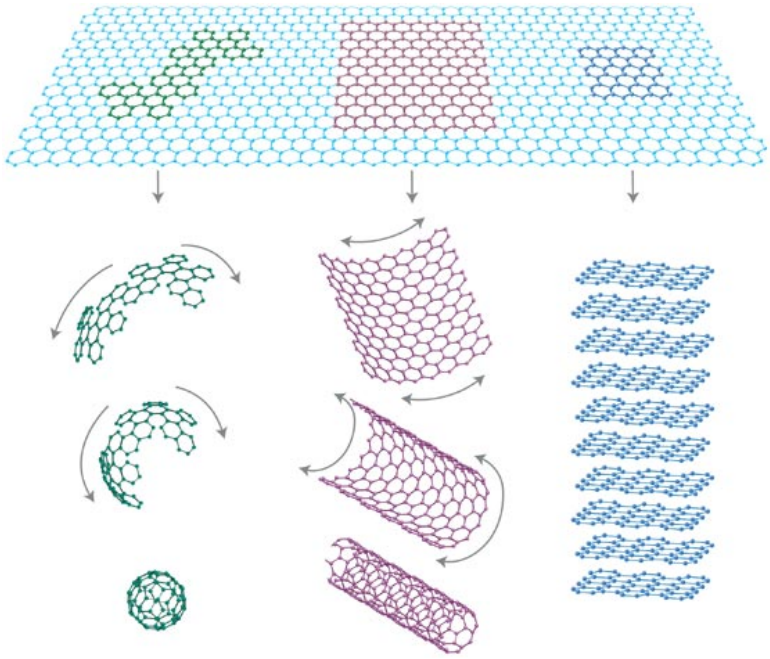


Figure 1.1.2: Graphene-based nanostructures [5]

struct highly sensitive nanobioelectronic devices including sensors and chips [48]. Graphene and DNA can also be used as the basic building blocks for bioelectronics, especially for bacterial DNA-protein and polyelectrolyte chemical transistors, and provide new opportunities in the design of systems for the study of nucleic acid and biosensors [49,50]. Furthermore, the adsorption of DNA on an electrode surface may lead to different rates of hybridization or new approaches to deliver drugs in DNA grooves [51]. Gowtham et al. [52] conduct a first-principles investigation of the interaction between nucleobases and graphene by using DFT together with Hartree-Fock (HF) and second-order Møller-Plesset (MP) perturbation theory. They show that the nucleobases exhibit significantly different interaction strengths when physisorbed on graphene. Antony and Grimme [53] determine the interaction energy of the DNA nucleobases with graphene by using a DFT method, and they established the ordering G>A>T>C. Zhao [54] examines the interaction of the dsDNA molecule (8 or 12 base pairs) with the graphene surface in aqueous solution using MD simulations to

detect the dominant role of the hydrophobic π stacking in the interaction between nucleotides and carbon nanosurfaces. This shows that the dsDNA molecule can be rotated from a parallel orientation to a perpendicular orientation with respect to the graphene surface. Kabelac et al. [55] use MD simulations to investigate the linker of ssDNA and dsDNA molecules to graphene. The structures of both the double-stranded and single-stranded molecules were assumed to have the B-form with the base sequence $5'$-CCACTAGTGG-$3'$. It is found that the dsDNA molecule is orientated roughly perpendicular to the graphene surface, with an average deviation from the perpendicular of approximately 18°, and the ssDNA molecule becomes parallel to the graphene surface in such a way that not all of the bases are simultaneously attached to the substrate. Oliveira-Brett and Chiorcea [51] employ magnetic AC mode atomic force microscopy (MAC mode AFM) to describe the adsorption of ssDNA and dsDNA molecules on highly orientated pyrolytic graphite (HOPG). They show that the ssDNA molecule interacts with and adsorbs to the graphene surface more strongly than the dsDNA molecule. Varghese et al. [56] employ isothermal titration calorimetry (ITC) to investigate the binding energy of DNA nucleobases and nucleotides with graphene in an aqueous environment, and they find that the experimental binding energies are generally small.

In this thesis, we investigate the interaction of DNA molecules with a graphene sheet. Employing classical applied mathematical modelling and using the basic principles of mechanics, we exploit the 6-12 Lennard-Jones potential and the continuum approximation. We derive analytical expressions for the binding energies between the DNA molecules adsorbing onto a graphene surface. We minimize the binding energies to determine the preferred locations of the DNA molecules with respect to the graphene sheet.

1.1.3 The binding of C_{60} fullerene to DNA

The term fullerene describes a closed cage molecule composed entirely of carbon. C_{60} fullerene comprises 60 carbon atoms. It was discovered in 1985 [57] and may have many biomedical, electronic, and semiconductor applications. C_{60} is the smallest stable fullerene, with a radius of approximately 3.55 Å. Because of their unique mechanical properties arising from the van der Waals interaction and their electronic properties arising from a large surface to volume ratio [58, 59], fullerenes make possible the creation of many future nanoscale devices. At present, this thesis is one of the few quantitative studies on the interactions of C_{60} fullerene with DNA molecules. Although C_{60} fullerene is one of the most important nanocarriers for drug delivery, the interactions between C_{60} fullerene and DNA molecules are still not fully understood.

Pang et al. [60] examine the interaction of the dsDNA molecule with the C_{60} molecule by developing a surface-based electrochemical method. They show that the C_{60} molecule interacts strongly with the major groove and the phosphate backbone that acts as the binding sites of the dsDNA molecule. Zhao et al. [61] use MD simulations to investigate the stability of complexes composed of ssDNA or dsDNA molecules and C_{60} in aqueous solution. For the dsDNA molecule, they find that the C_{60} binds with the DNA at either the hydrophobic ends or the minor groove of the nucleotide, but this binding does not affect the overall shape of the B-form of the DNA molecule. For the ssDNA molecule, they find that the C_{60} binds strongly with the DNA and leads to deformation of the nucleotides. Xu et al. [62] use MD simulations and thermodynamic analysis to investigate the dynamic binding of C_{60} fullerene with the dsDNA molecule. They find that the C_{60} fullerene binds with the minor groove of the dsDNA molecule. Zhao [63] performs MD simulations to study the binding of the C_{60} molecule to the ssDNA molecule. This shows that in a highly saline buffer solution the C_{60} fullerene can bind to the ssDNA and form energetically

stable hybrids with a binding energy of about -47 kcal/mol ($\approx$ -2.0 eV).

Here, we adopt the continuum approximation for modelling nanostructures in order to investigate the binding of C_{60} fullerene to DNA molecules and describe the interaction of DNA molecules with C_{60} fullerene. We obtain an analytical expression for the interaction energy, which can then be readily computed using a computer algebra package.

1.1.4 Continuum approximation and Lennard-Jones potential

Nanostructures can be modelled using the continuum approximation, which assumes that intermolecular structures can be approximated using average atomic surface densities. The continuum approximation can be utilized to obtain the potential energy of the intermolecular interaction, which can be derived from the classical Lennard-Jones potential function [43]. The researchers have been employed successfully the continuum approximation to model various types of nanomaterials. Girifalco et al. [4] apply the continuum approach to a calculation of the potential between carbon nanotubes. Based on the assumption of a Lennard-Jones potential for the interaction between carbon atoms in the continuum approach, they computed the van der Waals potential energy of interactions in graphitic structures for different carbon nanostructures. They show that the interaction between these carbon nanostructures in the continuum approximation may be obtained by averaging over the surface of each entity. Cox et al. [64, 65] use the continuum approximation together with the Lennard-Jones potential function to propose a new model that describes the adsorption of fullerenes onto the interior surfaces of carbon nanotubes. They are modelled the fullerene as an averaged atomic mass distributed over the surface of a sphere, and the carbon nanotube as an averaged atomic mass distributed over the surface of an open semi-infinite cylinder. Baowan et al. [66]

use the Lennard-Jones potential and the continuum approximation to investigate the encapsulation of C_{60} fullerenes in SWCNTs. Baowan et al. [67] also employ the continuum approximation together with the Lennard-Jones potential function to investigate the packing of C_{60} fullerene chains inside SWCNTs. They determine the interaction energy by averaging over the surface of a spherical fullerene and a cylindrical carbon nanotube.

We model the DNA molecules as an averaged atomic mass distributed over the surface of a helicoid, and we comment that the modelling of the DNA molecule which is developed here is entirely new. The dsDNA molecule is modelled as a surface with a double helicoid geometry, and the ssDNA molecule is modelled as a single helicoid geometry. With reference to a rectangular Cartesian coordinate system (x, y, z), the parametric equation for the dsDNA molecule is given by

$$\mathbf{G}(\Theta, t) = \left(\frac{R}{2}\left[\cos\Theta + \cos(\Theta - \phi) + t\Big(\cos\Theta - \cos(\Theta - \phi)\Big)\right], \right.$$
$$\left. \frac{R}{2}\left[\sin\Theta + \sin(\Theta - \phi) + t\Big(\sin\Theta - \sin(\Theta - \phi)\Big)\right], \frac{c\Theta}{2\pi} \right),$$

where $R = 10$ Å is the radius of the dsDNA helix, $c = 34$ Å is the unit cell length, ϕ is the helical phase angle parameter and the parametric variables t and Θ are such that $-1 < t < 1$, and $-\pi < \Theta < \pi$. Again with reference to a rectangular Cartesian coordinate system (x, y, z), a typical point on the surface of the ssDNA is given by

$$\mathbf{H}(\theta, t) = \left(rt\cos\theta, rt\sin\theta, c\theta/2\pi \right),$$

where r and c are the radius and the unit cell length of the ssDNA helix, respectively, and the two parametric variables t and θ are such that $0 < t < 1$ and $-\pi < \theta < \pi$. The interactions between the atoms can be derived from the Lennard-Jones potential, and the energy can be calculated by evaluating surface integrals over

the relevant molecules and nanostructures. The pairwise interaction within each structure can be ignored, and the interaction between two separate structures is given by the following expression:

$$E = \sum_{i=1}^{N}\sum_{j=1}^{M}\Phi(\rho_{ij}),$$

where i and j are indices for all the atoms in each structure, respectively, and ρ_{ij} denotes the distance between the ith atom in the first structure and the jth atom in the second structure. The Lennard-Jones potential for two unbonded atoms is given by

$$\Phi(\rho) = -A\rho^{-6} + B\rho^{-12},$$

where A and B represent the experimentally determined attractive and repulsive constants, respectively, these are related to the van der Waals, distance σ and the well-depth ε through the relations $\sigma = (B/A)^{1/6}$ and $\varepsilon = A^2/4B$. Table 1.1.1 gives numerical values of the Lennard-Jones constants for the particular elements studied in this thesis. Thus, utilizing the continuum approximation together with

	ε (eV $\times 10^{-2}$)	σ (Å)	A (eV Å^6)	B (eV Å^{12})
C-C	0.4119	3.88	56.21	191800
C-H	0.1336	3.54	10.52	20700
C-N	0.5089	3.788	60.09	177400
C-O	0.6197	3.695	63.08	160600
C-P	0.6197	4.088	115.6	539300

Table 1.1.1: Lennard-Jones parameters [1] .

the Lennard-Jones potential yields a formulation of the total potential energy

$$E = \eta_1\eta_2\int_{S_1}\int_{S_2}\Phi(\rho)dS_1dS_2,$$

where η_1 and η_2 represent the average atomic surface densities of the two interacting molecular structures and $\Phi(\rho)$ is the Lennard-Jones potential function for two unbonded atoms with typical surface elements dS_1 and dS_2 a distance ρ apart. Note that all of the integrals in this thesis are surface integrals that are evaluated over the surfaces. The reader is referred to Kreyszig [68, pp. 443–452] or Kaplan [69, pp. 313–319] about the evaluation of surface integrals.

In summary, mathematical modelling and numerical simulations are important complements to experiments. Mathematical modelling is an effective yet computationally efficient method for modelling the interactions of biomolecules with carbon nanostructures (such as carbon nanotubes, graphite, or fullerenes) by using the continuum approximation, which assumes that intermolecular interactions can be approximated by average atomic surface densities. The approach adopted herein may help to understand the interactions between carbon nanostructures and DNA molecules, and these may serve as the precursors of further studies in other fields of nanotechnology. This thesis formulates a fundamental model of ideal behaviour as a first step in elucidating the principal behaviour of such systems. Much work remains to be done on the models, especially with respect to DNA mobility and the interactions with other molecules, such as water molecules, which are often present in physical systems.

1.1.5 Thesis structure

This thesis is presented in seven chapters. In Chapter 1 we review the interactions of DNA molecules with carbon nanostructures; namely, carbon nanotubes, graphite, and C_{60} fullerene. In this chapter we also outline the continuum approximation and the Lennard-Jones potential, which constitute the approach taken in this thesis. In Chapter 2 we study the interaction of double-strand DNA inside single-walled carbon nanotubes. Next in Chapter 3 we investigate and determinate of the opti-

mal nanotube radius for encapsulation of single-strand DNA in a carbon nanotube. While in Chapter 4 we analyse the offset configurations for single-strand and double-strand DNA inside single-walled carbon nanotubes. Following in Chapter 5 we study the adsorption of DNA molecules on graphene, and in Chapter 6 we determine the binding energy of C_{60} fullerene to DNA molecules. Finally in Chapter 7 we present a concluding summary. The modelling of the DNA molecule is subsequently employed in a number of problems investigated throughout the thesis. We comment that this model may lead to the requirement of some repetition in wording, modelling and mathematical techniques through this thesis particularly in Chapters 2, 3 and 4.

1.1.6 Nomenclature

Symbol	Meaning
n, m	are the chiral vector numbers
$\Phi(\rho_{ij})$	is the Lennard-Jones potential function for two unbonded atoms
ρ_{ij}	is the distance between ith atom of the first molecule
	and jth atom of the second molecule
E	is the interaction energy
A	is the attractive Lennard-Jones constant
B	is the repulsive Lennard-Jones constant
η_1, η_2	are the atomic surface densities of the two interacting
	molecular structures
σ	is the equilibrium distance of two atoms
ε	is the depth of the potential well
ϕ	is the helical phase angle parameter
R	is the radius of the dsDNA
r	is the radius of the ssDNA
c	is the unit cell length

Chapter 2

Interaction of double-strand DNA inside single-walled carbon nanotubes

2.1 Abstract

Deoxyribonucleic acid (DNA) is the genetic material for all living organisms, and as a nanostructure offers the means to create novel nanoscale devices. In this chapter, we investigate the interaction of deoxyribonucleic acid inside single-walled carbon nanotubes. Using classical applied mathematical modeling, we derive explicit analytical expressions for the encapsulation of DNA inside single-walled carbon nanotubes. We adopt the 6-12 Lennard-Jones potential function together with the continuous approach to determine the preferred minimum energy position of the dsDNA molecule inside a single-walled carbon nanotube, so as to predict its location with reference to the cross-section of the carbon nanotube. An analytical expression is obtained in terms of hypergeometric functions which provides a computationally rapid procedure to determine critical numerical values. We observe that the double-strand

DNA can be encapsulated inside a single-walled carbon nanotube with a radius larger than 12.30 Å, and we show that the optimal single-walled carbon nanotube to enclose a double-stranded DNA has radius 12.8 Å.

2.2 Introduction

Classical applied mathematics and mechanics generate models to predict ideal behavior and to determine simple but relevant solutions which provide insight into complex physical processes. In many disciplines, applied mathematical modelling has been used to determine elegant solutions to problems, but thus far, few problems have been addressed in nanotechnology. Recently, the characterization of nano-materials and the design and realization of nanostructure based devices with advanced functionality has had an impact on the field of materials science and micro-engineering [15]. Since the discovery of the double helix structure of deoxyribonucleic acid (DNA) by Watson and Crick in 1953 [14], DNA has also generated much research interest, and recently several areas in modern biotechnology have shown considerable potential for DNA molecules in the construction of nanostructures and devices, such as the assembly of devices and computational elements, for the assembly of interconnects, or as the device element itself [70]. In addition, the encapsulation of biomolecules such as DNA has promised many applications in gene and drug delivery [71]. Furthermore, inorganic nanomaterials involving carbon nanotubes (CNTs), nanocrystals, and nanowires with their unique physical and chemical properties have generated attention for future applications such as drug delivery, enzyme immobilization, and DNA transfection [70, 72, 73]. The functionalization of CNTs with DNA has recently aroused interest in the developing area of nanobiotechnology due to many potential applications in molecular electronics, field devices and medical applications [18–20]. These applications of DNA with CNTs have increased the interest in CNT solubility in organic media and DNA assisted

CNT characterisation [40, 74–76].

Xu et al. [38] use a tight-binding method combined with molecular dynamics (MD) simulations to investigate the electrostatic signals generated by DNA segments inside short semiconducting single-walled carbon nanotubes, and they obtain stronger electrical signals for the semiconducting CNTs when DNA bases are present inside the CNT. Shim et al. [40] focus on encapsulating DNA molecules inside CNTs, while Cui et al. [41] show that the double stranded DNA molecules can be encapsulated inside multiwalled carbon nanotubes in water at 400 K and 3 Bar. In addition, by employing the (MD) simulation to study the translocating of dsDNA molecules through single wall carbon nanotube, Xue and Chen [36] investigate the translocation of the dsDNA molecule through the carbon nanotubes channel by the van der Waals interaction, and they assume that the dsDNA molecule simulated are comprised of eight base pairs. They show that the dsDNA molecules could be inserted into (20, 20) CNT within 100 ps in vacuo. Lau et al. [37] investigate the encapsulation of double-stranded DNA inside single-walled carbon nanotubes of diameters 30 and 40 Å, using (MD) simulation. They find that the structure of dsDNA is not significantly perturbed if the counterions are included inside the nanotube. Ito et al. [32] study the transport of the dsDNA molecule through a multiwalled carbon nanotube with 77 nm in diameter by fluorescence microscopy.

In this chapter, we study the equilibrium position for a double helix DNA molecule inside a single-wall carbon nanotube (SWCNT), and by minimizing the interaction energy between the DNA and the CNT, we deduce the optimal radius of the CNT which can be used to accommodate the DNA. In particular, we assume the B-DNA form which is the structure commonly found inside cells [3]. With reference to Fig. 2.3.1, we consider a unit cell comprising a DNA molecule over a distance of 34 Å. The DNA groove sites refer to the spaces between the strands, and there are two groove sites which are created by the coiling of the two helices around each other;

the wider one is called the major groove which is 22 Å in length, and the smaller is called the minor groove which is 12 Å in length [3]. We join the two helices with a continuum of straight, horizontal lines forming a surface which resembles that of a twisted ribbon and which we use to model the structure of the DNA unit cell. The DNA comprises five elements: carbon (C), oxygen (O), hydrogen (H), nitrogen (N) and phosphorus (P) [3,77–79]. There are approximately 21 nucleotides that make up one turn of the dsDNA; each nucleotide is composed of deoxyribose sugar attached to a single phosphate group and the base which may be either guanine (G), cytosine (C), adenine (A) and thymine (T). After taking the average of atoms of 21 bases and adding them to the atoms of the deoxyribose sugar and the phosphate group, we have 204.75 carbon atoms, 189 oxygen atoms, 299.25 hydrogen atoms, 78.75 nitrogen atoms and 21 phosphorus atoms, which gives a total average of 792.75 atoms in the unit cell. The modeling proposed here is not intended to compute all the detail of the underlying physics, but rather to represent the most important interactions for the purpose of determining the dominant phenomena of the system. In addition, the theoretical results presented in this chapter might pave the way toward further developing the area.

In §2.1, we introduce the Lennard-Jones potential and the continuum approach which assumes an average atomic surface density of the atoms on the DNA molecule and an average surface density of carbon atoms on the nanotube. We comment that Girifalco et al. [4] state that the continuum Lennard-Jones approach may in many instances be a good approximation for uniform atomic distributions. In §2.2.1, we present the details for the derivation of the total interaction energy per unit length for the DNA molecule which is assumed to be located inside the single-walled carbon nanotube. In addition, in §2.2.2, we also give the corresponding calculation for the special case of the interaction between the atoms of DNA and the carbon nanotube surface when the helical phase angle $\phi = \pi$, and some conclusions are presented in

§2.3.

2.3 Atomic interaction potentials

2.3.1 Lennard-Jones potential

The total non-bonded interaction energy E, may be obtained by summing the interaction energy for each atomic pair and is given by

$$E = \sum_i \sum_j P(\rho_{ij}),$$

where $P(\rho_{ij})$ is a potential function for atoms i and j which are separated by a distance ρ_{ij}. In the continuum approximation, the atoms are assumed to be uniformly distributed over the surface of the molecules, and so we replace the double summation by two surface integrals, thus

$$E = \eta_1 \eta_2 \int_{S_1} \int_{S_2} P(\rho)\, dS_1\, dS_2,$$

where η_1 and η_2 are atomic surface densities of the first and the second molecules, respectively, and ρ is the distance between two typical surface elements dS_1 and dS_2 on the two unbonded molecules. In this chapter, we adopt the 6-12 Lennard-Jones potential to determine the van der Waals interaction energy. The classical Lennard-Jones potential for two atoms at a distance ρ apart is given by

$$P(\rho) = 4\varepsilon\Big[-\Big(\frac{\sigma}{\rho}\Big)^6 + \Big(\frac{\sigma}{\rho}\Big)^{12}\Big],$$

where ρ is the distance between two atoms, ε is the magnitude of the energy at the equilibrium distance $\rho_0 = 2^{1/6}\sigma$, and σ is the atomic distance when the potential energy is zero. The constants ε and σ are determined experimentally and if given

the values ε_1, σ_1 for the interaction of the atoms of one species and ε_2, σ_2 for the interaction of the atoms of a second species, then these parameters for the interaction of atoms of species 1 with those of species 2 may be determined from the empirical mixing rules given by $\varepsilon_{12} = (\varepsilon_1\varepsilon_2)^{1/2}$, and $\sigma_{12} = (\sigma_1 + \sigma_2)/2$ [4, 80]. The 6-12 Lennard-Jones potential may also be expressed as

$$P(\rho) = -\frac{A}{\rho^6} + \frac{B}{\rho^{12}},$$

where A and B are called the attractive and the repulsive constants, respectively, and are given in terms of the previously given parameters given previously by $A = 4\varepsilon\sigma^6$ and $B = 4\varepsilon\sigma^{12}$. To determine the total interaction energy for two non-bonded molecules we use the Lennard-Jones potential function for two non-bonded molecules with the continuum approximation which is given by

$$E = \eta_1\eta_2 \int_{S_1}\int_{S_2} \left(-\frac{A}{\rho^6} + \frac{B}{\rho^{12}}\right) dS_1\, dS_2,$$

where η_1 and η_2 are atomic surface densities of the first and the second molecules, respectively.

2.3.2 DNA and CNT geometry

In this chapter, we model the DNA as a surface with the double helical geometry located on the z-axis, as shown in Fig. 2.3.1. With reference to a rectangular Cartesian coordinate system (x, y, z), a typical point on the surface of the DNA is given by

$$\mathbf{R}(\theta_1, t) = \Bigg(\frac{r}{2}\Big[\cos\theta_1 + \cos(\theta_1 - \phi) + t\Big(\cos\theta_1 - \cos(\theta_1 - \phi)\Big)\Big],$$
$$\frac{r}{2}\Big[\sin\theta_1 + \sin(\theta_1 - \phi) + t\Big(\sin\theta_1 - \sin(\theta_1 - \phi)\Big)\Big], \frac{c\theta_1}{2\pi}\Bigg),$$

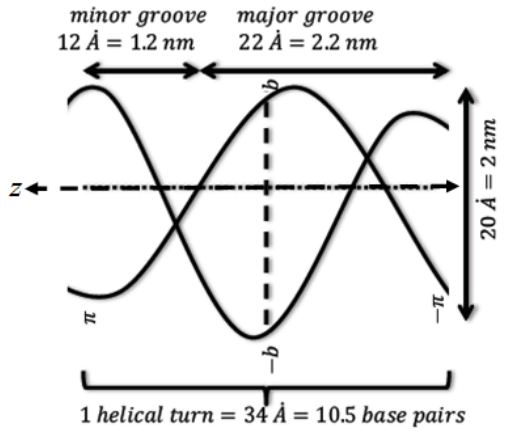


Figure 2.3.1: Assumed geometry of double helix B-DNA for one turn of helix (34 Å)

where $r = 10$ Å is the radius of the DNA helix, $c = 34$ Å is the unit cell length,

constant	Value
Radius of (18, 18)	12.21 Å
Radius of (19, 19)	12.88 Å
Radius of (20, 20)	13.56 Å
Radius of (21, 21)	14.24 Å
Mean surface density of carbon nanotube	η_g=0.3812 Å^{-2}
Mean surface density of DNA ($\phi = 12\pi/17$)	η_{d_1}=0.97 Å^{-2}
Mean surface density of DNA ($\phi = \pi$)	η_{d_2}=0.83 Å^{-2}
Attractive constant CNT-DNA	A=42.563 eV Å^6
Repulsive constant CNT-DNA	B=127534.91 eV Å^{12}

Table 2.3.1: Numerical values of constants used in this chapter.

$\phi = 12\pi/17$ is the helical phase angle parameter and the parametric variable t is such that $-1 < t < 1$, and $-\pi < \theta_1 < \pi$. Similarly, with reference to the rectangular Cartesian coordinate system (x, y, z) with origin located at the centre of the nanotube, a typical point on the surface of the tube has the coordinates $(a\cos\theta_2, a\sin\theta_2, z)$, where a is the radius of the carbon nanotube and $-\infty < z < \infty$ and $-\pi < \theta_2 < \pi$. Thus, the distance ρ between a typical surface element on the

CNT and another on the DNA is given by

$$\begin{aligned}\rho^2 &= a^2 - ar\big[\cos(\theta_1-\theta_2)+\cos(\theta_1-\theta_2-\phi)+t[\cos(\theta_1-\theta_2)-\cos(\theta_1-\theta_2-\phi)]\big]\\ &+ r^2[\cos^2(\phi/2)+t^2\sin^2(\phi/2)]+(z-c\theta_1/2\pi)^2.\end{aligned}$$

2.3.3 General case

In this section, we consider the general helical angle ϕ for which we have in mind the particular value $\phi = 12\pi/17$ which leads to the major and minor groove sites mentioned above. The equilibrium position is the location of the minimum potential energy for the DNA inside the CNT. We begin by considering the interaction of a carbon nanotube with a single point situated at a distance ξ from the tube axis, as shown in Fig. 2.3.2. We then integrate this potential for a single point over the surface of the DNA molecule, thus

$$\begin{aligned}\xi^2 &= \Big(\frac{r}{2}[\cos\theta_1+\cos(\theta_1-\phi)+t(\cos\theta_1-\cos(\theta_1-\phi))]\Big)^2\\ &+ \Big(\frac{r}{2}[\sin\theta_1+\sin(\theta_1-\phi)+t(\sin\theta_1-\sin(\theta_1-\phi))]\Big)^2\\ &= r^2[\cos^2(\phi/2)+t^2\sin^2(\phi/2)].\end{aligned}$$

Also, the distance ρ between two typical surface elements on the DNA and the CNT molecules is given by

$$\rho^2 = (a-\xi)^2 + z^2 + 4a\xi\sin^2(\theta_2/2),$$

where a is the radius of CNT, $r = 10$ Å, $c = 34$ Å, $-1 < t < 1$, $-\pi < \theta_2 < \pi$ and we have in mind the value $\phi = 12\pi/17$. Also, we have the interaction energy of point

with infinite carbon nanotube from [81], which is given by

$$E_c = \frac{3\pi^2\eta_g}{4a^4}\left[-AF\left(\frac{5}{2},\frac{5}{2};1;\left(\frac{\xi}{a}\right)^2\right)+\frac{21B}{32a^6}F\left(\frac{11}{2},\frac{11}{2};1;\left(\frac{\xi}{a}\right)^2\right)\right],$$

where η_g is the mean atomic surface density of CNT, and $F(a,b;c;z)$ is the standard hypergeometric function [82]. Thus, the total potential energy of the dsDNA with the CNT per unit length E, is given by

$$\begin{aligned} E &= \frac{rc\eta_{d_1}}{2\pi}\sin(\phi/2)\int_{-\pi}^{\pi}\int_{-1}^{1}E_c\left(1+\frac{4r^2\pi^2\sin^2(\phi/2)}{c^2}t^2\right)^{1/2}dt\,d\theta_2 \\ &= 2rc\eta_{d_1}\sin(\phi/2)\int_{0}^{1}E_c\left(1+\frac{4r^2\pi^2\sin^2(\phi/2)}{c^2}t^2\right)^{1/2}dt, \end{aligned} \tag{2.3.1}$$

where η_{d_1} represents the mean atomic surface density of DNA for the helical phase angle $\phi = 12\pi/17$. The details for the analytical evaluation of (2.3.1) are presented in Appendix A.1, from which we find that the total interaction energy for the DNA inside the CNT for any value of the helical phase angle ϕ is given by

$$E = \frac{3\pi^2 rc\eta_g\eta_{d_1}\sin(\phi/2)}{2a^4}\Big(-AR_3+\frac{21B}{32a^6}R_6\Big), \tag{2.3.2}$$

where R_n is defined by (A.1.1).

2.4 Interaction of carbon nanotube with DNA

Results and discussions for $\phi = 12\pi/17$

Although the final expression (2.3.2) with R_n defined by (A.1.1) appear to be quite complicated, the numerical solution is readily obtained using the algebraic computer package MAPLE using the parameter values given in Table. 2.3.1. We show graphically in Fig. 2.4.1 the relation between the potential energy and the radius

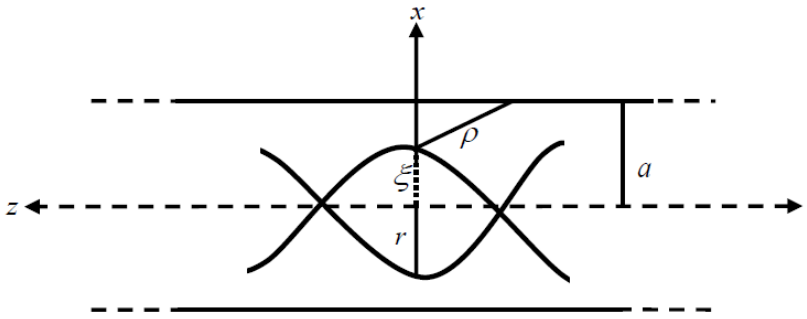


Figure 2.3.2: Double-strand DNA molecule inside a single-walled carbon nanotube

of the DNA (r) which are undertaken for each of the four specific armchair carbon nanotubes (i, i) for $i = 18, 19, 20$ and 21. As shown in Fig. 2.4.1, the radii of DNA molecules which minimize the interaction energy and which we refer to as the optimal radius are 8.96 Å, 9.63 Å, 10.31 Å and 11 Å for the (18, 18), (19, 19), (20, 20) and (21, 21) nanotubes, respectively. In addition, the larger the radius of the nanotube, the larger the optimal radius of DNA as larger radii nanotubes tend to accommodate larger DNAs. The DNA becomes unstable when the radii of DNA are beyond 9.48 Å, 10.17 Å, 10.85 Å and 11.54 Å for the (18, 18)-(21, 21) nanotubes, respectively, due to the mutually repulsive force between the DNA and the nanotube. Also, Fig. 2.4.2 shows the interaction energy as a function of the radius of the CNT. We observe that the encapsulation of dsDNA inside carbon nanotubes may occur for radii greater than 12.28 Å. In addition, as shown in Fig. 2.4.2 if we vary the CNT radius the preferred radius of carbon nanotube giving the maximum energy to enclose the double helix DNA for this case ($\phi = 12\pi/17$) is about 12.71 Å so we may infer that the (19, 19) tube is the preferred tube.

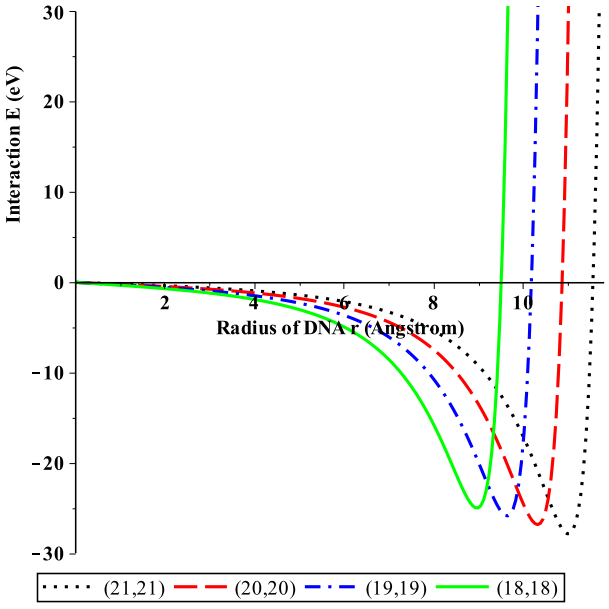


Figure 2.4.1: Total interaction potential between DNA molecule inside (18, 18)-(21, 21) CNTs as function of DNA radius r for $\phi = 12\pi/17$

2.4.1 Special case $\phi = \pi$

In this section, we assume that the value of ϕ is equal to π. In this special case the formal analytical details are slightly simpler than those for the general case. Again the equilibrium position arises from the location of the minimum potential energy for the DNA molecule inside the CNT, and we begin by considering the interaction of a carbon nanotube with a single point located at a distance ξ from the tube axis, also as shown in Fig. 2.3.2. We then integrate the potential for a single point over the surface of the DNA molecule, and for the second integration we make the substitution $\xi = rt$. Also, the distance between two typical points ρ is given by

$$\rho^2 = a^2 + \xi^2 + z^2 - 2a\xi\cos\theta_2.$$

Now to evaluate the total interaction in this case we, follow the same steps as in the previous case, and we find that the total potential energy per unit length E for the

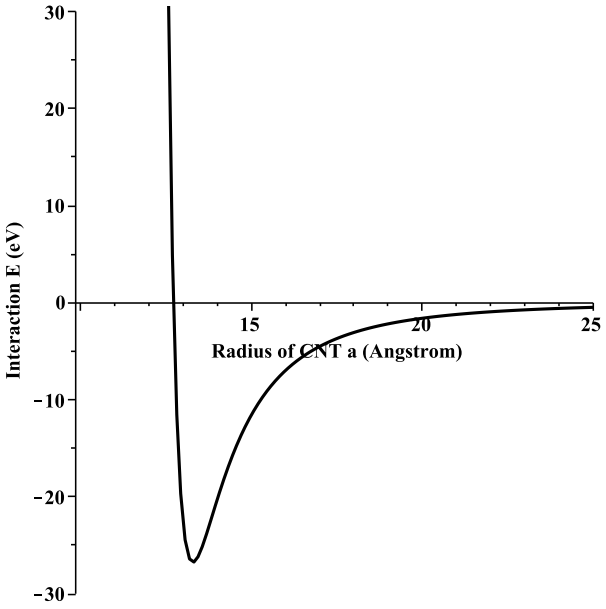


Figure 2.4.2: Total interaction potential between DNA molecule and CNT as function of tube radius a for $\phi = 12\pi/17$

offset DNA molecule in a carbon nanotube for $\phi = \pi$ is given by

$$E = \frac{3\pi^2 rc\eta_g\eta_{d_2}}{2a^4}\Big(- AI_3 + \frac{21B}{32a^6}I_6\Big), \tag{2.4.1}$$

where η_{d_2} represents the mean atomic surface density of DNA for the helical phase angle $\phi = \pi$. The formal details for the analytical evaluation of (2.4.1) are presented in Appendix A.2, and I_n is defined by (A.2.1).

Results and discussions for $\phi = \pi$

The numerical solution is evaluated using the algebraic computer package MAPLE with the parameter values as given in Table. 2.3.1. We show graphically in Fig. 2.4.3 the relation between the potential energy and the radius r of the DNA molecule. As shown in Fig. 2.4.3, the minimum energy is obtained when r= 8.95 Å, 9.61 Å, 10.30 Å and 10.99 Å for (18, 18), (19, 19), (20, 20) and (21, 21) carbon nanotubes,

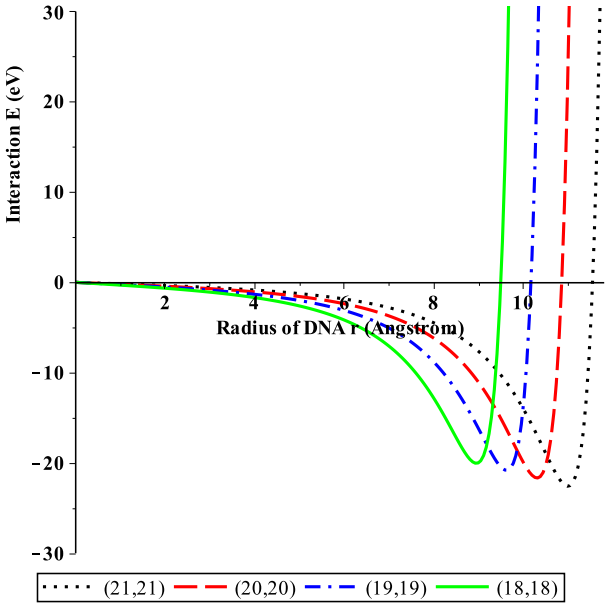


Figure 2.4.3: Total interaction potential between DNA molecule inside (18, 18)-(21, 21) CNTs as function of DNA radius r for the special case $\phi = \pi$

respectively. Thus, we observe that the optimal radii of the DNA which provide the lowest interaction energy for (18, 18)-(21, 21) carbon nanotubes are the radii of these tubes, respectively. In addition, these results give numerical values for the distances between the centre of the DNA and the wall of the nanotube. Moreover, the larger the nanotube radius, the larger the optimal radius of DNA as a larger radius nanotube tends to accommodate larger DNAs. The DNA becomes unstable as the radius is increased beyond 9.47 Å, 10.17 Å, 10.84 Å and 11.52 Å for (18, 18)-(21, 21) carbon nanotubes, respectively due to the mutually repulsive force between the DNA and the nanotube. Also, as shown in Fig. 2.4.4 the preferred radius of carbon nanotube to enclose the double helix DNA in the special case $\phi = \pi$ is about 12.73 Å, so we infer that the (19, 19) tube is the preferred tube.

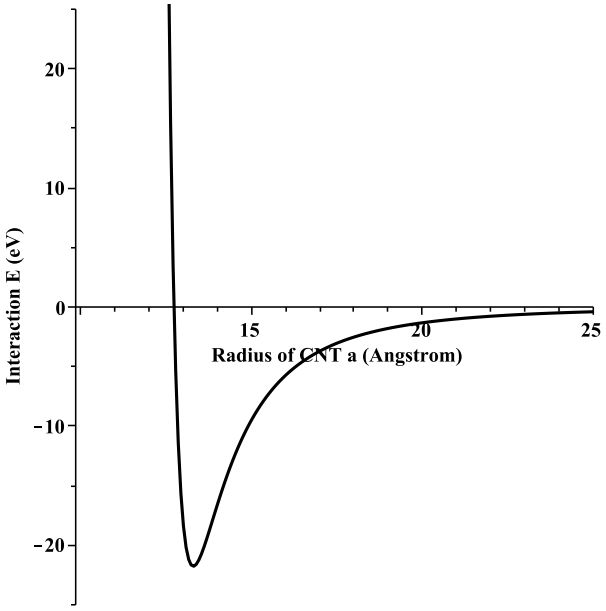


Figure 2.4.4: Total interaction potential between DNA molecule and CNT as function of tube radius a for the special case $\phi = \pi$

2.5 Conclusions

This chapter presents a new applied mathematical model to investigate the interaction energy between a double-strand DNA molecule (dsDNA) that is assumed to be inside a single-walled carbon nanotube. We employ the 6-12 Lennard-Jones potential together with the continuum approximation to calculate the van der Waals interaction energy which may be expressed in terms of the usual hypergeometric function. We examine the interaction energy for a dsDNA inside single-walled carbon nanotube for different armchair tubes, assuming that the DNA is already accepted into the tube. We refer to the location where the potential energy adopts the minimum value as the preferred optimal location. The numerical evaluations are performed using the algebraic computer package MAPLE. For the helical phase angle of the DNA, we study two cases for the interaction of the dsDNA inside a single-walled carbon nanotube, which are the general case with $\phi = 12\pi/17$, and a special case with

$\phi = \pi$. In both cases we observe that at the point where the minimum energy occurs, that the difference between the radii of the CNT and the DNA is approximately 3.25 Å ($a - r \approx 3.25$ Å). In addition, the results indicate that the encapsulation of the dsDNA molecule into a single-walled carbon nanotubes may occur for carbon nanotubes with radii greater than 12.30 Å. Moreover, the optimal radius of carbon nanotube to enclose the double helix DNA in both cases is approximately 12.8 Å, and we conclude that the preferred tube is (19, 19). These results are close to those determined by Xue and Chen [36], who propose that the dsDNA molecule can be encapsulated inside a (20, 20) CNT. We comment that the mathematical modelling employed in deriving these results is computationally instantaneous; moreover, it compares favourably with other methods such as molecular dynamics simulations and experiments for example [36,37] which together may serve as a solid background for understanding DNA mechanics in carbon nanotubes.

2.5.1 Nomenclature

Symbol	Meaning
$P(\rho_{ij})$	is the Lennard-Jones potential function for two unbonded atoms
ρ_{ij}	is the distance between ith atom of the first molecule and jth atom of the second molecule
E	is the interaction energy
A	is the attractive Lennard-Jones constant
B	is the repulsive Lennard-Jones constant
η_1, η_2	are the atomic surface densities of the two interacting molecular structures
σ	is the equilibrium distance of two atoms
ε	is the depth of the potential well
ρ	is the distance between a typical surface elements on the CNT and the DNA
ϕ	is the helical phase angle parameter
a	is the radius of the carbon nanotube
η_g	is the atomic surface density of the carbon nanotube
η_{d_1}	is the atomic surface density of the DNA (for $\phi = 12\pi/17$)
η_{d_2}	is the atomic surface density of the DNA (for $\phi = \pi$)
r	is the radius of the dsDNA
c	is the unit cell length of the DNA
ξ	is the distance from the tube axis
$F(a, b; c; z)$	is the standard hypergeometric function

Chapter 3

Determination of the optimal nanotube radius for single-strand DNA encapsulation

3.1 Abstract

We model the molecular interactions between a single-strand DNA molecule and a carbon nanotube to determine the suction force experienced by the DNA which is assumed to be located on the axis near the open end of a single-walled carbon nanotube. We determine the optimal nanotube radius for encapsulation, that is the radius of nanotube with the lowest interaction energy. The expression for the molecular interaction energy is derived from the 6-12 Lennard-Jones potential together with the continuum approach, which assumes that a discrete atomic structure can be replaced by a line or surface with constant average atomic density. We find that a single-strand DNA can be encapsulated inside a single-walled carbon nanotube with a radius larger than 8.2 Å, and we show that the optimal single-walled carbon nanotube needed to fully enclose the DNA molecule has radius 8.8 Å, which ap-

proximately corresponds to the chiral vector numbers (13, 13). This means that if we wish to encapsulate single-strand DNA into a carbon nanotube, an ideal single-walled carbon nanotube to do this is (13, 13) which has the required radius of 8.8 Å.

3.2 Introduction

Multi-walled carbon nanotubes (MWCNTs) and single-walled carbon nanotubes (SWCNTs) were first reported in 1991 and 1993 [28, 29], respectively. Carbon nanotubes are cylindrical macromolecules entirely comprising carbon atoms, with a geometric configuration defined by a pair of integers (n, m), which are known as the chiral vector numbers [27]. The discovery of carbon nanotubes has generated much interest owing to their outstanding physical and chemical properties such as high electrical conductance, mechanical stiffness, and light weight, leading to many possible applications such as field emission, electrochemical actuation and transistors [27, 83]. This has led to both single-walled and multi-walled carbon nanotubes becoming the focus of intensive research interest as possible electrodes to transmit electrical signals and as sensors to detect concentrations of chemical or biological material [27, 83, 84]. The possibility of using carbon nanotubes as engineered nanoscale flow channels has also attracted much attention in nanobiotechnology for the transport of water, proteins and macromolecules [36].

Watson and Crick [14] formulated the geometric model for the structure of deoxyribonucleic acid (DNA) in 1953, nearly one century after the discovery of DNA by Friedrich in 1869 [6], and it is now well established that the DNA molecule comprises two long polynucleotide helical chains composed of four nucleotide subunits [3, 14]. In the case of DNA, each nucleotide is composed of sugar attached to a single phosphate group with four possible bases; guanine (G), cytosine (C), adenine (A) and thymine (T) [3]. DNA's unique features make it an important and

a promising molecule with all the basic properties necessary for the self-assembly of nanomaterial electronic devices [76]. Using the molecular recognition between complementary strands of the double-strand DNA, various geometric objects at the nanometre scale have been constructed [7].

The functionalization and applications of carbon nanotubes (CNTs) and deoxyribonucleic acid (DNA) have emerged as novel areas in biomechanics, biochemistry with promising, thermodynamics, electronics, optics and magnetics [17]. In particular, the DNA molecule can be used to increase CNT solubility in organic media and further applications and in the advancement of DNA based nanostructures. The the DNA molecule can also be used to distinguish conducting from semiconducting CNTs [35]. In addition, DNA/CNT hybrids hold promise for new applications in many medical areas. For example, DNA/SWCNT can be used as vehicles for drug and gene delivery [22, 33, 34]. For these reasons, the interaction of single strand DNA (ssDNA) with CNTs has been the subject of several studies. Goa et al. [2] investigate the dynamics of ssDNA molecules being encapsulated inside CNT using molecular dynamics (MD) simulations, and they find that the ssDNA molecule may be encapsulated inside a (10, 10) CNT. Pei et al. [39] employ MD simulations to investigate the translocation of ssDNA inside CNT in water, and find that the ssDNA is unable to enter an (8, 8) CNT, but passes through larger carbon nanotubes with armchair chiralities in the range (10, 10)-(14, 14). Xue and Chen [36] also employ MD simulations to study the translocating of ssDNA molecules through single-walled carbon nanotubes both *in vacuo* and in an aqueous environment. They show that the insertion of the ssDNA molecule into a (10, 10) CNT is spontaneous within 100 ps *in vacuo*, but there is no corresponding spontaneous insertion of ssDNA into (10, 10) CNT for simulation times up to 2 ns at a temperature of 400 K and pressures of 3 bar in an aqueous environment. Kamiya and Okada [34] employ density functional theory (DFT) to investigate the encapsulation of ssDNA inside SWNTs, and

find that the encapsulation reaction is exothermic for nanotubes of radii larger than 6.15 Å. D'yachkov et al. [42] use a molecular docking method to study the complex formation of ssDNA with nanotubes as a function of the nucleotide composition of DNA and nanotube diameter, and find that a (14, 14) nanotube is too small for ssDNA to enter.

In this chapter, we adopt the 6-12 Lennard-Jones potential and the continuum approach which assumes that a discrete atomic structure can be replaced by an average atomic surface density of the atoms on the ssDNA molecule and an average surface density of carbon atoms on the nanotube. We comment that Girifalco et al. [4] state that the continuum Lennard-Jones approach may in many instances be a better approximation than a set of discrete atomic centres, since the former may be viewed as arising from an average over all possible electronic configurations. We first examine the suction behaviour for single-strand DNA entering a single-walled carbon nanotube, assumed to be semi-infinite in length, and due to the short range nature of the Lennard-Jones interactions, this is a reasonable approximation. Also, we determine the minimum potential energy equilibrium position for the ssDNA inside the SWCNT.

3.3 Energy between ssDNA molecule and carbon nanotube

We assume that a single-strand DNA has a helical geometry, and this assumption follows the previous experimental studies [8–11], as shown in Fig. 3.3.1. The unit cell of the single-strand DNA molecule used here is assumed to comprise 10 nucleotides, which give a total of 377.75 atoms in the unit cell. These ten nucleotides comprise 97.5 carbon, 142.5 hydrogen, 37.5 nitrogen, 90 oxygen and 10 phosphorus atoms, which gives an average of 37.75 atoms per nucleotide. With reference to the

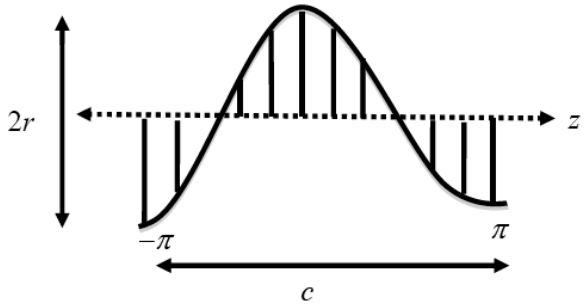


Figure 3.3.1: Assumed geometric profile of ssDNA molecule

rectangular Cartesian coordinate system (x, y, z), the ssDNA has coordinates

$$\mathbf{H}(\theta_1, t) = (rt\cos\theta_1, rt\sin\theta_1, c\theta_1/2\pi)\,,$$

where the numerical values of r the radius of the ssDNA helix and c the unit cell length are taken to be 5.4 Å and 34 Å, respectively [2,3]. The parametric variable t is such that $0 < t < 1$ and $-\pi < \theta_1 < \pi$. We comment that a helical curve is normally parameterized by the single parameter θ_1. In this case we have adopted two parameters to allow for variable internal points of the helicoid, so that we may integrate over all values of the DNA radius from zero to r. We also comment that single-strand DNA is a disordered polymer that is unlikely to have a precise helical conformation. Here we assume the ideal conformation as a first step towards modelling more realistic situations. Similarly, with reference to the same rectangular Cartesian coordinate system (x, y, z) with origin located at the centre of the nanotube, a typical point on the surface of the tube has coordinates $(a\cos\theta_2, a\sin\theta_2, z)$, where a is the radius of the carbon nanotube and $0 < z < \infty$ and $-\pi < \theta_2 < \pi$. Here we adopt the Lennard-Jones potential to determine the van der Waals interaction and the equilibrium position for the ssDNA inside SWCNT. The classical Lennard-Jones potential interaction energy between a pair of atoms at a distance ρ

apart is given by

$$P(\rho) = -\frac{A}{\rho^6} + \frac{B}{\rho^{12}},$$

where A and B denote the attractive and repulsive constants, respectively, and ρ denotes the distance from a typical point of the helicoid to a typical point on the cylindrical surface. The 6-12 Lennard-Jones potential may also be expressed as

$$P(\rho) = 4\varepsilon\Big[-\Big(\frac{\sigma}{\rho}\Big)^6 + \Big(\frac{\sigma}{\rho}\Big)^{12}\Big],$$

where $\varepsilon = A^2/4B$ is the magnitude of the energy at the equilibrium distance $\rho_0 = 2^{1/6}\sigma = (2B/A)^{1/6}$, and σ is the atomic distance when the potential energy is zero. Using the 6-12 Lennard-Jones potential, together with the continuum approximation, which assumes that discrete atoms may by replaced by a uniform density of atoms over the surface, the total non-bonded interaction energy E, may be deduced from

$$E = \eta_1\eta_2 \int_{S_1}\int_{S_2} \left(-\frac{A}{\rho^6} + \frac{B}{\rho^{12}}\right) dS_1\, dS_2,$$

where η_1 and η_2 denote the atomic surface densities of the first and the second molecules, respectively. The numerical values of the constants used throughout this chapter are as given in Tables 1.1.1 and 3.3.1.

3.3.1 Suction energy ssDNA entering carbon nanotube

In this section we determine the energy of the ssDNA molecule as it enters on axis into a single-walled carbon nanotube. The total work performed by the Lennard-Jones interaction on a molecule entering the carbon nanotube defines the suction energy. With reference to Fig. 3.3.2, the carbon nanotube is assumed to be semi-

Constant	Value
Radius of (8, 8)	5.4 Å
Radius of (9, 9)	6.1 Å
Radius of (10, 10)	6.8 Å
Radius of (11, 11)	7.5 Å
Radius of (12, 12)	8.1 Å
Radius of (13, 13)	8.8 Å
Radius of (14, 14)	9.5 Å
Radius of (15, 15)	10.2 Å
Radius of (16, 16)	10.9 Å
Radius of ssDNA r	5.4 Å
Length of ssDNA c	34 Å
Mean surface density of carbon nanotube	η_g=0.3812 Å^{-2}
Mean surface density of ssDNA	η_d=1.22 Å^{-2}
Attractive constant CNT-DNA	A=42.56 eV Å^6
Repulsive constant CNT-DNA	B=127500 eV Å^{12}

Table 3.3.1: Numerical values of constants used in this chapter.

infinite in length and of radius a, with parametric equations for the tube given by $(a\cos\theta_2, a\sin\theta_2, z)$. The single-stranded DNA is assumed to be a helix of radius r and centred on the z-axis so that a typical point on the helicoid is located at the position $z = Z$ and offset from the z-axis by a distance ξ. Owing to the symmetry of the CNT we may without loss of generality denote this point by the coordinates $(\xi, 0, Z)$, where $\xi = rt$ and $Z = Z_0 + c\theta_1/2\pi$. Thus, the distance from a typical point of the ssDNA molecule to a typical point on the cylindrical surface is given by

$$\begin{aligned}\rho^2 &= a^2 + \xi^2 - 2a\xi\cos\theta_2 + (z-Z)^2 \\ &= (a-\xi)^2 + 4a\xi\sin^2(\theta_2/2) + (z-Z)^2.\end{aligned}$$

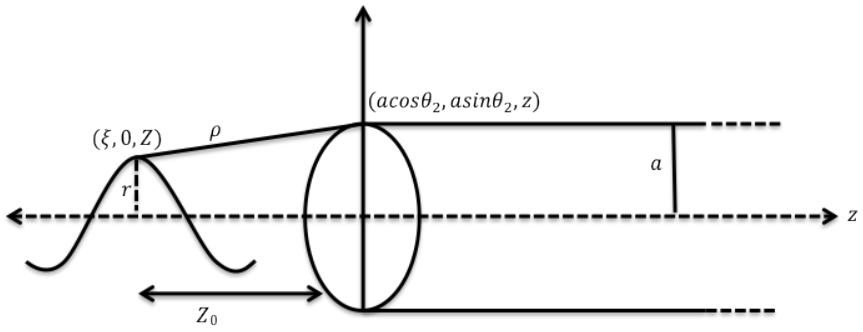


Figure 3.3.2: ssDNA molecule at entrance to single-walled carbon nanotube

Using the Lennard-Jones interaction energy and the continuum approximation, the total interaction energy may be written as

$$E = \frac{rca\eta_g\eta_d}{2\pi}\int_{-\pi}^{\pi}\int_{-\pi}^{\pi}\int_0^1\int_0^{\infty}\left(-\frac{A}{\rho^6}+\frac{B}{\rho^{12}}\right)\left[1+\left(\frac{2\pi r}{c}\right)^2 t^2\right]^{1/2} dz\,dt\,d\theta_1\,d\theta_2,$$

where η_g and η_d represent the mean atomic surface densities of CNT and DNA, respectively. Further, we define the integral T_n by

$$T_n = \int_{-\pi}^{\pi}\int_{-\pi}^{\pi}\int_0^1\int_0^{\infty}\rho^{-n}\left[1+\left(\frac{2\pi r}{c}\right)^2 t^2\right]^{1/2} dz\,dt\,d\theta_1\,d\theta_2, \qquad (3.3.1)$$

and we present the details for the analytical evaluation of T_n in Appendix B.1, and from which we find that the total interaction energy for the ssDNA molecule to be sucked into the CNT is given by

$$E = (rca\eta_g\eta_d/2\pi)\,(-AT_3 + BT_6)\,. \qquad (3.3.2)$$

Results and discussion

Using the algebraic software package MAPLE with the constants given in Table 3.3.1, the numerical calculations are performed, and in this section we present the numerical results showing the relationship between the interaction energy for different sizes of carbon nanotubes and a single ssDNA molecule. Fig. 3.3.3 shows the relation between the distance Z_0 and interaction energy for the ssDNA molecule encapsulated into armchair nanotubes in the range (10, 10)-(16,16) from the open-end of the tube as given in Fig. 3.3.2, we observe that the lowest interaction energy occurs for the case of the (13, 13) nanotube. Also, for the (13, 13), (14, 14), (15, 15) and (16,16) carbon nanotubes we observe that the energetically most favourable location for the ssDNA molecule is inside the tube in the positive z direction given rise to the possibility of encapsulation of the ssDNA molecule in all these cases. In addition, Fig. 3.3.3 shows that there is no possibility of encapsulation of the ssDNA molecule inside the (10, 10), (11, 11) and (12, 12) carbon nanotubes. These observations contrast to the results from [36], where they show that the ssDNA molecule could be inserted inside a (10, 10) carbon nanotube.

3.3.2 Preferred single-walled carbon nanotube to enclose ssDNA

Here we assume that the ssDNA molecule is symmetrically located on axis inside the CNT, and we look for the minimum interaction energy for the ssDNA molecule inside single-walled carbon nanotube. We begin by considering the interaction of a single atom with the carbon nanotube assuming that the single atom is located at a distance ξ from the tube axis, as shown in Fig. 3.3.4. We then integrate the potential energy for the single atom over the surface of the DNA molecule. For the second integration we make the substitution $\xi = rt$ and the distance between two

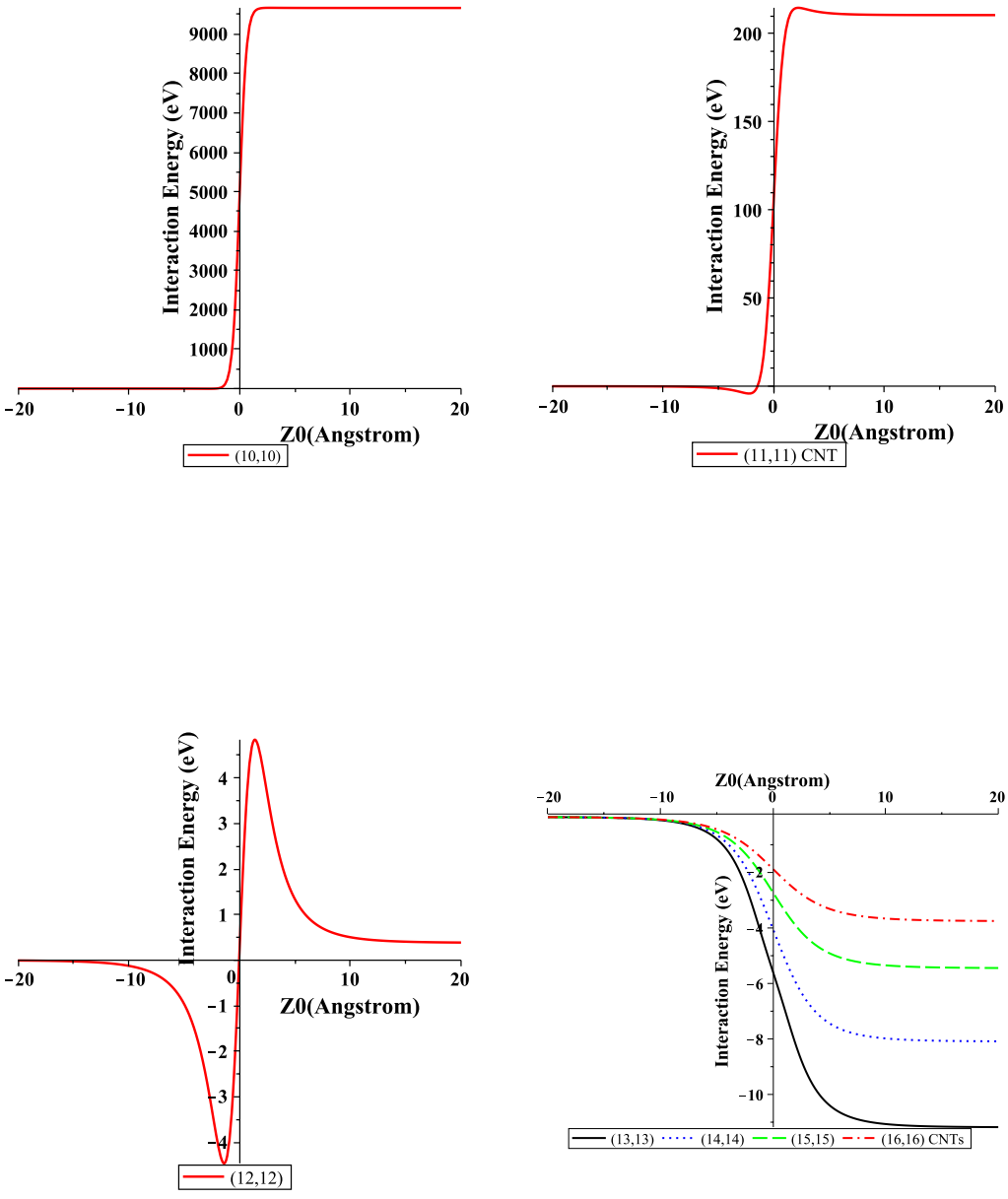


Figure 3.3.3: Interaction potential between ssDNA molecule and (10, 10)-(16, 16) carbon nanotubes

typical points ρ is given by

$$\rho^2 = a^2 + \xi^2 + z^2 - 2a\xi\cos\theta_2.$$

We have the interaction energy of point with infinite carbon nanotube from [81], which is given by

$$E_c = \frac{3\pi^2\eta_g}{4a^4}\left[-AF\left(\frac{5}{2},\frac{5}{2};1;\left(\frac{\xi}{a}\right)^2\right)+\frac{21B}{32a^6}F\left(\frac{11}{2},\frac{11}{2};1;\left(\frac{\xi}{a}\right)^2\right)\right],$$

where $F(a,b;c;z)$ is the standard hypergeometric function [82, §7.5]. Thus, the total potential energy of the dsDNA with the CNT per unit length E, is given by

$$E = \frac{rc\eta_d}{2\pi}\int_{-\pi}^{\pi}\int_0^1 E_c\left(1+\frac{4r^2\pi^2}{c^2}t^2\right)^{1/2} dt\, d\theta_1, \tag{3.3.3}$$

for the analytical evaluation of (3.3.3), we may follow the same steps which we present in Appendix A.2 for the analytical evaluation of (2.4.1), from which we find that the total interaction energy for the ssDNA inside the CNT is given by

$$E = \frac{3\pi^2 rc\eta_g\eta_d}{4a^4}\Big(-AR_3+\frac{21B}{32a^6}R_6\Big), \tag{3.3.4}$$

where R_n is defined by

$$R_n = \sum_{\ell=0}^{\infty}\left[\frac{((2n-1)/2)_\ell\, r^\ell}{(2\ell+1)^{1/2}\ell!a^\ell}\right]^2 F\left(\frac{-1}{2},\ell+\frac{1}{2};\ell+\frac{3}{2};-\delta\right). \tag{3.3.5}$$

Results and discussion

Using the algebraic computer package MAPLE together with the constants given in Table. 3.3.1, numerical solutions for ssDNA molecule inside (8, 8)-(13, 13) CNTs

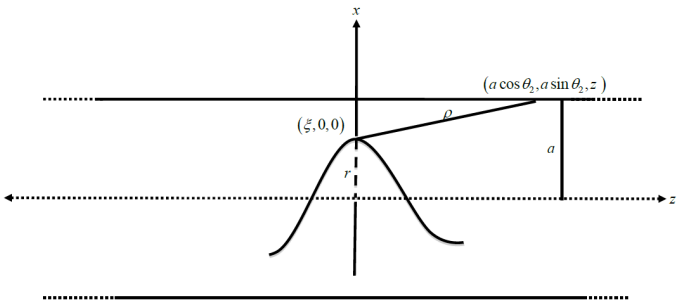


Figure 3.3.4: Single-strand DNA molecule inside single-walled carbon nanotube

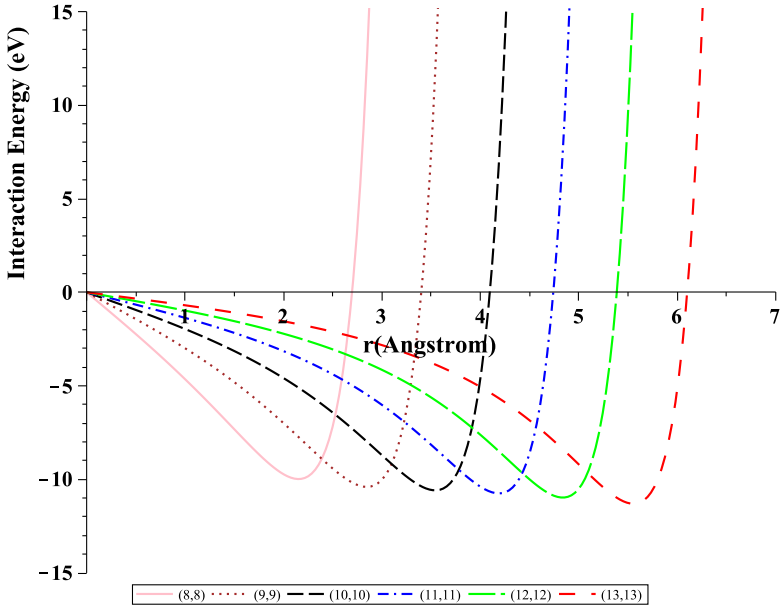


Figure 3.3.5: Interaction potential between ssDNA molecule inside (8, 8)-(13, 13) CNTs as function of ssDNA radius r

are shown in Fig. 3.3.5 with respect to the radius of the ssDNA r. We are observed that the minimum energy occurs at $r = 2.2$ Å, $r = 2.9$Å, $r = 3.5$ Å, $r = 4.2$ Å, $r = 4.8$ Å and $r = 5.6$ Å, for (8, 8)-(13, 13) CNTs, respectively. Also, we observe that at the point where the minimum energy occurs, that the difference between the radii of the CNT and the DNA is approximately 3.3 Å ($a - r \approx 3.3$ Å). In addition, Fig. 3.3.5 shows that the optimal radii of the ssDNA molecule to enclose inside the

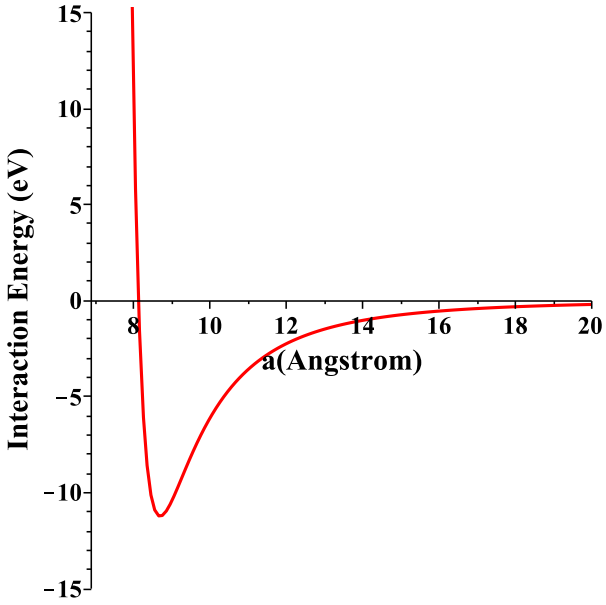


Figure 3.3.6: Interaction potential between ssDNA molecule and CNT as function of tube radius a

(8, 8)-(13, 13) CNTs are $r = 2.1$ Å, $r = 2.8$ Å, $r = 3.5$ Å, $r = 4.2$ Å, $r = 4.8$ Å and $r = 5.6$ Å, respectively. In other words, Fig. 3.3.6 shows that the optimal radius of CNT which is required to enclose the ssDNA with a radius of approximately 5.4 Å is (13, 13) CNT with a radius of approximately 8.8 Å, where the minimum energy occurrs.

3.4 Conclusions

In this chapter, we present a model for the encapsulation of a single-strand DNA molecule inside a single-walled carbon nanotube assuming a vacuum environment. We employ the 6-12 Lennard-Jones potential together with the continuum approximation to calculate the Lennard-Jones interaction energy, which we find may be expressed in terms of a series of hypergeometric functions. These analytical expressions can be readily evaluated numerically using the algebraic computer package

MAPLE. An expression for the suction energy of a ssDNA molecule assumed to enter on axis into a semi-infinite carbon nanotube is obtained. We observe that the suction behaviour depends on the radius of the carbon nanotube, and here we predict that it is less likely for an ssDNA molecule to be accepted into the CNT when the value of the tube radius is less than 8.1 Å. In addition, we observe that the lowest interaction energy for all carbon nanotubes considered in this study occurs for the (13, 13) carbon nanotube, assuming that the ssDNA molecule remains on the tube axis. Thus we are predicted the encapsulation of an ssDNA molecule is more likely to be into the (13, 13) carbon nanotube. This differs from [2, 36] who show that the ssDNA can be accepted inside a (10, 10) CNT. It also differs from [42] who show that a (14, 14) nanotube diameter turns out to be too small for ssDNA to enter into its cylindrical channel. The discrepancy between our results and these results may be attributed to the rigid geometric structure of the ssDNA which we have adopted here. Generally, there will be an elastic energy effect in the CNT as the ssDNA molecule enters the tube.

We also examine the interaction energy for a ssDNA inside single-walled carbon nanotube for different armchair tubes, assuming that the ssDNA is already accepted into the carbon nanotube tube. The results indicate that the encapsulation of the ssDNA molecule into a single-walled carbon nanotubes may occur for carbon nanotubes with radii greater than 8.2 Å. Moreover, the optimal radius of carbon nanotube to enclose the single-strand DNA is approximately 8.8 Å, and we conclude that the preferred armchair tube is (13, 13). The benefit of the approach adopted here is the prediction of whether or not certain DNA molecule will be encapsulated into a carbon nanotube, which will become an important issue for applications including drug and gene delivery research.

3.4.1 Nomenclature

Symbol	Meaning
$P(\rho)$	is the Lennard-Jones potential function
E	is the interaction energy
A	is the attractive Lennard-Jones constant
B	is the repulsive Lennard-Jones constant
η_1, η_2	are the atomic surface densities of the two interacting molecular structures
σ	is the equilibrium distance of two atoms
ε	is the depth of the potential well
ρ	is the distance between typical surface elements on the CNT and the DNA
a	is the radius of the carbon nanotube
η_g	is the atomic surface density of the carbon nanotube
η_d	is the atomic surface density of the ssDNA
r	is the radius of the ssDNA
c	is the unit cell length of the ssDNA
ξ	is the distance from the tube axis
Z_0	is the distance from the tube opening
$F(a, b; c; z)$	is the standard hypergeometric function

Chapter 4

Offset configurations for single and double strand DNA inside single-walled carbon nanotubes

4.1 Abstract

Nanotechnology is a rapidly expanding research area, and it is believed that the unique properties of molecules at the nano-scale will prove to be of substantial benefit to mankind especially so in medicine and electronics. Here we use applied mathematical modelling exploiting the basic principles of mechanics and the 6-12 Lennard-Jones potential function together with the continuum approximation, which assumes that intermolecular interactions can be approximated by average atomic surface densities. We consider the equilibrium offset positions for both single-strand and double-strand DNA molecules inside a single-walled carbon nanotube, and we predict offset positions with reference to the cross-section of the carbon nanotube. For the double-strand DNA, the potential energy is determined for the general case for any helical phase angle ϕ, but we also consider a special case when $\phi = \pi$, which

leads to a substantial simplification in the analytical expression for the energy. As might be expected, our results confirm that the global minimum energy positions for a single-strand DNA molecule and a double-strand DNA molecule will lie off axis and they become closer to the tube wall as the radius of the tube increases.

4.2 Introduction

The discovery of carbon nanotubes by Iijima in 1991 [28] has had an enormous impact on research into new nanomechanical devices exploiting their unique physical and mechanical properties, such as low weight, high strength, flexibility and thermal stability [20, 27, 83, 85]. Carbon nanotubes comprise carbon atoms and it has been established that carbon nanotubes are one of the strongest known materials [86]. For more information on the exceptional properties of carbon nanotubes, we refer the reader to [87]. Single-walled carbon nanotubes (SWCNTs) can be envisaged as a graphene sheet that is rolled up to form a seamless cylinder. The first report on deoxyribonucleic acid (DNA) appeared in 1869 by Friedrich Miescher and in 1944 Avery, MacLeod, and McCarty showed that DNA is the basic hereditary material for all living species [6]. The formulation of the geometric model for DNA occured in 1953 by Watson and Crick [14]. DNA consists of two long polymers of simple units called nucleotides, comprising five elements: carbon (C), oxygen (O), hydrogen (H), nitrogen (N) and phosphorus (P) [3, 14]. Each nucleotide is composed of a sugar attached to a single phosphate group with four possible bases; guanine (G), cytosine (C), adenine (A) and thymine (T), and the nucleotides are linked together in a chain by sugar-phosphates. Moreover, double-strand DNA forms a double helical structure that has two grooves which are created by the coiling of the two helices around each other; the wider one is termed the major groove which is 22 Å in length, and the smaller is called the minor groove which is in 12 Å in length, these two grooves together create a unit cell comprising a DNA molecule over a distance

of 34 Å [3]. Their small size together with their unique mechanical and electronic properties, carbon nanotubes and DNA molecules comprise potential new materials for uses in many areas of nanotechnology [17]. Examples of the functionalization of DNA-CNT are DNA molecules with CNT used to develop CNTs in drug and gene delivery, and CNT-DNA hybrids for biological sensing [22, 33, 34, 73]. In addition, the DNA molecule can be used to control length and to increase the solubility of CNTs [35, 73]. There are many experiments and molecular dynamical simulations that study the interaction and the possibility of encapsulation of ssDNA and ds-DNA molecules inside carbon nanotubes (see for example [2,19,34,36,39,40,42,88]), but there is very little work to date adopting conventional applied mathematical modelling. In the previous chapters, we have investigated the interaction energy between single and double strand DNA molecules and a single-walled carbon nanotube. The DNA molecules are assumed to be inside the tube, and we determine the radius of carbon nanotube that is necessary to enclose the DNA molecules, and this turns out to be approximately 12.8 Å for the dsDNA molecule, and 8.8 Å for the ssDNA molecule. Here we investigate the equilibrium offset position of both ssDNA and dsDNA molecules inside a single-walled carbon nanotube and we use classical applied mathematical modelling using the basic principles of mechanics to exploit the 6-12 Lennard-Jones potential and the continuum approximation, which assumes that the inter-atomic interactions can be modelled by smearing the atoms uniformly across an ideal surface. We comment that Girifalco et al. [4] state that the continuum Lennard-Jones approach may in many instances be a better approximation for uniform atomic distributions than for a set of discrete atomic centers. We use the continuum Lennard-Jones approach to deduce analytical approximations. In this paper we assume the B-form of DNA, which is the structure commonly found inside cells [3] and we comment that the assumption that the DNA retains its B form, assumes that there is sufficient water to solvate the backbone. We also comment

that this is a critical assumption when the DNA is within a nanotube and especially when the DNA is near the surface, since the surface interaction can also distort the DNA. We derive analytical expressions for the potential energy between a ssDNA or dsDNA molecule inside a single-walled carbon nanotube. In §4.2, we present the details for the derivation of the total interaction energy for an offset ssDNA molecule inside a SWCNT. In §4.3.1, we give the corresponding calculation for the special case of the interaction of an offset dsDNA molecule inside a SWCNT when the helical phase angle $\phi = \pi$, and in §4.3.2, we give the corresponding calculation for the interaction of an offset dsDNA molecule inside a SWCNT for any value of the helical phase angle ϕ. Some brief conclusions are presented in §4.4.

4.3 Continuum approximation and Lennard-Jones potential

The unit cell of the double-strand B-DNA molecule used here is assumed to comprise 10.5 base-pairs, which give a total of 792.75 atoms in the unit cell. We assume also that the unit cell for the single-strand DNA has a helical geometry, and this assumption follows the previous experimental studies [8–11]. The single-strand DNA comprises 11 bases which gives a total of 415.25 atoms in the unit cell. With reference to Fig. 4.3.1, we consider a unit cell comprising a DNA molecule over a distance of 34 Å. We derive the total interaction energy for a DNA molecule into a carbon nanotube using the Lennard-Jones potential together with the continuum approximation. The classical Lennard-Jones potential interaction energy between a pair of atoms at a distance ρ apart is given by

$$P(\rho) = -\frac{A}{\rho^6} + \frac{B}{\rho^{12}},$$

where A and B are the attractive and repulsive constants, respectively. The 6-12 Lennard-Jones potential may also be expressed as

$$P(\rho) = 4\varepsilon\Big[-\Big(\frac{\sigma}{\rho}\Big)^6 + \Big(\frac{\sigma}{\rho}\Big)^{12}\Big],$$

where $\varepsilon = A^2/4B$ is the magnitude of the energy at the equilibrium distance $\rho_0 = 2^{1/6}\sigma = (2B/A)^{1/6}$, and σ is the atomic distance when the potential energy is zero. Using the 6-12 Lennard-Jones potential, together with the continuum approximation, which assumes that discrete atoms may by replaced by a uniform by distributed surface density of atoms so that the total non-bonded interaction energy E, may be obtained from

$$E = \eta_1\eta_2 \int_{S_1}\int_{S_2} \left(-\frac{A}{\rho^6} + \frac{B}{\rho^{12}}\right) dS_1\, dS_2,$$

where η_1 and η_2 denote the atomic liner surface densities of the first and the second molecules, respectively. We comment that this double integral and all the subsequent integrals in this chapter are surface integrals that are evaluated over the surface of a helicoid and we refer the reader to Kreyszig [68, pp.443-452] or Kaplan [69, pp.313-319] for the evaluation of surface integrals. The numerical values of the constants that are used throughout this chapter are as given in Tables 1.1.1 and 4.3.1. We comment that in real experiments, the insertion into the carbon nanotube is most likely to occur in an aqueous solution, which may be partially modelled with modified Lenard-Jones parameters.

4.4 Offset ssDNA molecule inside SWCNT

In this section we assume that the ssDNA molecule may be modeled by a single helicoid, which is a ruled surface having a helix as its boundary, such that with

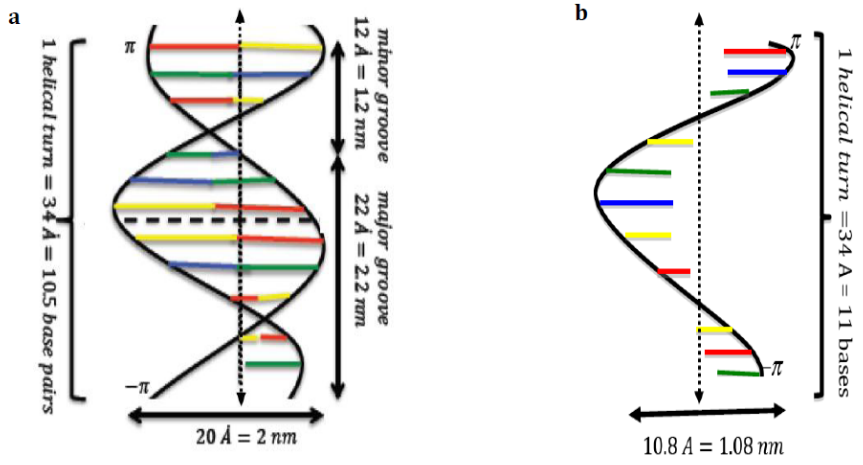


Figure 4.3.1: Geometry for (a) double and (b) single helicoid of B-DNA for one complete rotation of helix (34 Å)

Constant	Value
Radius of (13, 13)	8.8 Å
Radius of (16, 16)	10.9 Å
Radius of (20, 20)	13.6 Å
Radius of (23, 23)	15.6 Å
Radius of (26, 26)	17.6 Å
*Radius of ssDNA r	5.4 Å
**Radius of dsDNA R	10 Å
**Length of DNA c	34 Å
Mean surface density of carbon nanotube η_g	0.3812 Å^{-2}
Mean surface density of ssDNA η_d	0.83 Å^{-2}
Mean surface density of dsDNA ($\phi = \pi$) η_{D_1}	0.84 Å^{-2}
Mean surface density of dsDNA ($\phi = 12\pi/17$) η_{D_2}	0.97 Å^{-2}
Attractive constant CNT-DNA A	42.6 eV Å^6
Repulsive constant CNT-DNA B	127500 eV Å^{12}

Table 4.3.1: Numerical values of constants used in this chapter (* denotes data from [2] and ** denotes data from [3]).

reference to the rectangular Cartesian coordinate system (x, y, z), a typical point on

the surface of an offset ssDNA molecule specialised by the coordinates

$$\mathbf{H}(\theta, t) = (rt\cos\theta + \delta, rt\sin\theta, c\theta/2\pi)\,,$$

where δ is the offset distance measured along the x-axis, r and c are the radius and the unit cell length of the ssDNA helix, respectively, and the two parametric variables t and θ are such that $0 < t < 1$ and $-\pi < \theta < \pi$. We comment that a helical curve is normally parameterized by the single parameter θ. In this case we have adopted two parameters to allow for variable internal points of the helicoid, so that we may integrate over all values of the DNA radius from zero to r. We also comment that single-strand DNA is a disordered polymer that is unlikely to have a precise helical conformation. Here we assume the ideal conformation as a first step towards modelling more realistic situations. With reference to the same rectangular Cartesian coordinate system (x, y, z), a typical point on the surface of the tube has coordinates $(a\cos\omega, a\sin\omega, z)$, where a is the radius of the carbon nanotube and $-\infty < z < \infty$ and $-\pi < \omega < \pi$. Thus, the distance ρ between typical surface and line elements on the CNT and on the DNA is given by

$$\rho^2 \;=\; a^2 + r^2t^2 - 2art\cos(\omega - \theta) + 2rt\cos\theta - 2a\delta\cos\omega + \delta^2 + (z - c\theta/2\pi)^2.$$

We now determine the position with reference to the cross-section of a carbon nanotube the ssDNA molecule has its minimum potential energy. The total potential energy E of the ssDNA molecule inside the CNT, becomes

$$E \;=\; \frac{arc\eta_d\eta_g}{2\pi}\int_{-\pi}^{\pi}\int_{-\pi}^{\pi}\int_{0}^{1}\int_{-\infty}^{\infty}\left(-\frac{A}{\rho^6} + \frac{B}{\rho^{12}}\right)\left(1 + \frac{4r^2\pi^2}{c^2}t^2\right)^{1/2} dz\,dt\,d\theta\,d\omega,$$

and using the rotational symmetry of the tube, without loss of generality, we may assume that a typical point on the ssDNA molecule is located at $(\xi, 0, 0)$, which

means that the point of interaction is fully prescribed by a distance ξ from the z-axis, and the CNT of infinite extent, as shown in Fig. 4.4.1. Thus,

$$\xi^2 = (rt\cos\theta+\delta)^2+(rt\sin\theta)^2 = (rt+\delta)^2-4\delta rt\sin^2(\theta/2).$$

From [81] we have the interaction energy of a single atom with an infinite carbon nanotube is given by

$$E_c = \frac{3\pi^2\eta_g}{4a^4}\left[-AF\left(\frac{5}{2},\frac{5}{2};1;\left(\frac{\xi}{a}\right)^2\right)+\frac{21B}{32a^6}F\left(\frac{11}{2},\frac{11}{2};1;\left(\frac{\xi}{a}\right)^2\right)\right], \quad (4.4.1)$$

where $F(a,b;c;z)$ is the usual hypergeometric function [82, §7.5]. Thus, the total potential energy of the ssDNA molecule inside the CNT E, is given by

$$E = \frac{rc\eta_d}{2\pi}\int_{-\pi}^{\pi}\int_0^1 E_c\left(1+\frac{4r^2\pi^2}{c^2}t^2\right)^{1/2}dt\,d\theta. \quad (4.4.2)$$

Some brief details for the analytical evaluation of equation (4.4.2) are presented in Appendix C.1, from which we find that the total interaction energy for the ssDNA molecule inside the CNT is given by

$$E = \frac{3\pi^2 rc\eta_g\eta_d}{4a^4}\Big(-AR_3+\frac{21B}{32a^6}R_6\Big), \quad (4.4.3)$$

where R_n is defined by (C.1.1). In the final evaluation of the energy, these equations are computed for each atom species and then summed, using the Lennard-Jones parameters given in Table 1.1.1 for the five types of atoms. In Fig. 4.4.2, we use the algebraic computer package MAPLE together with the parameter values given in Table 4.3.1 to plot the potential energy E as given by equation (4.4.3) with respect to δ for an ssDNA molecule inside the carbon nanotube (13, 13) (a= 8.8 Å), (16, 16) (a=10.9 Å) and (20, 20) (a= 13.6 Å). As shown in Fig. 4.4.2, the preferred

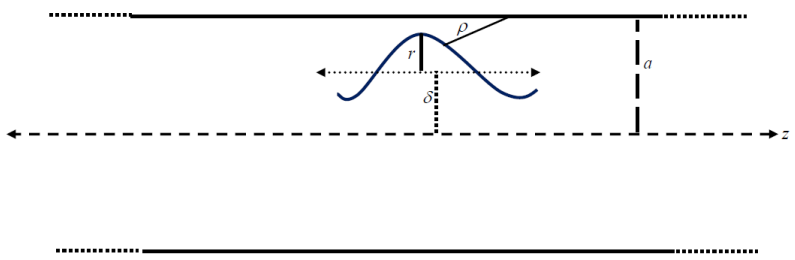


Figure 4.4.1: Schematic for offset ssDNA molecule inside single-walled carbon nanotube

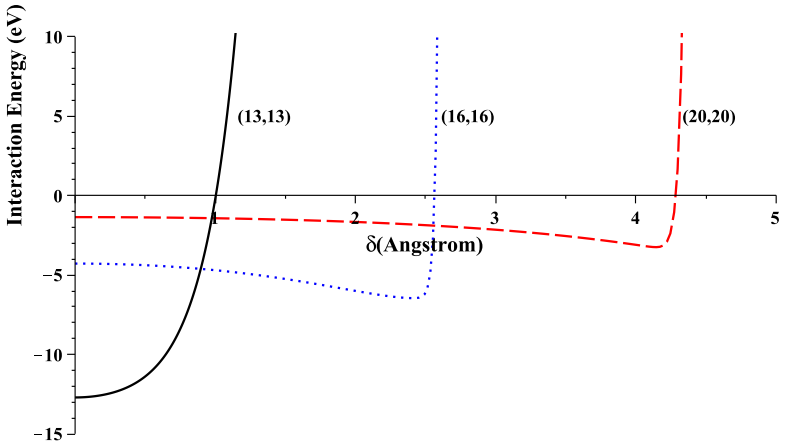


Figure 4.4.2: Total potential energy for offset ssDNA molecule inside (13, 13), (16, 16) and (20, 20) SWCNTs with respect to the offset distance δ

location of the ssDNA molecule inside the carbon nanotube (13, 13) is with the axis of the ssDNA molecule lying on the tube axis. In the cases of (16, 16) and (20, 20) carbon nanotubes, we obtain $\delta = 2.4$ Å and $\delta = 4.1$ Å, respectively. These results are equivalent to the distance between the centre of the ssDNA molecule and the wall of the nanotube being 8.8 Å, 8.5 Å and 9.5 Å, respectively.

4.5 Offset dsDNA molecule inside SWCNT

In this section, the location of the minimum potential energy is determined which corresponds to the preferred position of the dsDNA molecule inside a single-walled

carbon nanotube. We study two cases for an offset dsDNA molecule inside a single-walled carbon nanotube, depending on the helical phase angle ϕ. We assume that the dsDNA molecule is inside the SWCNT and that Δ is the perpendicular distance between the axes of the dsDNA molecule and the SWCNT as shown in Fig. 4.5.1. Firstly, we consider the interaction energy for the special helical phase angle $\phi = \pi$, and then we examine the general case for any value of the helical phase angle ϕ. As before, we model the dsDNA molecule as a surface with a double helicoid geometry, and the parametric equation for an offset dsDNA molecule is given by

$$\mathbf{G}(\Theta, t) = \left(\frac{R}{2}\left[\cos\Theta + \cos(\Theta - \phi) + t\Big(\cos\Theta - \cos(\Theta - \phi)\Big)\right] + \Delta, \right.$$
$$\left. \frac{R}{2}\left[\sin\Theta + \sin(\Theta - \phi) + t\Big(\sin\Theta - \sin(\Theta - \phi)\Big)\right], \frac{c\Theta}{2\pi}\right),$$

where $R = 10$ Å is the radius of the dsDNA helix, $c = 34$ Å is the unit cell length, ϕ is the helical phase angle parameter and the parametric variables t and Θ are such that $-1 < t < 1$, and $-\pi < \Theta < \pi$. With reference to the same rectangular Cartesian coordinate system (x, y, z), a typical point on the surface of the tube has coordinates $(a\cos\omega, a\sin\omega, z)$, where a is the radius of the carbon nanotube and $-\infty < z < \infty$ and $-\pi < \omega < \pi$. Thus, the distance ρ between two typical points on the surface of the dsDNA molecule and the tube can be written as

$$\begin{aligned}\rho^2 &= \left\{ \frac{R}{2}\left[\cos\Theta + \cos(\Theta - \phi) + t\Big(\cos\Theta - \cos(\Theta - \phi)\Big)\right] + \Delta - a\cos\omega \right\}^2 \\ &+ \left\{ \frac{R}{2}\left[\sin\Theta + \sin(\Theta - \phi) + t\Big(\sin\Theta - \sin(\Theta - \phi)\Big)\right] - a\sin\omega \right\}^2 + \left(\frac{c\Theta}{2\pi} - z \right)^2.\end{aligned}$$

As before, with reference to the cross-section of the carbon nanotube, we determine the position where the dsDNA molecule has its minimum potential energy. We may assume that a typical point on the dsDNA molecule is located at $(\Xi, 0, 0)$ and the

CNT is of infinite extent, as shown in Fig. 4.5.1. Thus,

$$\begin{aligned}\Xi^2 &= \Big(\frac{R}{2}[\cos\Theta+\cos(\Theta-\phi)+t(\cos\Theta-\cos(\Theta-\phi))]+\Delta\Big)^2 \\ &+ \Big(\frac{R}{2}[\sin\Theta+\sin(\Theta-\phi)+t(\sin\Theta-\sin(\Theta-\phi))]\Big)^2 \\ &= R^2\left[\cos^2(\phi/2)+t^2\sin^2(\phi/2)\right]+R\Delta\left[(1+t)\cos\Theta+(1-t)\cos\left(\Theta-\phi\right)\right]+\Delta^2.\end{aligned}$$

4.5.1 Offset dsDNA molecule inside SWCNT for $\phi = \pi$

In this section, we consider the special case of the helical angle ϕ, by assuming that the value of ϕ is equal to π. Thus

$$\Xi^2 = R^2t^2+2R\Delta t\cos\Theta+\Delta^2=(Rt+\Delta)^2-4R\Delta t\sin^2(\Theta/2).$$

Using the interaction energy of a single atomic point with an infinite carbon nanotube which is given by equation (4.4.1) thus the total potential energy of the dsDNA molecule inside the CNT E, is given by

$$E = \frac{rc\eta_{D_1}}{2\pi}\int_{-\pi}^{\pi}\int_{-1}^{1}E_c\left(1+\frac{4r^2\pi^2}{c^2}t^2\right)^{1/2}dt\,d\Theta, \tag{4.5.1}$$

for the analytical evaluation of equation (4.5.1), we follow the same steps which are shown in Appendix C.1. Thus, the total interaction energy for the dsDNA molecule inside the CNT for $\phi = \pi$, which is given by

$$E = \frac{3\pi^2rc\eta_g\eta_{D_1}}{2a^4}\Big(-AR_3+\frac{21B}{32a^6}R_6\Big), \tag{4.5.2}$$

where R_n is defined by (C.1.1), and using the algebraic computer package MAPLE and employing the parameter values given in Table 4.3.1, we may evaluate the total potential energy E for the dsDNA molecule inside a single-walled carbon nanotube. In Fig. 4.5.2, we show the relation of the the potential energy and the offset position

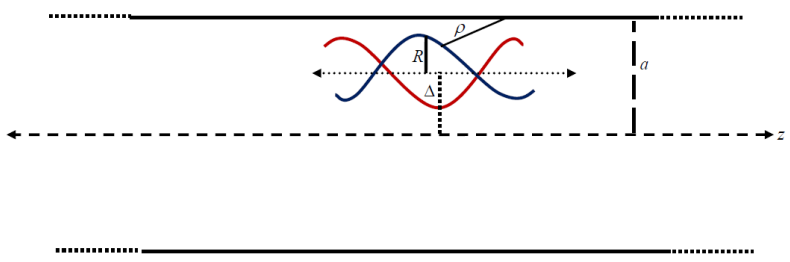


Figure 4.5.1: Schematic for offset dsDNA molecule inside a single-walled carbon nanotube

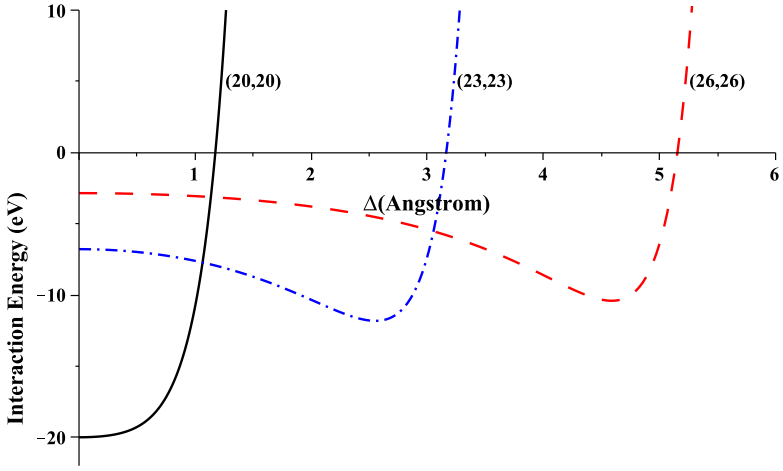


Figure 4.5.2: Total potential energy for offset dsDNA molecule inside (20, 20), (23, 23) and (26, 26) SWCNTs with respect to the offset distance Δ for $\phi = \pi$

for a dsDNA molecule inside (20, 20), (23, 23) and (26, 26) carbon nanotubes. We find that the value of Δ for the dsDNA molecule inside the (20, 20), (23, 23) and (26, 26) carbon nanotubes is approximately 0, 2.6 Å and 4.6 Å, respectively. The corresponding distances $(a - \Delta)$ between the of the dsDNA and the wall of the tube are 13.6 Å, 13 Å and 13 Å, respectively. We observe that as expected as the radius of the tube gets larger, the location where the minimum energy occurs tends to be closer to the nanotube wall.

4.5.2 Offset dsDNA molecule inside SWCNT for $\phi = 12\pi/17$

In this section, we consider the general helical angle ϕ for which we have in mind the particular value $\phi = 12\pi/17$, which is the physical value of the helical angle ϕ, leading to the measured major and minor groove sites, as shown in Fig. 4.3.1. Thus

$$\Xi^2 = R^2\left[\cos^2(\phi/2) + t^2\sin^2(\phi/2)\right] + R\Delta\left[(1+t)\cos\Theta + (1-t)\cos\left(\Theta-\phi\right)\right] + \Delta^2.$$

Using the interaction energy for an atom with an infinite carbon nanotube which is given by equation (4.4.1), the total potential energy of the dsDNA molecule inside the CNT per unit length E, is given by

$$E = \frac{rc\eta_{D_2}}{2\pi}\sin(\phi/2)\int_{-\pi}^{\pi}\int_{-1}^{1} E_c\left(1 + \frac{4r^2\pi^2\sin^2(\phi/2)}{c^2}t^2\right)^{1/2} dt\, d\Theta, \quad (4.5.3)$$

and the total interaction energy for the dsDNA molecule inside the CNT for $\phi = 12\pi/17$, is given by

$$E = \frac{3\pi^2 rc\eta_g\eta_{D_2}\sin(\phi/2)}{4a^4}\Big(-AJ_3 + \frac{21B}{32a^6}J_6\Big), \quad (4.5.4)$$

and we show the derivation of the analytical evaluation for J_n in Appendix C.2. In Fig. 4.6.1, we use the algbraic computer package MAPLE to evaluate (4.5.3), and plot the relation between the potential energy and the offset position for a dsDNA molecule for the general helical angle ϕ inside the (20, 20), (23, 23) and (26, 26) carbon nanotubes. As shown in Fig. 4.6.1, we observe that as the radius of the tube gets larger, the minimum energy location tends to be closer to the nanotube wall.

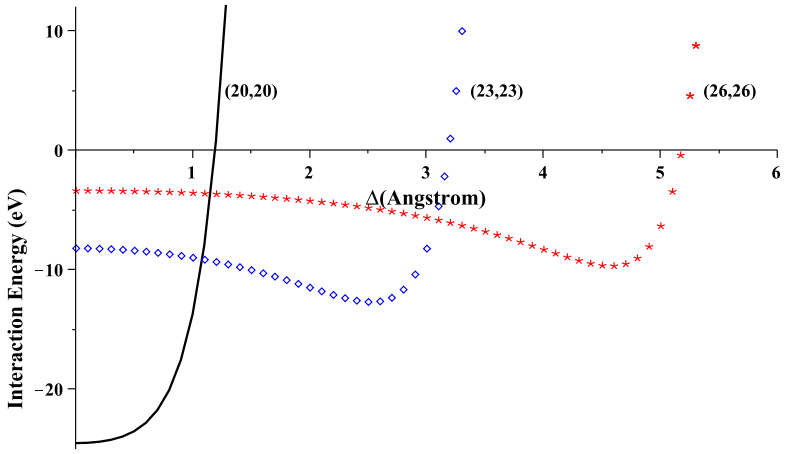


Figure 4.6.1: Total potential energy for offset dsDNA molecule inside (20, 20), (23, 23) and (26, 26) SWCNTs with respect to the offset distance Δ for $\phi = 12\pi/17$

4.6 Conclusions

In this chapter, we employ the 6-12 Lennard-Jones potential together with the continuum approach, for which the discrete atoms are modelled by an average distribution over a surface for each molecule. We determine the offset equilibrium positions for both single-strand and double-strand DNA molecules inside a single-walled carbon nanotube. In the modelling we assume that the DNA is already accepted inside the single-walled carbon nanotube. We find that the global minimum energy equilibrium positions of the offset ssDNA and dsDNA tend to be closer to tube wall as the radius of the tube increases. We may also adopt a similar modelling approach to predict whether or not molecules can be accepted into a carbon nanotube, which has become an important issue in terms of developing drug and gene delivery.

4.6.1 Nomenclature

Symbol	Meaning
$P(\rho)$	is the Lennard-Jones potential function for two unbonded atoms
E	is the interaction energy
E_c	the interaction energy of a single atom with an infinite carbon nanotube
A	is the attractive Lennard-Jones constant
B	is the repulsive Lennard-Jones constant
η_1, η_2	are the atomic surface densities of the two interacting molecular structures
σ	is the equilibrium distance of two atoms
ε	is the depth of the potential well
ρ	is the distance between typical surface elements on the CNT and the DNA
ϕ	is the helical phase angle parameter
a	is the radius of the carbon nanotube
η_g	is the atomic surface density of the carbon nanotube
η_d	is the atomic surface density of the ssDNA
η_{D_1}	is the atomic surface density of the dsDNA (for $\phi = \pi$)
η_{D_2}	is the atomic surface density of the dsDNA (for $\phi = 12\pi/17$)
R	is the radius of the dsDNA
r	is the radius of the ssDNA
c	is the unit cell length
δ	is the perpendicular distance between the axes of the ssDNA and the SWCNT
Δ	is the perpendicular distance between the axes of the dsDNA and the SWCNT
$F(a, b; c; z)$	is the standard hypergeometric function

Chapter 5

DNA adsorption on graphene

5.1 Abstract

Here we use classical applied mathematical modeling to determine surface binding energies between single-strand and double-strand DNA molecules interacting with a graphene sheet. We adopt basic mechanical principles to exploit the 6-12 Lennard-Jones potential function and the continuum approximation, which assumes that intermolecular interactions can be approximated by average atomic line or surface densities. The minimum binding energy occurs when the single-strand DNA molecule is centred 20.2 Å from the surface of the graphene and the double-strand DNA molecule is centred 20.3 Å from the surface, noting that these close values apply for the case when the axis of the helix is perpendicular to the surface of graphene. For the case when the axis of the helix is parallel to the surface, the minimum binding energy occurs when the axis of the single-strand molecule is 8.3 Å from the surface, and the double-strand molecule has axis 13.3 Å from the surface. For arbitrary tilted axis, we determine the optimal angles Ω of the axis of the helix, which give the minimum values of the binding energies, and we observe that the optimal rotational angles tend to occur in the intervals $\Omega \in (\pi/4, \pi/2)$ and

$\Omega \in (\pi/7, \pi/5)$ for the single and double-strand DNA molecules, respectively.

5.2 Introduction

Graphene is a single-layer carbon crystal, which is highly electronically conducting through the plane of the material. The first reported existence of graphene sheet occurred in 2004 [44], and because of its unique physicochemical properties, such as high surface area, excellent thermal conductivity and strong mechanical strength, graphene has considerable promise for many applications, such as in electronics, energy storage (supercapacitors, batteries, fuel cells, solar cells), bioscience and biotechnologies [44, 46, 47]. Deoxyribonucleic acid (DNA) is one of the most promising chemical moieties to facilitate the self-assembly process at the nanoscale. The DNA molecule comprises two long polynucleotide helical chains composed of four nucleotide subunits [3, 14]. Each nucleotide is composed of sugar attached to a single phosphate group with four possible bases; guanine (G), cytosine (C), adenine (A) and thymine (T), and the nucleotides are linked together in a chain by sugar-phosphates [3]. The key geometric design parameters for the predicted helical structures constitute a wide major groove and a narrower minor groove [3]. The DNA molecule has generated much research interest in several areas of modern biotechnology, and there is considerable potential for DNA molecules to be used in the construction of nanostructures and devices, such as the self assembly of devices and computational elements, for interconnects, or for the device element itself [70].

The DNA molecule and graphene sheet are ideal nanostructues to fabricate novel nanobio hybrid materials through different arrangements, to construct highly sensitive nanobio electronic devices including sensors and chips [48]. Graphene and DNA can also be used as the basic building blocks for bioelectronics, especially for bacterial DNA-protein and polyelectrolyte chemical transistors, and opening up new opportunities for the design of graphene/DNA-base systems for the study of nucleic acid and

biosensors [49,50]. Furthermore, the adsorption of DNA on an electrode surface may lead to new approaches to deliver drugs in the DNA grooves or to different rates of hybridization [51]. Gowtham et al. [52] provide a first-principles investigation of the interaction of the nucleobases with graphene using density-functional theory (DFT) together with Hartree-Fock and a second-order Møller-Plesset perturbation theory. They show that the nucleobases exhibit significantly different interaction strengths when physisorbed on graphene. Antony and Grimme [53] determine the interaction energy of the DNA nucleobases with graphene using a DFT method, and establish the ordering G>A>T>C. Zhao [54] examines the interaction of the dsDNA molecule with the graphene surface in aqueous solution using molecular dynamics (MD) simulations to detect the dominant role of the hydrophobic π stacking in the interaction between nucleotides and carbon nanosurfaces, where the dsDNA molecule in the study consists of 8 or 12 base pairs. Zhao [54] shows that the dsDNA molecule can be rotated from a parallel to a perpendicular position with respect to the graphene surface. Kabelac et al. [55] use MD simulations to investigate the linker of single-strand and double-strand DNA molecules to the graphene; the structures of both the double-strand and single-stranded molecules are assumed to be in the B-form with the base sequence 5'-CCACTAGTGG-3'. These authors find that the dsDNA molecule is orientated more or less perpendicularly to the graphene surface, with an average deviation from perpendicularity of approximately 18 degrees, and the ssDNA molecule becomes parallel to the graphene surface such that not all of the bases are simultaneously attached to the substrate. Oliveira Brett and Chiorcea [51] employe Magnetic AC mode atomic force microscopy (MAC Mode AFM) to describe the process of adsorption of ssDNA and dsDNA molecules on a highly oriented pyrolytic graphite (HOPG), and show that the ssDNA molecule interacts and adsorbs strongly to the graphene surface, as compared to the dsDNA molecule. Varghese et. al [56] employ the isothermal titration calorimetry (ITC) to

investigate the binding energy of DNA nucleobases and nucleosides with graphene in an aqueous environment, and find that the experimental binding energies are generally small.

In this chapter, we investigate the interaction of single-strand and double-strand DNA molecules with a graphene sheet. Employing classical applied mathematical modeling and using the basic principles of mechanics we exploit the 6-12 Lennard-Jones potential and the continuous approximation. The modelling approach adopted here has the major advantage of computational efficiency to determine accurate energy values which would be otherwise arduous to obtain. We derive analytical expressions for the binding energies between a ssDNA and dsDNA molecules adsorbing onto a graphene surface. We minimize the binding energies so as to determine the preferred locations of single-strand and double-strand DNA molecules with respect to the graphene sheet. For the two situations reported in [54, 55], when the helical axis of the DNA molecule is perpendicular to the surface of graphene and secondly, when the helical axis of the DNA molecule is parallel to the surface of graphene, are presented in sections 5.2 and 5.3, respectively. In section 5.4, we present the interaction of ssDNA and dsDNA molecules with graphene sheet for different orientations of the helix axis in order to determine the minimum energy angle of tilt. A summary is given in the final section of the chapter.

5.3 Method

The assumptions underlying the mathematical modelling employed here are outlined in this section. We assume the B-DNA form, which is the structure commonly found inside cells [3]. We comment that the assumption that the DNA retains its B form, assumes that there is sufficient water to solvate the backbone. We also comment that this is a critical assumption when the DNA is within a graphene and especially when the DNA is near the surface, since the surface interaction can also distort the

DNA. The double-strand DNA investigated in this study is assumed to consist of 10.5 base pairs, while the single-strand DNA is assumed to have a helical geometry comprising 11 bases, and we consider a unit cell comprising a DNA molecule over a distance of 34 Å. The interaction between a pair of atoms at distance ρ apart is usually modelled by the 6-12 Lennard-Jones potential [89], which is given by

$$V(\rho) = 4\varepsilon\Big[-\Big(\frac{\sigma}{\rho}\Big)^6 + \Big(\frac{\sigma}{\rho}\Big)^{12}\Big] = -\frac{A}{\rho^6} + \frac{B}{\rho^{12}},$$

where $\varepsilon = A^2/4B$ is the magnitude of the energy at the equilibrium distance $\rho_0 = 2^{1/6}\sigma = (2B/A)^{1/6}$, and σ is the atomic distance when the potential energy is zero. In addition, A and B denote the attractive and repulsive constants, respectively. Using the 6-12 Lennard-Jones potential, together with the continuum approximation, which assumes that a discrete atomic structure may by replaced by a uniform distribution of atoms over a line or surface, so that for example, in the case of surfaces, the total non-bonded interaction energy E, may be deduced from

$$E = \eta_1\eta_2 \int_{S_1}\int_{S_2} \left(-\frac{A}{\rho^6} + \frac{B}{\rho^{12}} \right) dS_1\, dS_2,$$

where η_1 and η_2 denote the atomic surface densities of the first and the second molecules, and dS_1 and dS_2 denote respective surface elements. The numerical values of the various constants that are used throughout this chapter are as given in Tables 1.1.1 and 5.3.1.

Constant	Value
*Radius of ssDNA b	5.4 Å
**Radius of dsDNA r	10 Å
**Length of DNA c	34 Å
Mean surface density of grapene sheet η_g	0.3812 Å^{-2}
Mean surface density of ssDNA η_d	0.83 Å^{-2}
Mean surface density of dsDNA ($\phi = \pi$) η_{D_1}	0.84 Å^{-2}
Mean surface density of dsDNA ($\phi = 12\pi/17$) η_{D_2}	0.97 Å^{-2}
Attractive constant graphene-DNA A	42.6 eV Å^6
Repulsive constant graphene-DNA B	127500 eV Å^{12}

Table 5.3.1: Numerical values of constants used in this chapter (* denotes data from [2] and ** denotes data from [3]).

5.4 Interaction of ssDNA and dsDNA molecules with graphene sheet when helix axis is perpendicular to sheet

In this section, we examine the surface binding energy between ssDNA and dsDNA molecules interacting with graphene as shown in Fig. 5.4.1. Here the binding energy is defined as the potential energy between the bound DNA and the surface, assuming that the graphene configuration is infinite in extent and remains planar. The coordinate system is chosen as follows: the origin O is the intersection point between the line passing through to the center of the helix and perpendicular to the graphene surface. The xy-plane is assumed to coincide with the graphene surface and the z-axis is assumed to pass through the center of the helix. The coordinates of a typical point on the graphene sheet are given by $(x, y, 0)$. In the following subsections we present the interaction between the dsDNA molecule and the ssDNA molecule onto the graphene surface, respectively.

5.4.1 Interaction of dsDNA molecule and graphene sheet

With reference to the rectangular Cartesian coordinate system, a typical point on the surface of the dsDNA has coordinates

$$\mathbf{G}(\theta,t)=\Bigg(\frac{r}{2}\bigg[\cos\theta+\cos(\theta-\phi)+t\Big(\cos\theta-\cos(\theta-\phi)\Big)\bigg],\\ \frac{r}{2}\bigg[\sin\theta+\sin(\theta-\phi)+t\Big(\sin\theta-\sin(\theta-\phi)\Big)\bigg],\frac{c\theta}{2\pi}+\Delta\Bigg),$$

where r and c are the radius and the unit cell length of the dsDNA helix, respectively, ϕ is the helical phase angle and the parametric variables t and θ are such that $-1<t<1$ and $-\pi<\theta<\pi$. We assume that the dsDNA molecule above the graphene surface has its centre situated a distance Δ from the surface and we define a three-dimensional Cartesian coordinate system (x,y,z) with the point located at $(0,0,P)$. We may therefore calculate the binding energy from the following integral expression

$$\begin{aligned}E &= \frac{rc\sin(\phi/2)\eta_{D_i}\eta_g}{2\pi}\int_{-\infty}^{\infty}\int_{-\infty}^{\infty}\int_{-\pi}^{\pi}\int_{-1}^{1}\left(\frac{-A}{\rho^6}+\frac{B}{\rho^{12}}\right)\\ &\times \left(1+\frac{4r^2\pi^2\sin^2(\phi/2)}{c^2}t^2\right)^{1/2}dt\,d\theta\,dx\,dy,\end{aligned}$$

where $\rho^2=x^2+y^2+(c\theta/2\pi+\Delta)^2$, and η_g and η_{D_i} $(i\in\{1,2\})$ are the average atomic density on the dsDNA molecule and on graphene sheet, respectively, and from [81] we have the interaction between a point and a plane E_{pp} may give by

$$E_{pp}=\pi\left(\frac{-A}{2P^4}+\frac{B}{5P^{10}}\right), \tag{5.4.1}$$

where here $P = c\theta/2\pi + \Delta$, and we may write E as follows

$$E = \frac{rc\sin(\phi/2)\eta_{D_i}\eta_g}{\pi} F\left(\frac{-1}{2}, \frac{1}{2}; \frac{3}{2}; \frac{-4r^2\pi^2\sin^2(\phi/2)}{c^2}\right) \int_{-\pi}^{\pi} E_{pp} d\theta,$$

where $F(a_1, a_2; a_3; w)$ donates the usual hypergeometric function [82, §7.5], which is defined by

$$F(a_1, a_2; a_3; w) = \sum_{k=0}^{\infty} \frac{(a_1)_k (a_2)_k}{k!(a_3)_k} w^k,$$

and $(a_j)_k = a_j(a_j+1)(a_j+2)...(a_j+k-1)$ denotes the Pochhammer symbol, where $j \in \{1, 2, 3\}$. Thus, the total binding energy between the dsDNA molecule and graphene surface is given by

$$\begin{aligned} E &= 2r\pi\sin(\phi/2)\eta_{D_i}\eta_g F\left(\frac{-1}{2}, \frac{1}{2}; \frac{3}{2}; \frac{-4r^2\pi^2\sin^2(\phi/2)}{c^2}\right) \\ &\times \left(\frac{-A}{2} I_2 + \frac{B}{5} I_5\right), \end{aligned} \tag{5.4.2}$$

where I_n for $n = 2$ and 5 are defined by

$$I_n = (-2n+1)^{-1}\left[(c/2+\Delta)^{-2n+1} - (-c/2+\Delta)^{-2n+1}\right].$$

5.4.2 Interaction of ssDNA molecule and graphene sheet

Now, we determine the binding energy between an ssDNA and graphene sheet. Again, with reference to the rectangular Cartesian coordinate system, a typical point on the surface of the ssDNA has the coordinates

$$\mathbf{H}(\upsilon, t) = (bt\cos\upsilon, bt\sin\upsilon, c\upsilon/2\pi + \delta),$$

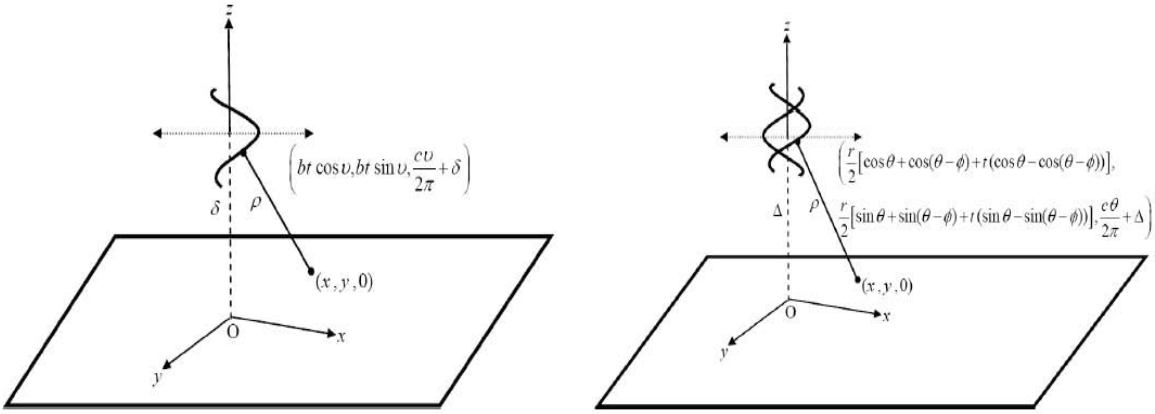


Figure 5.4.1: Interaction between ssDNA and dsDNA molecules with helix axis for the perpendicular to sheet

where b and c are the radius and the unit cell length of the ssDNA helix, respectively, and the parametric variables t and υ are such that $0 < t < 1$ and $-\pi < \upsilon < \pi$. Thus, the total binding energy between the ssDNA molecule and the graphene is given by

$$E = b\pi\eta_d\eta_g F\left(\frac{-1}{2}, \frac{1}{2}; \frac{3}{2}; \frac{-4b^2\pi^2}{c^2}\right)\left(\frac{-A}{2}J_2 + \frac{B}{5}J_5\right), \tag{5.4.3}$$

where J_n for $n = 2$ and 5 are defined by

$$J_n = (-2n+1)^{-1}\left[(c/2+\delta)^{-2n+1} - (-c/2+\delta)^{-2n+1}\right].$$

Using the algebraic computer package MAPLE together with the parameter values given in Table 5.3.1, we show in Fig. 5.4.2 the variation of the binding energies with equilibrium distances for single-strand and double-strand DNA molecules interacting with graphene sheet for the case when the helix axis is perpendicular to the graphene surface. Thus, Fig. 5.4.2 shows the relation between the potential energy and the equilibrium distance as measured from the center of the helix. Our results

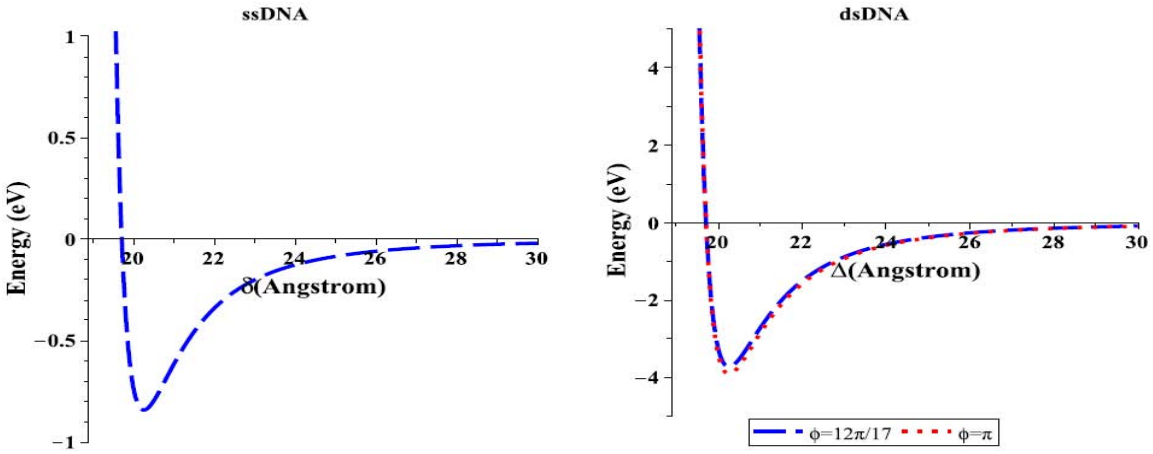


Figure 5.4.2: Total potential energy when axis of DNA helix is perpendicular to graphene sheet

show that the equilibrium location for the ssDNA and dsDNA molecules to the graphene surface are 20.2 and 20.3 Å with a corresponding energy of 0.86 and 3.85 eV, respectively. In addition, The distance from the edge of the double-strand and single-strand molecules to the graphene surface are approximately 3.3 Å and 3.2 Å, respectively.

5.5 Interaction of ssDNA and dsDNA molecules with graphene sheet when helix axis is parallel to sheet

In this section, we consider the binding energy of a single-strand and double-strand DNA molecules with graphene sheet. With reference to Fig. 5.5.1, we assume that the helix axis of the single-strand and double-strand DNA molecules lie on axis in the xy-plane which are parallel to the graphene surface. We begin by considering the interaction of a single atom with the graphene sheet, we denote this point by

the coordinates $(0, 0, P)$ without loss of generality, and assuming that the graphene configuration is infinite in extent with the coordinates $(x, y, 0)$.

5.5.1 Interaction of dsDNA molecule and graphene sheet

With reference to the rectangular Cartesian coordinate system, a typical point on the surface of the dsDNA molecule has coordinates

$$\mathbf{G}(\theta, t) = \left(\frac{c\theta}{2\pi}, \frac{r}{2}\Big[\sin\theta + \sin(\theta - \phi) + t\Big(\sin\theta - \sin(\theta - \phi)\Big)\Big], \right.$$
$$\left. \frac{r}{2}\Big[\cos\theta + \cos(\theta - \phi) + t\Big(\cos\theta - \cos(\theta - \phi)\Big)\Big] + \Delta \right).$$

Using the interaction energy of point with plane which is given by equation (5.4.1), where here P is given by

$$P = \frac{r}{2}\Big[\cos\theta + \cos(\theta - \phi) + t\Big(\cos\theta - \cos(\theta - \phi)\Big)\Big] + \Delta.$$

Thus the total potential energy of the dsDNA molecule interacting with the graphene sheet E can be shown to be given by

$$E = \frac{rc\sin(\phi/2)\eta_{D_i}\eta_g}{2}\left(\frac{-A}{2} I_2^* + \frac{B}{5} I_5^* \right), \tag{5.5.1}$$

and the details for the analytical evaluation of I_n^* are presented in Appendix D.1.

5.5.2 Interaction of ssDNA molecule and graphene sheet

Again, with reference to the rectangular Cartesian coordinate system, a typical point on the surface of the ssDNA molecule has coordinates

$$\mathbf{H}(\upsilon, t) = \left(c\upsilon/2\pi, bt\sin\upsilon, bt\cos\upsilon + \delta \right).$$

Using the interaction energy of point with plane which is given by equation (5.4.1), where here

$$P = bt\cos\upsilon + \delta,$$

and the total potential energy of the ssDNA molecule intracting with the graphene sheet E can be shown to be given by

$$E = \frac{bc\eta_d\eta_g}{2}\left(\frac{-A}{2}J_2^* + \frac{B}{5}J_5^*\right),$$

where

$$\begin{aligned} J_n^* &= \sum_{\gamma=0}^{\infty}\sum_{\mu=0}^{\infty}\binom{-2n-\gamma}{\mu}\frac{(2n)_\gamma(1/2)_\gamma 2^\gamma r^{\gamma+\mu}\delta^{-2n-\gamma-\mu}}{(\gamma!)^2(\gamma+2\mu+1)} \\ &\times F\left(\frac{-1}{2}, \gamma+\mu+\frac{1}{2}; \gamma+\mu+\frac{3}{2}; \frac{-4b^2\pi^2}{c^2}\right), \end{aligned}$$

and $\binom{d}{v} = d!/v!(d-v)!$ is the binomial coefficient.

In Fig. 5.5.2, we plot the potential energy E with respect to the distance from the graphene sheet, either δ and Δ for the single-stranded or double-stranded DNA molecules, respectively. As shown in Fig. 5.5.2, the preferred location of the ssDNA molecule is 8.3 Å ($\delta = 8.3$ Å) above the surface of the graphene, and the preferred location of the dsDNA molecule to be 13.3 Å ($\Delta = 13.3$ Å) above the surface of the graphene.

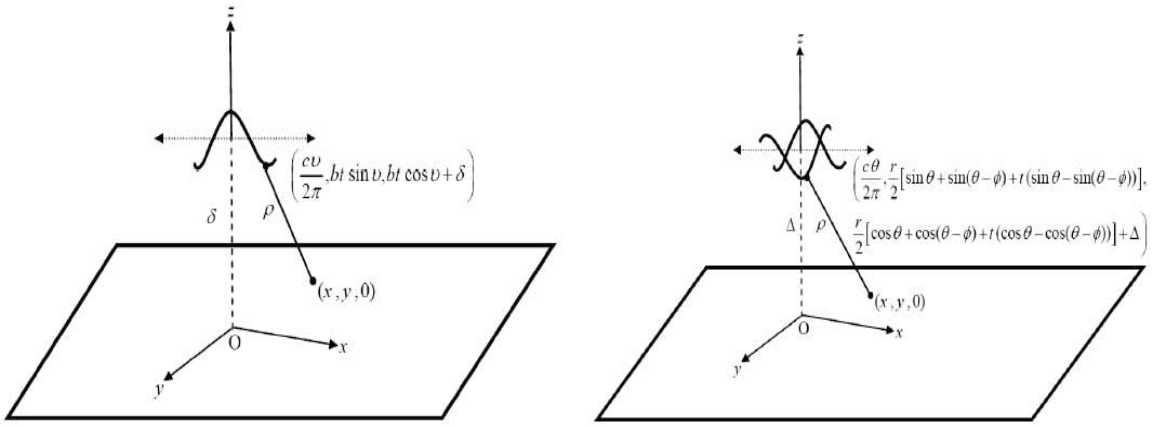


Figure 5.5.1: Interaction between ssDNA and dsDNA molecules with helix axis parallel to sheet

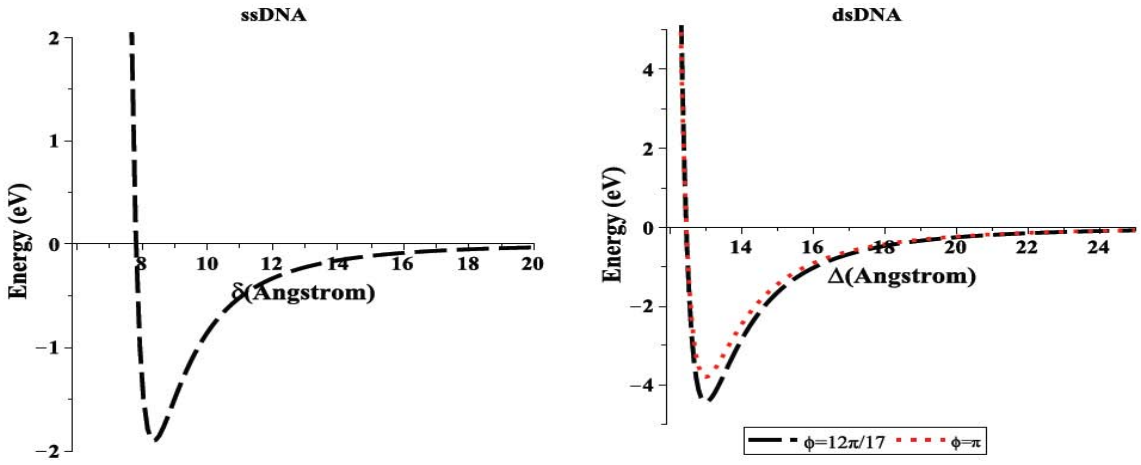


Figure 5.5.2: Total potential energy of DNA molecule when helix axis is parallel to graphene sheet

5.6 Interaction of ssDNA and dsDNA molecules with graphene sheet for different helix axis orientations

In this section, we determine the optimal orientation of the DNA molecule with respect to the graphene sheet by minimising the interaction energy. In the case of the dsDNA molecule, we assume that the helical phase angle ϕ is equal to π ($\phi = \pi$). With reference to Fig. 5.6.1, a typical point on the surface of the dsDNA molecule has coordinates

$$\mathbf{G}(\theta, t) = (rt\cos\theta, rtsin\theta\cos\Omega - (c\theta/2\pi)\sin\Omega, (c\theta/2\pi)\cos\Omega + rt\sin\theta\sin\Omega)\,.$$

In addition, a typical point on the surface of the ssDNA molecule has coordinates

$$\mathbf{H}(\upsilon, t) = (rb\cos\upsilon, rb\sin\upsilon\cos\Omega - (c\upsilon/2\pi)\sin\Omega, (c\upsilon/2\pi)\cos\Omega + rb\sin\upsilon\sin\Omega)\,,$$

and we assume that the graphene configuration is infinite in extent with coordinates $(x, y, -Z_0)$. By following the same steps as in sections 5.2 and 5.3, we may deduce that the total binding energy between the single-strand and double-strand DNA molecules and the graphene is given by

$$E = \frac{\chi c\eta_\kappa\eta_g}{2\pi}\int_{-\pi}^{\pi}\int_{\varrho}^{1} E_{pp}\left(1 + \frac{4\chi^2\pi^2}{c^2}t^2\right)^{1/2} dt\, d\xi, \tag{5.6.1}$$

where E_{pp} is given by (5.4.1) and P is defined by

$$P = (c\xi/2\pi)\cos\Omega + \chi t\sin\xi\sin\Omega + Z_0,$$

where for the dsDNA molecule $\chi = r$, $\kappa = D_1$, $\varrho = -1$ and $\xi = \theta$, and for the ssDNA molecule $\chi = b$, $\kappa = d$, $\varrho = 0$ and $\xi = \upsilon$. Thus the total potential energy of the DNA molecule interacting with the graphene sheet E, is given by

$$E = \frac{\chi c \eta_\kappa \eta_g}{2} \left(\frac{-A}{2} Y_2 + \frac{B}{5} Y_5 \right), \tag{5.6.2}$$

and we show the derivation of the analytical expressions for Y_n in Appendix D.2.

In Fig. 5.6.2 and Table 5.6.1, we use the algbraic computer package MAPLE to evaluate (5.6.1), and plot the relation between the potential energy and the distance Z_0 for a single-strand and double-strand DNA molecules above the graphene sheet for different values of the rotational angle Ω, where we use the units of radians for the rotational angle. Also, we note that $\Omega = 0$ indicates that the axis of the helix is perpendicular to the graphene surface, and $\Omega = \pi/2$ indicates that the axis of the helix is parallel to the plane. For the dsDNA molecule the minimum energy is obtained when $\Omega \in (0.44, 0.62)$, indicating that the dsDNA molecule remains more or less perpendicular to the graphene. In addition, the minimum energy for the ssDNA molecule occurs when $\Omega \in (0.79, 1.57)$. Our results are in close agreement with the results obtained in [54, 55].

Moreover, Fig. 5.6.3 shows the binding energies for both dsDNA and ssDNA molecules interacting with the graphene sheet for different lengths of DNA. In Fig. 5.6.3 (a), we show the binding energies as a function of S where $0 < \xi < S\pi$, for single-strand and double-strand DNA molecules interacting with graphene sheet for the case when the helix axis of the DNA molecule is perpendicular to the sheet (i.e. $\Omega = 0$). We observe that after the first single turn of the DNA molecule (i.e. $S = 2$), the values of the energies are approximately unchanged, that is because the major contribution to the interaction occurs between the atoms of the DNA molecule which are closest to the graphene sheet, and the effect of the other atoms further from the surface, is negligible. In addition, in Fig. 5.6.3 (b), we show the binding energies

for single-strand and double-strand DNA molecules interacting with graphene sheet for the case when the helical axis of the DNA molecule is parallel to the graphene surface (i.e. $\Omega = \pi/2$) as a function of S where $0 < \xi < 2S\pi$. We observe that for both ssDNA and dsDNA molecules, the binding energies are equal to (SE_f), where E_f is the total energy of the interaction between a single turn of the DNA molecule and a graphene sheet, which means that the binding energy of the interaction of the DNA molecule and a graphene sheet increases as the length of the DNA molecule increases.

Ω (rad)	ssDNA		dsDNA	
	Z_0(Å)	E (eV)	Z_0(Å)	E (eV)
0	20.3	-0.84	20.3	-3.9
$\pi/16$	19.9	-0.94	19 .9	-4.07
$\pi/8$	19	-1.12	19.8	-4.90
$3\pi/16$	17.5	-1.43	17.8	-5.7
$\pi/4$	15.4	-1.93	17.1	-4.2
$5\pi/16$	13.4	-2.30	16.6	-2.9
$3\pi/8$	11.7	-2.05	15.7	-2.4
$7\pi/16$	10	-1.82	14.5	-3.39
$\pi/2$	8.4	-1.90	13	-3.80

Table 5.6.1: Interaction energy for different values of the rotational angle Ω.

5.7 Conclusions

In this chapter we present an applied mathematical model for the interaction energy between both single-strand and double-strand DNA molecules and a graphene sheet. We employ the 6-12 Lennard-Jones potential together with the continuum approximation to calculate the van der Waals interaction energy, which may be expressed in terms of the hypergeometric function, to determine the surface binding energies between an ssDNA molecule and dsDNA molecule interacting with a graphene sheet. The binding energy for the DNA-graphene system is derived as a function of the

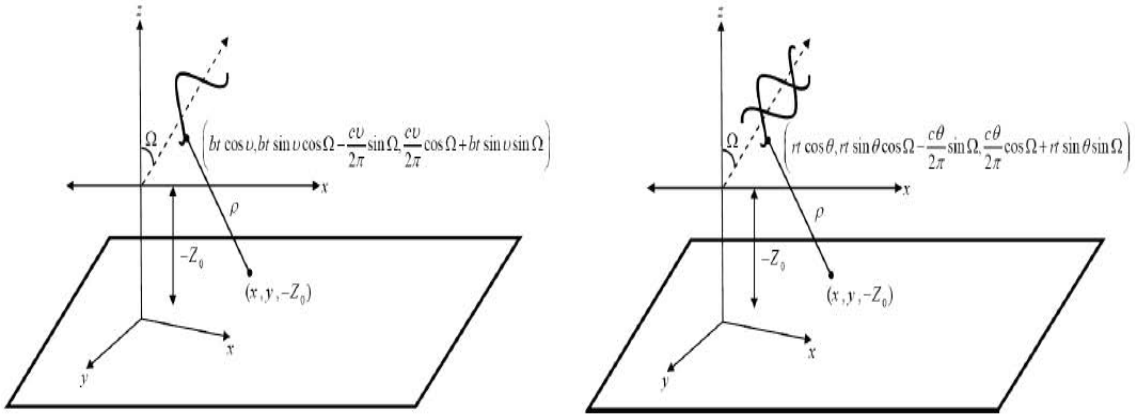


Figure 5.6.1: Interaction between ssDNA and dsDNA molecules with graphene sheet for arbitrary helix axis inclination.

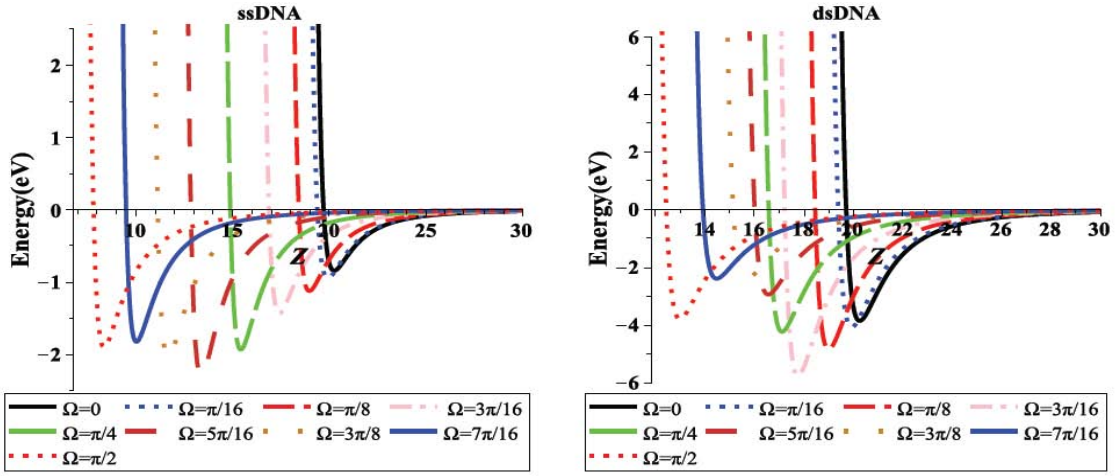


Figure 5.6.2: Total potential energy of the DNA molecule with graphene sheet for different values of the rotational angle Ω.

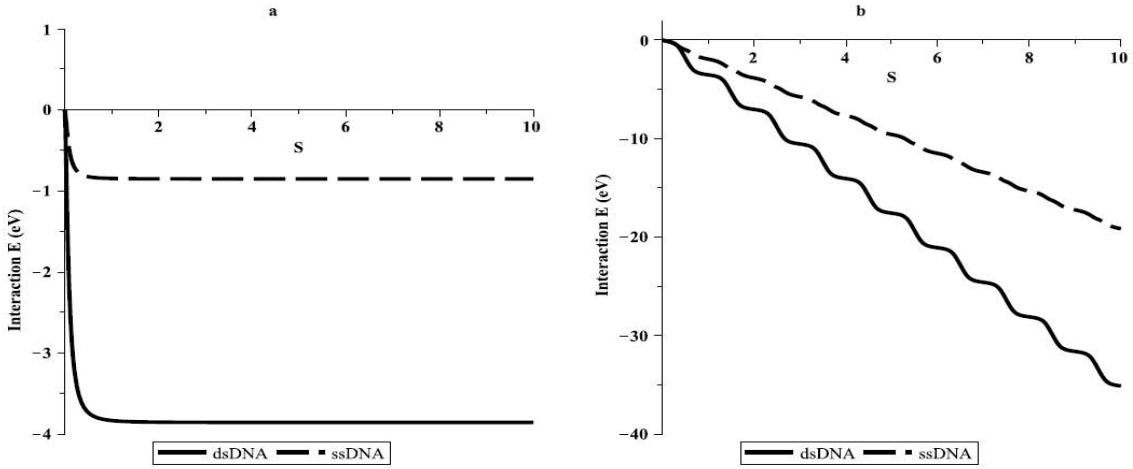


Figure 5.6.3: Interaction between the DNA molecule for helix axis (a) perpendicular (b) parallel to graphene sheet for different lengths of DNA.

distance from the centre of the DNA molecule and the graphene surface, and we refer to the location where the potential energy adopts a minimum value as the preferred optimal location. The numerical evaluations are performed using the algebraic computer package MAPLE. We determine the equilibrium distance of the DNA-graphene for two possible situations of the helix axis of the DNA molecule to the surface of graphene as shown in [54, 55], by minimizing their respective binding energies. Firstly, when the helical axis of both ssDNA and dsDNA molecules are perpendicular to the graphene surface, we observe that the binding energy for both ssDNA and dsDNA-graphene are minimized when the ssDNA and dsDNA molecules are centred 20.2 Å and 20.3 Å from the surface of the graphene, respectively. We comment that these close numerical values are almost the same because the major contribution to the interaction occurs between the atoms of the DNA molecule which are closest to the graphene sheet, and the effect of the other atoms further from the surface, very quickly becomes negligible. When the helical axis of the ssDNA and dsDNA molecules lie parallel to the graphene sheet, we show that the minimum values of the binding energies of both ssDNA and dsDNA molecules with the graphene

sheet, occur when the axis of the ssDNA and dsDNA molecules are 8.3 Å and 13.3 Å from the surface of the graphene, respectively. Moreover, by minimising the potential energies for arbitrary tilt angles we determine the most stable configuration of the single-strand and double-strand DNA molecules from the graphene sheet. For the ssDNA molecule, it occurs when the axis of the helix is almost parallel to the graphene surface, and for the dsDNA molecule, when the axis of the helix remains more or less perpendicular to the graphene. Our results for a single turn of the DNA molecule are in good agreement with those given in [54, 55]. For more than a single turn of the DNA molecule, we observe that for both single and double-strand DNA molecules, the parallel orientation shows a much stronger binding than does the perpendicular orientation. Graphene and DNA origami may be exploited to construct DNA-graphene nanobiosensors, and they may also serve as precursors for further studies in other fields of nanotechnology.

5.7.1 Nomenclature

Symbol	Meaning
$V(\rho)$	is the Lennard-Jones potential function for two unbonded atoms
E	is the interaction energy
E_{pp}	the interaction energy between a point and a plane
A	is the attractive Lennard-Jones constant
B	is the repulsive Lennard-Jones constant
η_1, η_2	are the atomic surface densities of the two interacting molecular structures
σ	is the equilibrium distance of two atoms
ε	is the depth of the potential well
ρ	is the distance between a typical surface elements on the plane and the DNA
ϕ	is the helical phase angle parameter
η_g	is the atomic surface density of the grapene sheet
η_d	is the atomic surface density of the ssDNA
η_{D_1}	is the atomic surface density of the dsDNA (for $\phi = \pi$)
η_{D_2}	is the atomic surface density of the dsDNA (for $\phi = 12\pi/17$)
r	is the radius of the dsDNA
b	is the radius of the ssDNA
c	is the unit cell length
δ	is the equilibrium distance between the axes of the ssDNA and the grapene
Δ	is the equilibrium distance between the axes of the dsDNA and the grapene
Z_0	is the distance for the DNA molecules above the graphene
$F(a, b; c; z)$	is the standard hypergeometric function
Ω	is the rotational angle of the helix axis
$(a_j)_k$	is the Pochhammer symbol

Chapter 6

C_{60} fullerene binding to DNA

6.1 Abstract

Fullerenes have attracted considerable attention in various areas of science and technology. Owing to their exceptional physical, chemical, and biological properties, they have many applications, particularly in cosmetic and medical products. Using the Lennard-Jones 6-12 potential function and the continuum approximation, which assumes that intermolecular interactions can be approximated by average atomic surface densities, we determine the binding energies of a C_{60} fullerene with respect to both single-strand and double-strand DNA molecules. We assume that all configurations are in a vacuum and that the C_{60} fullerene is initially at rest. Double integrals are performed to determine the interaction energy of the system. We find that the C_{60} fullerene binds to the double-strand DNA molecule, at either the major or minor grooves, with binding energies of -4.7 eV or -2.3 eV, respectively, and that the C_{60} molecule binds to the single-strand DNA molecule with a binding energy of -1.6 eV. Our results suggest that the C_{60} molecule is most likely to be linked to the major groove of the dsDNA molecule.

6.2 Introduction

Nowadays, nanoparticles are used in the industrial and manufacturing sectors, as well as in medicine for the purposes of imaging and diagnosis as well as for drug and gene delivery. This is due to their small size, unique mechanical, electronic, and geometric properties [17,34,62]. Nanomaterials include a wide variety of chemical structures such as fullerenes, nanotubes, nanopeapods, and carbon onions. Fullerenes are a class of carbon nanomaterials which may have many biomedical, electronic and semiconductor applications, and their discovery in 1985 [57] has made possible the creation of many future nanoscale devices. This is because of their unique mechanical properties arising from the van der Waals interaction force and their electronic properties arising from a large surface to volume ratio [58, 59].

Double-strand DNA (dsDNA) consists of two polynucleotide strands that are linked together by hydrogen bonds between complementary nucleotide bases and comprise five elements: carbon (C), oxygen (O), hydrogen (H), nitrogen (N), and phosphorus (P) [3]. In addition, double-strand DNA (dsDNA) is composed of two helices and has two grooves that are formed by the coiling of the helices around each other; the narrower one is called the minor groove, and the wider one is called the major groove [3]. The discovery of the geometric structure of DNA in 1954 [14] marked the beginning of a process that has transformed the foundations of biology and medicine, giving rise to the development of new fields such as molecular biology and genetic engineering.

The C_{60} fullerene is one of the most important nanocarriers for drug delivery, although the interactions between a C_{60} fullerenes and a DNA molecule are still not fully understood. Pang et al. [60] examine the interaction of the double-strand DNA molecule with the C_{60} molecule by developing a surface-based electrochemical method. They show that the C_{60} molecule interacts strongly with the major groove and the phosphate backbone that acts as the binding sites of the double-strand DNA

molecule. Zhao et al. [61] use molecular dynamics (MD) simulations to investigate the stability of complexes composed of single- and double-strand DNA molecules and C_{60} in aqueous solution. For the double-strand DNA (dsDNA) molecule, they find that the C_{60} binds to dsDNA, at either the hydrophobic ends or the minor groove of the nucleotide, but this binding does not affect the overall shape of the B form of the DNA molecule. For the single-strand DNA (ssDNA) molecule, they find that the C_{60} binds strongly with ssDNA and leads to deformation of the nucleotides. Xu et al. [62] use (MD) simulations and thermodynamic analysis to investigate the dynamic bindings of C_{60} fullerene with the dsDNA molecule, and they find that the C_{60} fullerene binds with the minor groove of the dsDNA molecule. Zhao [63] performs (MD) simulations to study the binding of the C_{60} molecule to the ssDNA molecule, and shows that the C_{60} fullerene can bind to the ssDNA and form energetically stable hybrids in a highly saline buffer solution, and gives a binding energy of about -47 kcal/mol (≈ -2.0 eV).

In this chapter, the binding of C_{60} to DNA molecules is investigated by adopting the continuum approximation for modelling nanostructures. This approach allows the interaction energy between large molecular structures such as DNA molecules to be determined analytically, and in a much simpler manner than through a computational approach, such as molecular dynamics simulations. We obtain an analytical expression for the interaction energy, which can then be readily computed using computer algebra packages such as Maple. In §6.2.1, we give the corresponding calculation for the special case of the interaction of a C_{60} fullerene with a dsDNA molecule when the helical phase angle has the particular value $\phi = \pi$. In §6.2.2, we give the corresponding calculation for the interaction of a C_{60} fullerene with a dsDNA molecule for any value of the helical phase angle ϕ. In §6.3, we present the details for the derivation of the total interaction energy for a C_{60} fullerene and the ssDNA molecule. Some brief conclusions are presented in §6.4.

6.3 Mathematical modelling

The continuum approximation and the Lennard-Jones potential function for unbonded molecules are employed here to determine the interaction energy of the system. The total interaction energy for two unbonded molecules is obtained by performing two surface integrals and is given by

$$E = \eta_1 \eta_2 \int_{S_1} \int_{S_2} \left(-\frac{A}{\rho^6} + \frac{B}{\rho^{12}} \right) dS_1 \, dS_2,$$

where η_1 and η_2 denote the atomic surface densities of the first and the second molecules, respectively, and A and B donate the Lennard-Jones parameters. These are related to the van der Waals, distance σ and the well-depth ε through the relations $\sigma = (B/A)^{1/6}$ and $\varepsilon = A^2/4B$. The numerical values of the various constants that are used throughout this chapter are listed in Tables 1.1.1 and 6.3.1 . In this chapter, we assume the B form of DNA, which is the structure commonly found inside cells [3, 11]. We model a double-strand DNA molecule as a surface with a double helical geometry, assuming that it consists of 10.5 base pairs for a 360° rotation in the double helix of the B-form DNA. Moreover, the single-strand DNA molecule is composed of 11 bases, which are assumed to have a single helical geometry. We remark that the assumption that the DNA retains its B form entails the assumption that there is sufficient water to solvate the backbone. This is a critical assumption, especially so when the C_{60} molecule is near the water surface, since the surface interactions can distort the DNA.

6.4 Interaction between C_{60} and dsDNA

In this section, we examine the surface binding energy of a C_{60} molecule interacting with a dsDNA molecule. We assume that the C_{60} fullerene is at a distance Δ from

Constant	Value
Radius of C_{60} fullerene a	3.55 Å
*Radius of ssDNA r	5.4 Å
**Radius of dsDNA R	10 Å
**Length of DNA c	34 Å
Mean surface density of C_{60} fullerene η_f	0.3812 Å^{-2}
Mean surface density of ssDNA η_d	0.83 Å^{-2}
Mean surface density of dsDNA ($\phi = \pi$) η_S	0.84 Å^{-2}
Mean surface density of dsDNA ($\phi = 12\pi/17$) η_D	0.97 Å^{-2}
Attractive constant C_{60} fullerene-DNA A	42.6 eV Å^6
Repulsive constant C_{60} fullerene-DNA B	127500 eV Å^{12}
***Attractive constant C_{60}-C_{60} A_{cc}	20 eV Å^6
***Repulsive constant C_{60}-C_{60} B_{cc}	34800 eV Å^{12}

Table 6.3.1: Numerical values of constants used in this chapter (* denotes data from [2], ** denotes data from [3] and *** denotes data from [4]).

the z-axis of the dsDNA molecule. With respect to the Cartesian coordinate system (x, y, z), the centre of the C_{60} molecule is assumed to have coordinates $(x, y, 0)$, where the coordinates x and y can be expressed in terms of a polar angle Ω and distance Δ in the radial direction; that is, $x = \Delta\cos\Omega$ and $y = \Delta\sin\Omega$. Similarly, with respect to the Cartesian coordinate system (x, y, z), a typical point on the surface of the dsDNA molecule has the coordinates

$$\left(\frac{R}{2}\left[\cos\Theta + \cos(\Theta-\phi) + t\Big(\cos\Theta - \cos(\Theta-\phi)\Big)\right], \frac{R}{2}\right.$$
$$\left.\left[\sin\Theta + \sin(\Theta-\phi) + t\Big(\sin\Theta - \sin(\Theta-\phi)\Big)\right], \frac{c\Theta}{2\pi}\right),$$

where $R = 10$ Å is the radius of the dsDNA helix, $c = 34$ Å is the unit cell length, ϕ is the helical phase angle, and the parametric variables t and Θ are such that $-1 < t < 1$ and $-\pi < \Theta < \pi$, as shown in Fig. 6.4.1. The distance ρ from the C_{60}

fullerene to any given point on the dsDNA molecule is therefore given by

$$\begin{aligned}\rho^2 &= \left(\frac{R}{2}\Big[\cos\Theta+\cos(\Theta-\phi)+t\Big(\cos\Theta-\cos(\Theta-\phi)\Big)\Big]-\Delta\cos\Omega\right)^2 \\ &+ \left(\frac{R}{2}\Big[\sin\Theta+\sin(\Theta-\phi)+t\Big(\sin\Theta-\sin(\Theta-\phi)\Big)\Big]-\Delta\sin\Omega\right)^2+\left(\frac{c\Theta}{2\pi}\right)^2.\end{aligned}$$

We first consider the molecular interaction energy between an atomic point and a double helix, which is given in [64] as

$$E_c = \frac{\pi a\eta_f}{\rho}\left\{\frac{A}{2}\left[\frac{1}{(a+\rho)^4}-\frac{1}{(a-\rho)^4}\right]-\frac{B}{5}\left[\frac{1}{(a+\rho)^{10}}-\frac{1}{(a-\rho)^{10}}\right]\right\}.$$

By expressing the fractions with common denominators, expanding, and reducing to fractions with denominators involving powers of (ρ^2-a^2), it can be shown that

$$\frac{1}{2\rho}\left[\frac{1}{(a+\rho)^4}-\frac{1}{(a-\rho)^4}\right]=-4a\left[\frac{1}{(\rho^2-a^2)^3}+\frac{2a^2}{(\rho^2-a^2)^4}\right],$$

and

$$\begin{aligned}\frac{1}{5\rho}\left[\frac{1}{(a+\rho)^{10}}-\frac{1}{(a-\rho)^{10}}\right] &= -\frac{4a}{5}\left[\frac{5}{(\rho^2-a^2)^6}+\frac{80a^2}{(\rho^2-a^2)^7}\right. \\ &\left.+\frac{336a^4}{(\rho^2-a^2)^8}+\frac{512a^6}{(\rho^2-a^2)^9}+\frac{256a^8}{(\rho^2-a^2)^{10}}\right].\end{aligned}$$

Thus, the total energy of interaction between the C_{60} fullerene and the dsDNA molecule is given by

$$E = \frac{Rc\eta_i\sin(\phi/2)}{2\pi}\int_{-\pi}^{\pi}\int_{-1}^{1}E_c\left(1+\frac{4R^2\pi^2\sin^2(\phi/2)}{c^2}t^2\right)^{1/2}dt\,d\Theta,$$

where $i\in\{S,D\}$. We first consider the interaction energy for the special helical phase angle $\phi=\pi$, and then we examine the general case of arbitrary helical phase

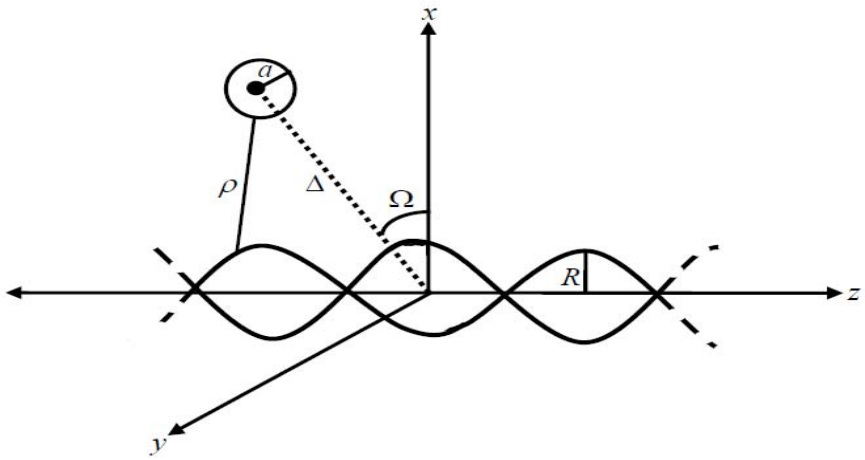


Figure 6.4.1: C_{60} fullerene binding to dsDNA molecule

angle ϕ.

6.4.1 Interaction of C_{60} and dsDNA for $\phi = \pi$

In this section, we consider the special case of the helical angle ϕ equal to π, so that

$$\begin{aligned} \rho^2 &= (Rt)^2 - 2Rt\Delta\cos(\Theta-\Omega) + \Delta^2 + (c\Theta/2\pi)^2 \\ &= (Rt-\Delta)^2 + 4Rt\Delta\sin^2(\Theta-\Omega/2) + (c\Theta/2\pi)^2\,, \end{aligned}$$

and the total interaction energy between the C_{60} fullerene and the dsDNA molecule is given by

$$E = \frac{Rc\eta_S}{2\pi}\int_{-\pi}^{\pi}\int_{-1}^{1} E_c\left(1+\frac{4R^2\pi^2}{c^2}t^2\right)^{1/2} dt\,d\Theta. \qquad (6.4.1)$$

The details of the analytical evaluation of equation (6.4.1) are presented in Appendix E. The numerical evaluation of equation (6.4.1) is readily obtained using the computer algebra package Maple together with the parameter values in Table 6.3.1. Fig. 6.4.2 shows the total interaction energy for the C_{60} fullerene and the dsDNA

molecule as a function of the distance Δ for $\phi = \pi$ and $\Omega \in [0, 2\pi]$. In addition, Fig. 6.4.3 shows the total interaction energy for the C_{60} fullerene and the dsDNA molecule as a function of the rotational angle Ω for $\phi = \pi$ and different values of Δ. The computational results indicate that the minimum interaction energy is obtained at $\Delta \approx 7.7$ Å and $\Omega = \pi/2$ or $\Omega = 3\pi/2$. In other words, the interaction energy is minimal for either of the parallel orientations. We note that in this case (i.e. for $\phi = \pi$), he major and minor grooves are of equal size (i.e. 17 Å). Fig. 6.4.4 shows a three-dimensional plot of the C_{60} fullerene binding to the dsDNA molecule for $\phi = \pi$ at $\Delta = 7.7$ Å and $\Omega = \pi/2, 3\pi/2$.

6.4.2 Interaction of C_{60} and dsDNA for $\phi = 12\pi/17$

In this section, we consider the case for the general helical angle ϕ, but we have in mind the case when the value of ϕ is equal to $12\pi/17$, which is the physical value of the helical angle ϕ that leads to the measured locations of the major and minor grooves. By minimising the interaction energy, we determine the binding energy of the C_{60} fullerene with respect to the major and minor grooves of the dsDNA molecule. Accordingly, the total interaction energy between the C_{60} fullerene and the dsDNA molecule is given by

$$E = \frac{Rc\eta_D \sin(\phi/2)}{2\pi} \int_{-\pi}^{\pi} \int_{-1}^{1} E_c \left(1 + \frac{4R^2\pi^2 \sin^2(\phi/2)}{c^2} t^2\right)^{1/2} dt\, d\Theta. \quad (6.4.2)$$

For the general helical angle, the evaluation of these integrals becomes extremely complicated and we therefore use a standard integration packages such as Maple to provide some numerical results. The interaction energy between the C_{60} molecule and the dsDNA molecule is determined using the computer algebra package Maple together with equation (6.4.2) and the parameter values in Table 6.3.1. Fig. 6.4.5 shows the total interaction energy for the C_{60} fullerene and the dsDNA molecule as

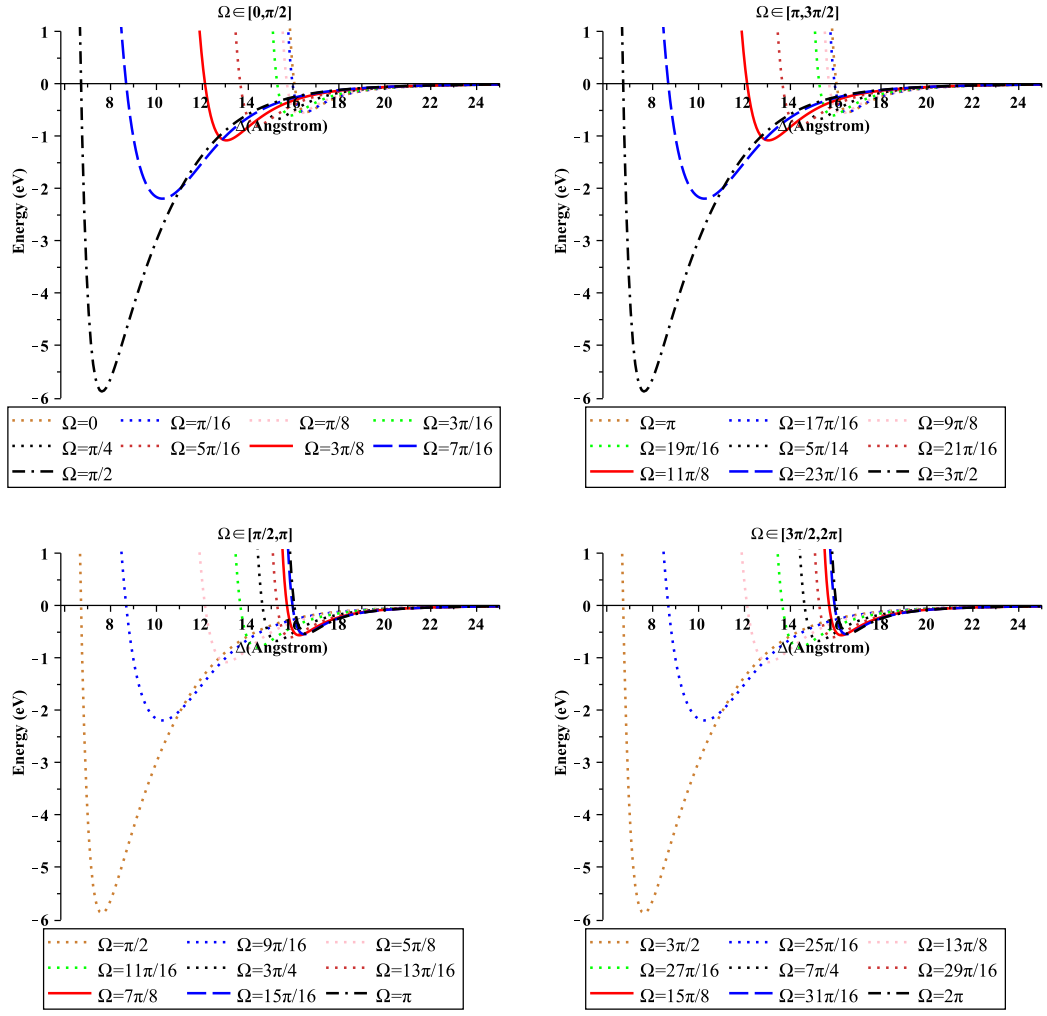


Figure 6.4.2: Energy profile of C_{60} binding to dsDNA with respect to distance Δ for $\phi = \pi$

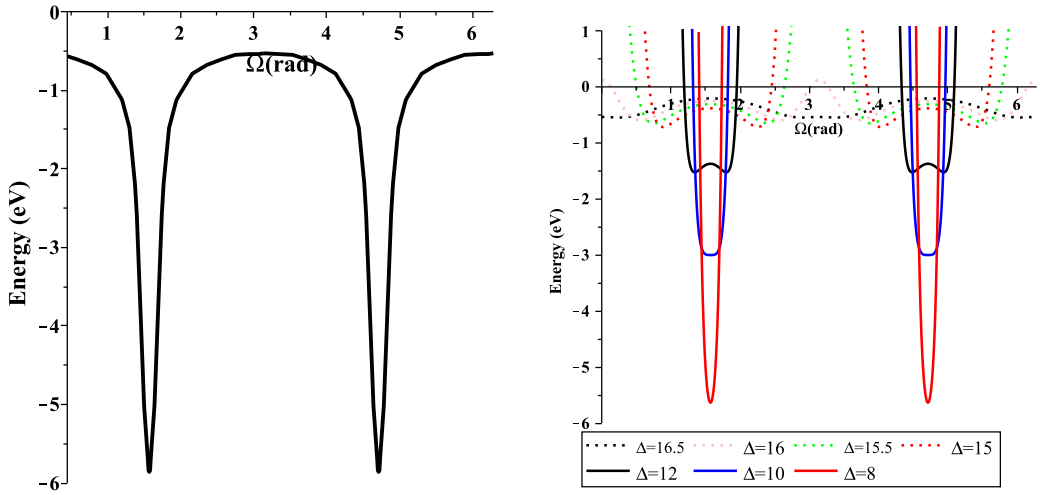


Figure 6.4.3: Energy profile of C_{60} binding to dsDNA molecule with respect to rotational angle Ω for $\phi = \pi$

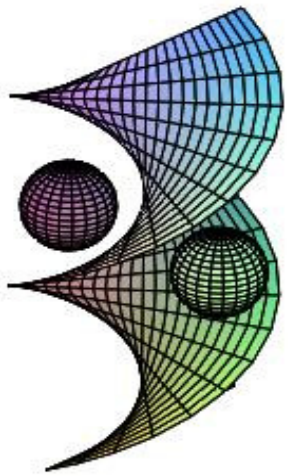


Figure 6.4.4: 3D plot of C_{60} binding to dsDNA at $\Omega = \pi/2, 3\pi/2$ and $\Delta = 7.7$ Å for $\phi = \pi$

a function of the distance Δ for $\phi = 12\pi/17$ and $\Omega \in [0, 2\pi]$. In addition, Fig. 6.4.6 shows the total interaction energy for the C_{60} fullerene and the dsDNA molecule as a function of the rotational angle Ω for $\phi = 12\pi/17$ and different values of Δ. In this case, we observe that the C_{60} fullerene interacts strongly with the major groove of the dsDNA molecule. The interaction thus depends on the rotational angle Ω, which lies in the range $(0, \pi)$ for the major groove and $(\pi, 2\pi)$ for the minor groove. As shown in Fig. 6.4.6, the minimum interaction energy between the C_{60} fullerene and the dsDNA molecule occurs for $\Omega = 2.01$ rad. These results are in good agreement with those given in [60], which showed that the C_{60} molecule can interact strongly with the major groove and phosphate backbone that act as the binding sites of the dsDNA molecule. Fig. 6.4.5 shows that the optimal distance Δ from the z-axis of the dsDNA molecule to the centre of the C_{60} molecule is approximately 2.4 Å for the major groove and 14.5 Å for the minor groove. In addition, Fig. 6.4.6 shows that the minimum interaction energies for the major and minor grooves are obtained at $\Omega \approx 2.1$ rad, located in the region of the major groove and $\Omega \approx 5.4$ rad, located in the region of the minor groove. Fig. 6.4.7 shows a three-dimensional plot of the C_{60} fullerene binding to the dsDNA molecule at these values of Ω and Δ for $\phi = 12\pi/17$.

6.5 Interaction of C_{60} and ssDNA

6.5.1 Binding energy of C_{60} fullerene to ssDNA

In this section, we consider the binding energy of the C_{60} fullerene with respect to an ssDNA molecule, assuming that the C_{60} fullerene is a distance δ from the z-axis of the ssDNA molecule, as shown in Fig. 6.5.1. With reference to the same Cartesian coordinates, we locate the centre of the C_{60} fullerene at $(\delta\cos\Omega, \delta\sin\Omega, 0)$ and the ssDNA molecule at $(rt\cos\theta + \delta, rt\sin\theta, c\theta/2\pi)$, where r and c are the radius and

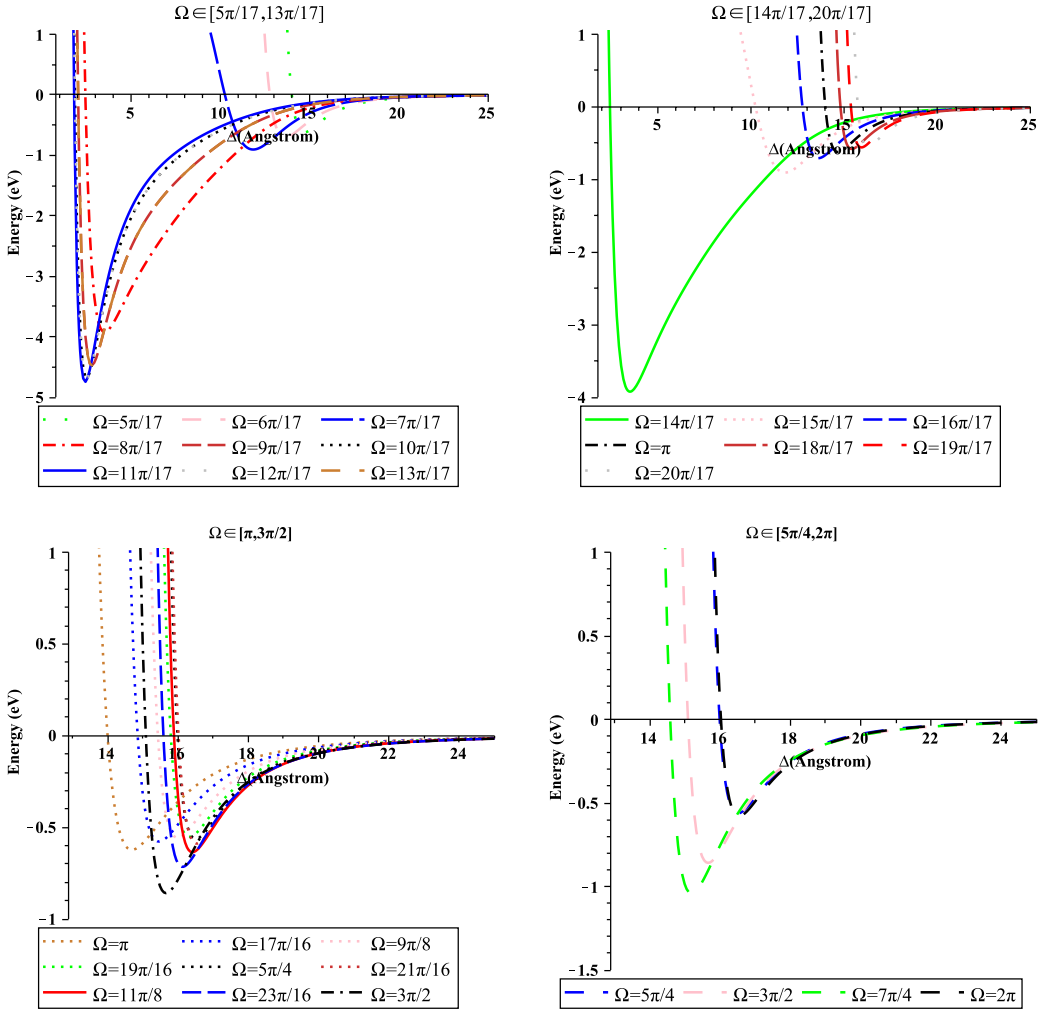


Figure 6.4.5: Energy profile of C_{60} binding to dsDNA with respect to distance Δ for $\phi = 12\pi/17$

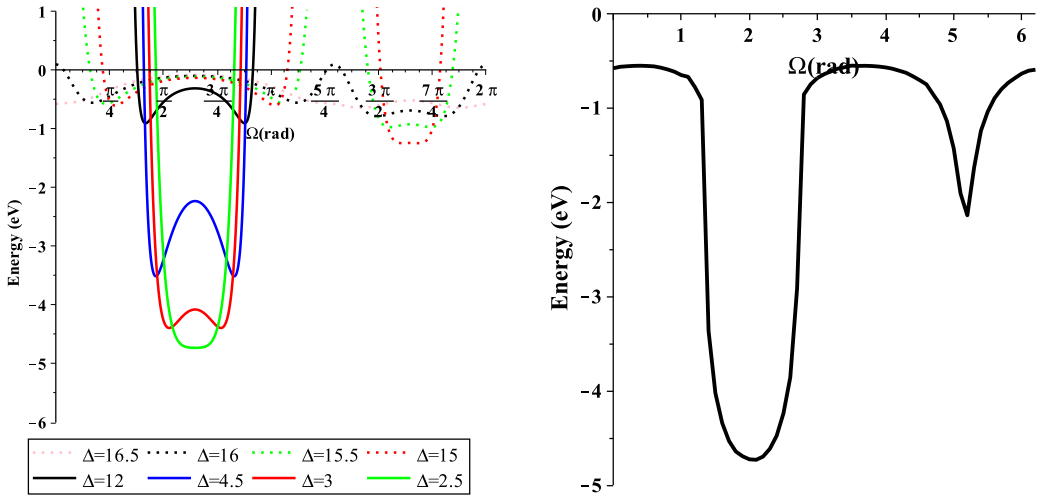


Figure 6.4.6: Energy profile of C_{60} binding to dsDNA with respect to rotational angle Ω for $\phi = 12\pi/17$

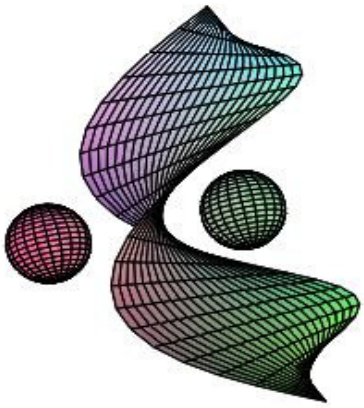


Figure 6.4.7: 3D plot of C_{60} binding to dsDNA at $\Omega = 2.1, 5.4$ rad and $\Delta = 2.4, 14.5$ Å for $\phi = 12\pi/17$

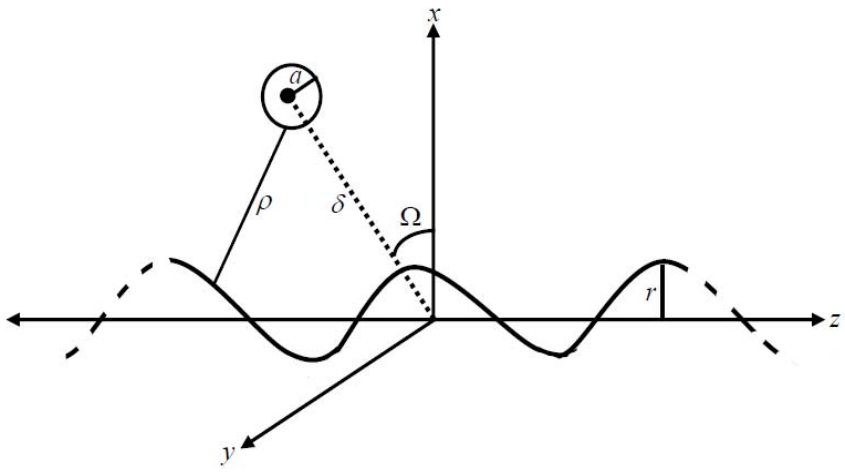


Figure 6.5.1: C_{60} fullerene binding to ssDNA molecule.

unit cell length of the ssDNA helix, respectively, and the parametric variables t and θ are such that $0 < t < 1$ and $-\pi < \theta < \pi$. Thus, the distance ρ from the C_{60} fullerene to any given point on the ssDNA molecule is given by

$$\rho^2 = (rt - \delta)^2 + 4rt\delta \sin^2(\theta - \Omega/2) + (c\theta/2\pi)^2 \,,$$

and the total interaction energy between the C_{60} fullerene and the ssDNA molecule is given by

$$E = \frac{rc\eta_d}{2\pi} \int_{-\pi}^{\pi} \int_0^1 E_c \left(1 + \frac{4r^2\pi^2}{c^2} t^2\right)^{1/2} dt\, d\theta. \tag{6.5.1}$$

To evaluate equation (6.5.1) analytically, we can follow the steps which are shown in the appendix E.1 to evaluate equation (6.4.1). The numerical evaluation for equation (6.5.1) is readily obtained using the computer algebra package Maple together with the parameter values as given in Tables 1.1.1 and 6.3.1. Fig. 6.5.2 and Fig. 6.5.3 show that the optimal distance δ from the z-axis of the ssDNA molecule to the centre of the C_{60} molecule is approximately 6.5 Å and the minimum interaction energy is obtained at $\Omega \approx \pi/2$ rad. Fig. 6.5.4 shows the binding of the C_{60} molecule to the

ssDNA in three dimensions. In other words, the orientation at which the interaction energy is minimum is the parallel orientation to the axis of the helix, and the lowest interaction energy is approximately -1.6 eV at $(\delta, \Omega) = (6.5, \pi/2)$. Fig. 6.5.4 shows the binding energy of the C_{60} molecule to the ssDNA in three dimensions, and these numerical results are in close agreement with to those given in [63]. Despite the fact that the binding between a ssDNA molecule and a C_{60} fullerene may in reality lead to deformation of the DNA due to the flexibility of the ssDNA molecule, our results serve as a first approximation and will help to predict optimal physical parameters for the binding of the ssDNA and C_{60} fullerene.

6.5.2 Interaction of fullerenes assuming helical configuration to axis of ssDNA

In this section, a helical configuration is assumed for N C_{60} fullerenes, which are located around the axis of the ssDNA helix, as shown in Fig. 6.5.5. We determine the angular spacing Φ by minimizing the energy the system. With reference to a rectangular Cartesian coordinate system (x, y, z) with the origin located at the centre of the left most C_{60} molecule, the centres of the C_{60} fullerenes have coordinates $(-\delta\cos(N\Phi), -\delta\sin(N\Phi), cN\Phi/2\pi)$. With reference to Fig. 6.5.5, we assume that the total potential energy of the system comprises five types of interactions between the C_{60} fullerenes which are labelled as I, II, III, IV and V. From the previous section we determine the interaction energy between the ssDNA molecule and a C_{60} fullerene, and we find that the distance δ from the z-axis of the ssDNA molecule to the centre of the C_{60} molecule is approximately 6.5 Å. Thus, the total interaction energy is given by

$$\begin{aligned} E_{cc} &= (N-1)E^*(M_1) + (N-2)E^*(M_2) + (N-3)E^*(M_3) \\ &+ (N-4)E^*(M_4) + (N-5)E^*(M_5), \end{aligned}$$

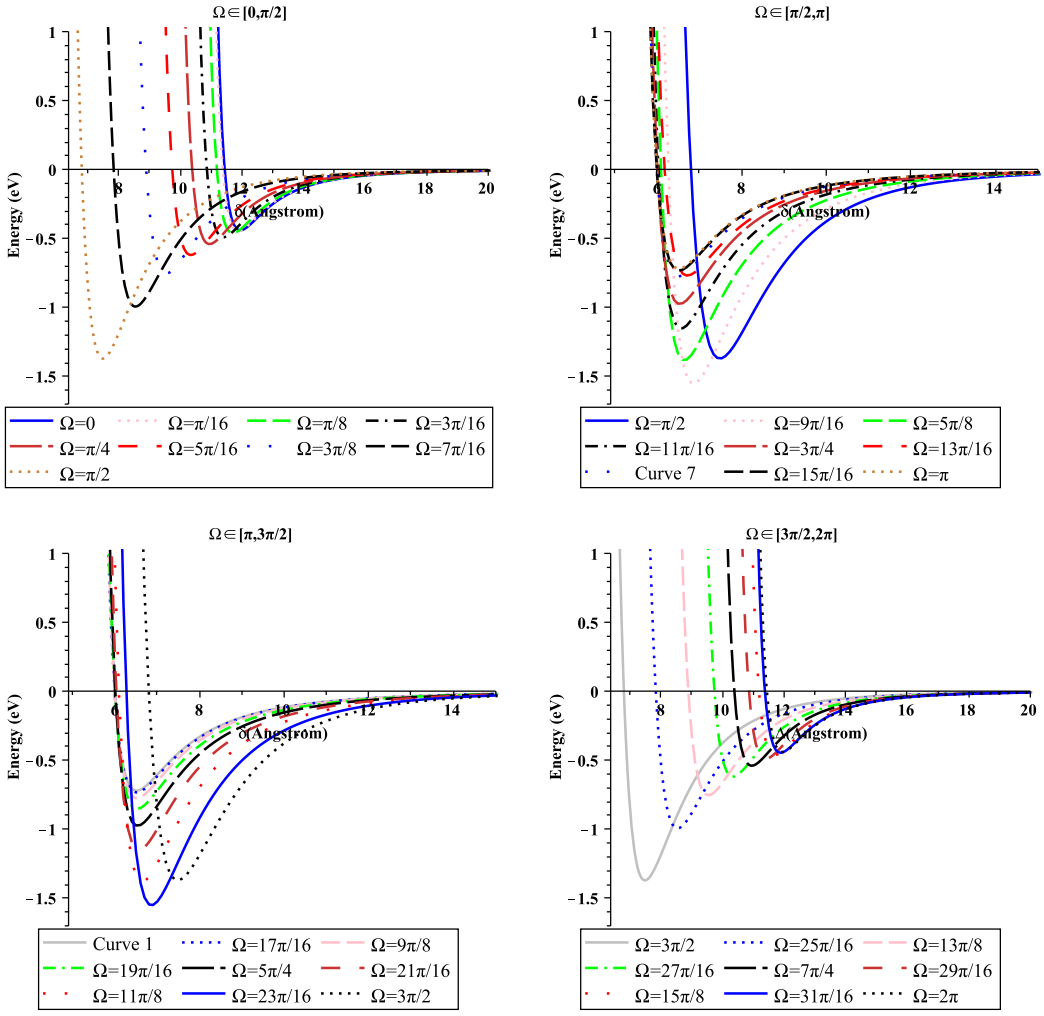


Figure 6.5.2: Energy profile of C_{60} binding to ssDNA with respect to distance δ

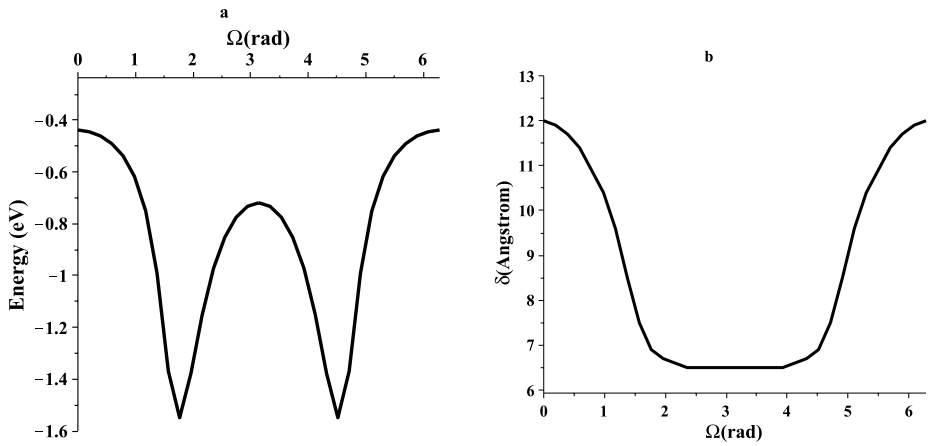


Figure 6.5.3: (a) energy profile for C_{60} binding to ssDNA with respect to rotational angle Ω, (b) relation between distances δ and tilting angle Ω

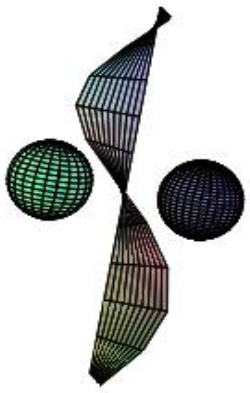


Figure 6.5.4: 3D plot of C_{60} binding to ssDNA at $\Omega = \pi/2, 3\pi/2$ rad and $\delta = 6.5$ Å

where $M_k (k = 1, 2, 3, 4, 5)$ are the distances between centres of C_{60} fullerenes as shown in Fig. 6.5.5 and

$$M_k^2 = 4\delta^2 \sin^2 (N\Phi/2) + (cN\Phi/2\pi)^2 .$$

The potential function $E^* (M_k)$ represents types I, II, III, IV and V interactions which are the potential energies between a pair of C_{60} fullerenes. We may determine $E^* (M_k)$ using the formula given in [67] for the potential energy between two spherical fullerenes, thus

$$E^* = -A_{cc} P_6 (M_k) + B_{cc} P_{12} (M_k) ,$$

where A_{cc} and B_{cc} represent the Lennard-Jones potential constants for a pair of C_{60} fullerenes, respectively, and P_l is defined by

$$P_l = \frac{4\pi^2 a^2 \eta_f^2}{M (2-l)(3-l)} \left(\frac{1}{(2a+M)^{l-3}} - \frac{1}{(2a-M)^{l-3}} + \frac{2}{M^{l-3}} \right) .$$

The energy minimization technique is employed here to determine the stable configurations of a helical chain of C_{60} fullerenes with respect to the axis of the ssDNA molecule. We assume that the system has N C_{60} molecules with five possible nearest neighbour interactions for two C_{60} molecules, and we already have the interaction between the ssDNA molecule and a C_{60} molecule which gives the offset distance δ= 6.5 Å. Again, using the algebraic computer package MAPLE and the parameter values in Tables 1.1.1 and 6.3.1, we obtain numerical values for the angular spacing Φ and the potential energy of the system $E_{cc}/N - 1$ for a pair of C_{60} fullerenes, which are shown in Table 6.5.1. We observe that the angular spacing Φ is approximately 1.23 radians. In addition, we may obtain the potential energies for the interaction types I, II, III, IV and V, which are $E^* (M_1) = -0.2796$, $E^* (M_2) = -0.003$,

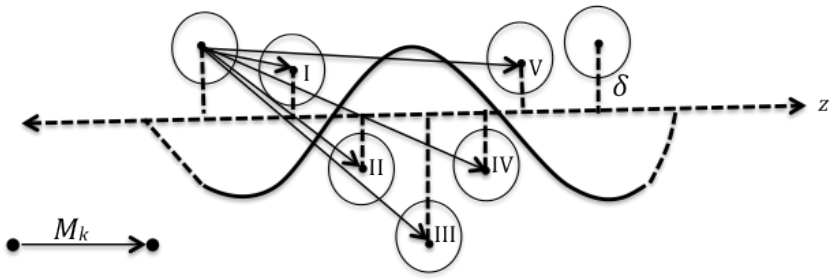


Figure 6.5.5: Helical configuration for N C_{60} fullerenes binding to ssDNA for $\delta = 6.5$ Å

$E^*(M_3) = -0.0005$, $E^*(M_4) = -0.0002$ and $E^*(M_5) = -0.00005$ (eV). Fig. 6.5.6 shows a three-dimensional plot of several C_{60} fullerenes binding to the ssDNA molecule at the values of $\Phi = 1.23$ radians and $\delta = 6.5$ Å in the helical configuration to the axis of the ssDNA molecule.

N	Φ	$E_{cc}/N - 1$ (eV)	N	Φ	$E_{cc}/N - 1$ (eV)
2	1.23359	-0.2796	20	1.23334	-0.2833
3	1.23348	-0.2812	30	1.23334	-0.2833
4	1.23343	-0.2818	40	1.23334	-0.2834
5	1.23341	-0.2823	50	1.23334	-0.2834
6	1.23339	-0.2825	65	1.23334	-0.2834
10	1.23336	-0.2830	80	1.23334	-0.2835
15	1.23335	-0.2831	100	1.23334	-0.2835

Table 6.5.1: Angular spacing Φ and energy of system $E_{cc}/N - 1$ (eV) for a pair of C_{60} fullerenes in helical configuration comprising N C_{60} molecules.

6.6 Conclusions

In this chapter, we use a classical modelling approach and demonstrate that an improved computational efficiency can be achieved using applied mathematical modelling to obtain an analytical expression for the interaction energy between a C_{60} molecule and a DNA molecule. We then use this result to describe the mechanism by which C_{60} molecules bind to ssDNA and dsDNA molecules, and the method

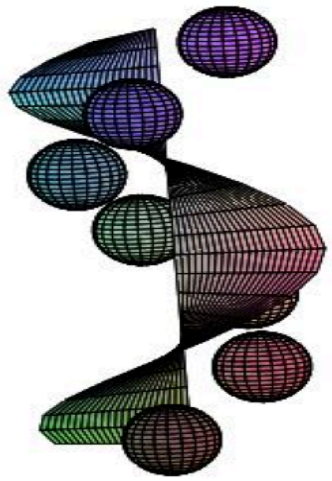


Figure 6.5.6: 3D plot of several C_{60} binding to ssDNA at $\Phi = 1.23$ rad and $\delta = 6.5$ Å.

adopted can be extended to investigate the interactions between more complicated molecules. By minimising the potential energies for arbitrary tilt angles and arbitrary distances from the helix axis of the DNA molecule to the centre of the C_{60} fullerene, we determine the binding energy of the C_{60} fullerene to the single-strand and double-strand DNA molecules. We show that the C_{60} fullerene binds to the major groove of the dsDNA, and that the results are in good agreement with those given in [60]. The C_{60} molecule binds to the ssDNA molecule with a binding energy of about -1.6 eV, and the results are in close agreement with those given in [61,63].

Here, we formulate a fundamental model of ideal behaviour as a first step in elucidating the principal behaviour of such systems. However, much work still remains to be done, particularly for the mobility of DNA and the interactions of DNA with other molecules such as water, which is often present in real physical systems.

6.6.1 Nomenclature

Symbol	Meaning
E	is the interaction energy
E_c	is the interaction energy for a point and a sphere
A	is the attractive Lennard-Jones constant
B	is the repulsive Lennard-Jones constant
η_1, η_2	are the atomic surface densities of the two interacting molecular structures
σ	is the equilibrium distance of two atoms
ε	is the depth of the the potential well
ρ	is the distance between a typical surface elements on the plane and the DNA
ϕ	is the helical phase angle parameter
η_f	is the atomic surface density of the C_{60} fullerene
η_d	is the atomic surface density of the ssDNA
η_S	is the atomic surface density of the dsDNA (for $\phi = \pi$)
η_D	is the atomic surface density of the dsDNA (for $\phi = 12\pi/17$)
R	is the radius of the dsDNA
r	is the radius of the ssDNA
c	is the unit cell length
δ	is the distance between the axes of the ssDNA and the C_{60} fullerene
Δ	is the distance between the axes of the dsDNA and the C_{60} fullerene
$F(a, b; c; z)$	is the standard hypergeometric function
Ω	is the rotational angle
Φ	is the angular spacing

Chapter 7

Summary

Nanotechnology is an emerging research area involving various disciplines. The combining of DNA with carbon nanostructures yields features that are important for researchers in chemistry, physics, biology, material sciences, engineering, and medicine. This thesis presents ideal applied mathematical models to determine the interaction energies between a DNA molecule and certain carbon nanostructures namely, carbon nanotubes, graphite, and C_{60} fullerene. We employ the 6-12 Lennard-Jones potential together with the continuum approximation to calculate the van der Waals interaction energy. The main objective of the applied mathematical approach adopted herein is to formulate a mathematical model that characterizes the dominant features of the interactions between DNA molecules and carbon nanostructures. Such mathematical modelling may generate deep insights into otherwise complex processes and often provides optimal parameters for special cases that may be otherwise time consuming or almost impossible to discern. Conventional nanostructures such as nanotubes, graphene and fullerenes can be modelled using the continuum approximation to formulate analytical expressions for their interactions, such as with DNA molecules. The continuum approximation assumes that molecular structures can be approximated using a constant average atomic surface densities,

obtained by assuming that the atoms are smeared over a surface. The work carried out for this thesis is summarized below.

In Chapter 2, we investigate the interaction energy between a dsDNA molecule and an SWCNT. We model the DNA molecule as a surface with a double helical geometry. The dsDNA molecule is assumed to be inside the tube, and we determine the radius of carbon nanotube that is necessary to enclose the double helix of the DNA. Then, the total interaction energy between the dsDNA molecule and the carbon nanotube is calculated for this model. We refer to the optimal or preferred location as the location where the potential energy attains a minimum value. The results in Chapter 2 indicate that the encapsulation of the dsDNA molecule in the SWCNT may occur for a carbon nanotube with radius greater than 12.30 Å. Moreover, the optimal radius of carbon nanotube to enclose the double helix of the DNA is approximately 12.8 Å, and we conclude that the optimal tube to encapsulate a dsDNA molecule is (19, 19).

In Chapter 3, we employ the 6-12 Lennard-Jones potential together with the continuum approximation to examine the suction behaviour for a ssDNA molecule entering a SWCNT, which is assumed to be semi-infinite in length, because of the short-range nature of the Lennard-Jones interaction. We determine the equilibrium position where the potential energy is minimum for the ssDNA inside the SWCNT, assuming a helical geometry for the ssDNA molecule. The numerical results show that the suction behaviour depends on the radius of the carbon nanotube, and it seems unlikely that an ssDNA molecule will be accepted into the SWCNT when the radius of the nanotube is less than 8.1 Å. Additionally, we examine the interaction energy of a ssDNA molecule inside the SWCNT for different tube sizes, assuming that the ssDNA molecule has already been accepted into the carbon nanotube. The results indicate that the encapsulation of the ssDNA molecule in the SWCNT may occur for a carbon nanotube with radius greater than 8.2 Å. Moreover, the

optimal radius of carbon nanotube to encapsulate the single helix of the DNA is approximately 8.8 Å, and so we conclude that the preferred armchair tube is (13, 13).

In Chapter 4, we investigate the equilibrium offset positions for both ssDNA and dsDNA molecules inside a SWCNT. The unit cell of the dsDNA molecule is assumed to comprise 10.5 base pairs that have a helical geometry. We further assume that the unit cell of the ssDNA molecule has a helical geometry and comprises 11 bases. Again we employ the 6-12 Lennard-Jones potential and the continuum approximation for the modelling and the assumption that the DNA has already been accepted into the SWCNT. The numerical results indicate that the equilibrium positions of the global minimum energy for the offset ssDNA and dsDNA tend to become closer to the tube wall as the radius of the tube increases.

In Chapter 5, the dsDNA is again assumed to consist of 10.5 base pairs, while the ssDNA is assumed to comprise 11 bases. Furthermore, both are assumed to have a helical geometry, and we consider a basic unit cell over a distance of 34 Å with a DNA molecule, and we investigate the interactions of ssDNA and dsDNA molecules with a graphene sheet. We derive analytical expressions for the binding energies between ssDNA or dsDNA molecules adsorbing onto a graphene surface. We then minimize the binding energies to determine the preferred locations of ssDNA and dsDNA molecules with respect to the graphene sheet. We determine the equilibrium DNA–graphene distance for two possible orientations of the helical axis of the DNA molecule with respect to the surface of the graphene. First, if the helical axis of the ssDNA or dsDNA molecule is perpendicular to the graphene surface, then we observe that the binding energy of the ssDNA–graphene or dsDNA–graphene is minimal when the ssDNA or dsDNA molecule is centred at 20.2 Å or 20.3 Å from the surface of the graphene, respectively. However, if the helical axis of the ssDNA or dsDNA molecule is parallel to the graphene sheet, then we observe that the minimum value

of the binding energy of the ssDNA or dsDNA molecule with the graphene sheet occurs when the axis of the ssDNA or dsDNA molecule is 8.3 Å or 13.3 Å from the surface of the graphene, respectively. Moreover, by minimizing the potential energy for an arbitrary tilt angle, we determine the most stable configuration of the ssDNA or dsDNA molecules with respect to the graphene sheet. For the ssDNA molecule, it occurs when the axis of the helix is almost parallel to the graphene surface, while for the dsDNA molecule, it occurs when the axis of the helix is almost perpendicular to the graphene surface. In addition, the results for more than a single turn of the DNA molecule show that for both ssDNA and dsDNA molecules the binding energy is much stronger in the parallel orientation than in the perpendicular orientation.

In Chapter 6, the binding of C_{60} molecules to DNA molecules is investigated, again by adopting the 6-12 Lennard-Jones potential and the continuum approximation for modelling nanostructures and we determine the interaction energy. The results obtained are used to describe the mechanism by which C_{60} molecules bind to ssDNA and dsDNA molecules. By minimizing the potential energies for arbitrary tilt angles and arbitrary distances from the helix axis of the DNA molecule to the centre of the C_{60} fullerene, we may determine the binding energy of the C_{60} fullerene to the ssDNA or dsDNA molecule. We show that the C_{60} fullerene binds to the major groove of the dsDNA. Moreover, the results show that the C_{60} molecule binds to the ssDNA molecule with a binding energy of about -1.6 eV.

The methods adopted in this thesis can be extended to investigate the interactions between more complicated molecules. Moreover, the formulated models describe ideal behaviour as a first step in elucidating the actual behaviour of such systems. The results show a good agreement with other methods such as molecular dynamics simulations and experiments. The studies have indicated that the DNA molecules could be encapsulated inside carbon nanotubes (see for example [2, 19, 34, 36, 39, 40, 42, 88]). Moreover, some experiments have predicted that

the ssDNA and dsDNA molecules can be absorbed on graphene sheet, they show that the dsDNA molecule can be rotated from a parallel orientation to a perpendicular orientation with respect to the graphene surface and the ssDNA molecule becomes parallel to the graphene surface (see for example [51–55]). The study of the C_{60} molecule binds to the DNA molecules can be used to complement the efforts of experimentalists and to confirm observed experimental outcomes (see for example [54, 60–63]). The major advantage of the approach adopted here is that the calculations can be readily obtained comparing to other methods. Much work still remains to be done on such models in terms of steadily improving the accuracy of the approach, especially with respect to DNA mobility and the interactions with other molecules, such as with water molecules, which are often present in real physical systems.

Appendix A

A.1 Analytical evaluation of (2.3.1)

In this appendix, we present the analytical evaluation of (2.3.1). By defining the integral R_n as

$$R_n = \int_0^1 \left(1 + \frac{4r^2\pi^2 \sin^2(\phi/2)}{c^2} t^2\right)^{1/2} F\left(\frac{2n-1}{2}, \frac{2n-1}{2}; 1; \left(\frac{\xi}{a}\right)^2\right) dt,$$

since

$$\xi^2 = r^2\left[\cos^2(\phi/2) + t^2 \sin^2(\phi/2)\right] = \left[r\cos(\phi/2)\right]^2\left[1 + t^2\tan^2(\phi/2)\right],$$

thus

$$\begin{aligned} R_n &= \int_0^1 \left(1 + \frac{4r^2\pi^2 \sin^2(\phi/2)}{c^2} t^2\right)^{1/2} \\ &\times F\left((2n-1)/2, (2n-1)/2; 1; \left[r\cos(\phi/2)/a\right]^2\left[1 + t^2\tan^2(\phi/2)\right]\right) dt, \end{aligned}$$

on making the substitution $x = t^2 \Rightarrow dt = (1/2)x^{-1/2}dx$, when $t = 0 \Rightarrow x = 0$, and when $t = 1 \Rightarrow x = 1$, and by letting $\alpha = \left[2r\pi\sin(\phi/2)/c\right]^2$. Thus, the integral R_n

becomes

$$\begin{aligned} R_n &= \frac{1}{2}\int_0^1 x^{-1/2}\left(1+\alpha x\right)^{1/2} \\ &\times F\left((2n-1)/2,(2n-1)/2;1;\left[r\cos(\phi/2)/a\right]^2\left[1+x\tan^2(\phi/2)\right]\right)\,dx, \end{aligned}$$

and on using the generalized hypergeometric series [90], we may deduce

$$\begin{aligned} R_n &= \frac{1}{2}\sum_{m=0}^{\infty}\left(\frac{\left(\left(2n-1\right)/2\right)_m r^m\cos^m(\phi/2)}{m!a^m}\right)^2 \\ &\times \int_0^1 x^{-1/2}\left(1+\alpha x\right)^{1/2}\left[1+x\tan^2(\phi/2)\right]^m\,dx. \end{aligned}$$

By taking

$$H_m=\int_0^1 x^{-1/2}\left(1+\alpha x\right)^{1/2}\left(1+\beta x\right)^m\,dx,$$

where $\alpha=\left[2r\pi\sin(\phi/2)/c\right]^2$ and $\beta=\tan^2(\phi/2)$, due to the positive power of the $(1+\beta x)^m$ terms, we may expand this as a binomial expansion to give

$$\left(1+\beta x\right)^m=\sum_{p=0}^{m}\binom{m}{p}\beta^p x^p,$$

where $\binom{i}{j}$ is the binomial coefficient. Thus the integral H_m becomes

$$H_m=\sum_{p=0}^{m}\binom{m}{p}\beta^p\int_0^1 x^{p-1/2}\left(1+\alpha x\right)^{1/2}\,dx,$$

by using form in [90] (p.59, Eq.10), thus

$$H_m=2\sum_{p=0}^{m}\binom{m}{p}\left[\beta^{2p}/(2p+1)\right]F(-1/2,p+1/2;p+3/2;-\alpha),$$

and we may deduce that R_n is given by

$$\begin{aligned} R_n &= \frac{1}{2}\sum_{m=0}^{\infty}\sum_{p=0}^{m}\binom{m}{p}\left[\beta^{2p}/(2p+1)\right]\left(\frac{\left((2n-1)/2\right)_m r^m\cos^m(\phi/2)}{m!a^m}\right)^2 \\ &\times F(-1/2,p+1/2;p+3/2;-\alpha), \end{aligned} \tag{A.1.1}$$

and this expression completes (2.3.2).

A.2 Analytical evaluation of (2.4.1)

In this appendix we evaluate (2.4.1), By defining the integral I_n as

$$I_n = \int_0^1 \left(1+\frac{4r^2\pi^2}{c^2}t^2\right)^{1/2} F\left(\frac{2n-1}{2},\frac{2n-1}{2};1;\left(\frac{\xi}{a}\right)^2\right)\,dt,$$

since $\xi = rt$, thus

$$I_n = \int_0^1 \left(1+\frac{4r^2\pi^2}{c^2}t^2\right)^{1/2} F\left((2n-1)/2,(2n-1)/2;1;(rt/a)^2\right)\,dt,$$

on making the substitution $y = t^2 \Rightarrow dt = (1/2)y^{-1/2}dy$, when $t = 0 \Rightarrow y = 0$, and when $t = 1 \Rightarrow y = 1$, and by letting $\alpha^* = (2r\pi/c)^2$. Thus, the integral I_n becomes

$$I_n = \frac{1}{2}\int_0^1 y^{-1/2}\left(1+\alpha^* y\right)^{1/2} F\left((2n-1)/2,(2n-1)/2;1;(r/a)^2\,y\right)\,dy,$$

using the generalized hypergeometric series [90], we may deduce

$$I_n = \frac{1}{2}\sum_{k=0}^{\infty}\left(\frac{\left((2n-1)/2\right)_k r^k}{k!a^k}\right)^2\int_0^1 y^{k-1/2}\left(1+\alpha^* y\right)^{1/2}\,dy,$$

by using form in [90] (p.59, Eq.10), thus

$$I_n = \sum_{k=0}^{\infty} \left(\frac{((2n-1)/2)_k \, r^k}{(2k+1)^{1/2} k! a^k} \right)^2 F\left(-1/2, k+1/2; k+3/2; -\alpha^*\right), \quad \text{(A.2.1)}$$

and this expression completes (2.4.1).

Appendix B

B.1 Analytical evaluation of (3.3.1)

In this appendix, we evaluate analytically the integrals T_n which is defined in (3.3.1). By defining the integral J_n

$$J_n = \int_0^\infty \left[\alpha + (z - Z)^2\right]^{-n} dz,$$

where $\alpha = (a - rt)^2 + 4art\sin^2(\theta_2/2)$ and $Z = Z_0 + c\theta_1/2\pi$, and by making the change of variable $x = z - Z$ which gives

$$\begin{aligned} J_n &= \int_{-Z}^0 \left[\alpha + x^2\right]^{-n} dx + \int_0^\infty \left[\alpha + x^2\right]^{-n} dx, \\ &= J_{n,1} + J_{n,2}. \end{aligned}$$

For evaluating $J_{n,1}$ we let $y = (x/Z)^2$, thus

$$J_{n,1} = -(1/2)Z\alpha^{-n} \int_0^1 y^{-1/2} \left[1 + \left(Z^2/\alpha\right) y\right]^{-n} dy,$$

using the definition of the hypergeometric function [82, §7.5], thus

$$J_{n,1} = -Z\alpha^{-n} F\left(n, 1/2; 3/2; -Z^2/\alpha\right),$$

using the generalized hypergeometric series [90], we may deduce

$$J_{n,1} = -\sum_{i=0}^{\infty} \frac{(n)_i (1/2)_i}{i!(3/2)_i} (-1)^i Z^{2i+1} \alpha^{-n-i}.$$

Now we evaluate $J_{n,2}$

$$J_{n,2} = \int_0^{\infty} \left[\alpha + x^2\right]^{-n} dx,$$

making the substitutions $X = x/a \Rightarrow dx = a\, dX$, thus $J_{n,2}$ becomes

$$J_{n,2} = a\alpha^{-n} \int_0^{\infty} \left[1 + (a^2/\alpha)X^2\right]^{-n} dX,$$

by making the substitutions $v = X^2$, and then $v = s/(1-s) \Rightarrow s = v/(1+v) \Rightarrow dv = ds/(1-s)^2$, thus

$$J_{n,2} = (1/2)a\alpha^{-n} \int_0^1 s^{-1/2}(1-s)^{n-3/2} \left[1 - \left(\alpha - a^2/\alpha\right) s\right]^{-n} ds,$$

using the definition of the hypergeometric function [82, §7.5], thus

$$J_{n,2} = \frac{a\sqrt{\pi}\alpha^{-n}\Gamma(n-1/2)}{2\Gamma(n)} F\left[n, 1/2; n; \left(\alpha - a^2/\alpha\right)\right].$$

using the generalized hypergeometric series [90], we may deduce

$$J_{n,2} = \frac{a\sqrt{\pi}\Gamma(n-1/2)}{2\Gamma(n)} \sum_{j=0}^{\infty} \frac{(1/2)_j}{i!} (\alpha - a^2)^j \alpha^{-n-j}.$$

Now we can easily evaluate the integrals T_n over θ_1, by defining the integral S_n

$$S_n = \int_{-\pi}^{\pi} (J_{n,1} + J_{n,2})\, d\theta_1,$$

thus,

$$S_n^* \;=\; \pi/c(i+1)\left[(Z_0+c/2)^{2i+2}-(Z_0+c/2)^{2i+2}\right]+2\pi.$$

To evaluate the integrals T_n over θ_2, we defined the integral W_n as

$$W_n \;=\; \int_{-\pi}^{\pi}(J_{n,1}+J_{n,2})\;d\theta_2,$$

and by introducing the integral $W_{n,1}=\int_{-\pi}^{\pi}J_{n,1}\,d\theta_2$, thus

$$W_{n,1}^* \;=\; \int_{-\pi}^{\pi}\left[\beta+\gamma\sin^2(\theta_2/2)\right]^{-n-i}\;d\theta_2, \tag{B.1.1}$$

where $\beta=(a-rt)^2$ and $\gamma=4art$, and making the change of variable $u=\theta_2/2$ which gives

$$W_{n,1}^*=4\int_0^{\pi/2}\left[\beta+\gamma\sin^2(u)\right]^{-n-i}\;du,$$

taking $\tau=\sin^2 u \Rightarrow d\tau=2\sin u\cos u\Rightarrow du=(1/2)\tau^{-1/2}(1-\tau)^{-1/2}d\tau$, when $u=0$ $\Rightarrow\tau=0$ and when $u=\pi/2\Rightarrow\tau=1$, thus $W_{n,1}^*$ becomes

$$W_{n,1}^*=2\beta^{-n-i}\int_0^1\tau^{-1/2}(1-\tau)^{-1/2}\left[1+(\gamma/\beta)\tau\right]^{-n-i}\;d\tau,$$

using the form given in [82, §7.5] and the generalized hypergeometric series [90], thus

$$\begin{aligned}W_{n,1}^* &= 2\pi\beta^{-n-i}F\left[n-i,1/2;1;-\gamma/\beta\right]\\ &= 2\pi\sum_{k=0}^{\infty}\frac{(n+i)_k(1/2)_k}{(k!)^2}(-1)^k\beta^{-n-i-k}\gamma^k.\end{aligned}$$

Now we introduce the integral $W_{n,2} = \int_{-\pi}^{\pi} J_{n,2}\, d\theta_2$, thus

$$W^*_{n,2} \;=\; \int_{-\pi}^{\pi} \left[\omega + \gamma \sin^2(\theta_2/2)\right]^j \left[\beta + \gamma \sin^2(\theta_2/2)\right]^j \, d\theta_2,$$

where $\omega = -2art + r^2t^2$, $\beta = (a - rt)^2$ and $\gamma = 4art$, and by making the change of variables as shown in (B.1.1), thus $W^*_{n,2}$ becomes

$$W^*_{n,2} = 2\omega^j \beta^{-n-j} \int_0^1 \chi^{-1/2}(1-\chi)^{-1/2} \left[1 + (\gamma/\omega)\chi\right]^j \left[1 + (\gamma/\beta)\chi\right]^{-n-i} \, d\chi,$$

using the definition of an Appell hypergeometric function [91], thus

$$W^*_{n,2} = 2\pi\omega^j \beta^{-n-j} F_1\left[1/2; -j, n+j; 1; -\gamma/\omega; -\gamma/\beta\right],$$

by using formula for the Appell hypergeometric function given in [91], which is given as

$$F_1\left(a'; b', b''; c'; x'; y'\right) \;=\; \sum_{m'=0}^{\infty} \sum_{n'=0}^{\infty} \frac{(a')_{m'+n'} (b')_{m'} (b'')_{n'}}{m'! n'! (c')_{m'+n'}} x'^{m'} y'^{n'},$$

thus $W^*_{n,2}$ becomes

$$W^*_{n,2} = 2\pi \sum_{p=0}^{\infty} \sum_{q=0}^{\infty} \frac{(1/2)_{p+q} (-j)_p (n+j)_q}{(p!)^2 (q!)^2} \omega^{j-p} \beta^{-n-j-q}.$$

To complete the evolution of the integrals T_n, we need to evaluate it over t. So, we defined the integral H_n as

$$H_n \;=\; \int_0^1 \left(J_{n,1} + J_{n,2}\right) \left(1 + \delta t^2\right)^{1/2} \, dt,$$

where $\delta = (2r\pi/c)^2$, and by introducing the integral $H_{n,1} = \int_0^1 W_{n,1}^* \left(1+\delta t^2\right)^{1/2}\, dt$, thus

$$H_{n,1}^* \;=\; (4r)^k a^{-2(n+i)-k} \int_0^1 t^k \left[1-(r/a)\,t\right]^{-2(n+i+k)} \left(1+\delta t^2\right)^{1/2}\, dt,$$

by expanding the term $\left[1-(r/a)\,t\right]^{-2(n+i+k)}$, thus

$$H_{n,1}^* \;=\; 4^k \sum_{g=0}^{\infty} \binom{-2(n+i+k)}{g} r^{k+g} a^{2(-n-i)-k-g} \int_0^1 t^{k+g} \left(1+\delta t^2\right)^{1/2}\, dt,$$

on making the substitution $\sigma = t^2$, thus $H_{n,1}^*$ becomes

$$H_{n,1}^* \;=\; 4^k/2 \sum_{g=0}^{\infty} \binom{-2(n+i+k)}{g} r^{k+g} a^{2(-n-i)-k-g} \int_0^1 \sigma^{(k+g-1)/2} \left(1+\delta\sigma\right)^{1/2}\, d\sigma,$$

using the definition of the hypergeometric function [82, §7.5], thus

$$H_{n,1}^* \;=\; 4^k \sum_{g=0}^{\infty} \binom{-2(n+i+k)}{g} \frac{r^{k+g} a^{2(-n-i)-k-g}}{(k+g+1)} F\left(\frac{-1}{2}, \frac{k+g+1}{2}; \frac{k+g+3}{2}; -\delta\right).$$

Now we introduce the integral $H_{n,2} = \int_0^1 W_{n,2}^* \left(1+\delta t^2\right)^{1/2}\, dt$. We follow the same steps for evaluating $H_{n,1}^*$ above to evaluate $H_{n,2}^*$.

Appendix C

C.1 Analytical evaluation of (4.4.2)

In this appendix we evaluate (4.4.2). By defining the integral R_n as

$$R_n = \int_{-\pi}^{\pi}\int_0^1 \left(1+\frac{4r^2\pi^2}{c^2}t^2\right)^{1/2} F\left[\frac{2n-1}{2},\frac{2n-1}{2};1;\left(\frac{\xi}{a}\right)^2\right] d\theta\, dt,$$

where $\xi^2 = (rt+\delta)^2 - 4\delta rt\sin^2(\theta/2)$, we perform the integration over θ, by defining the new integral S_n as

$$S_n = \int_{-\pi}^{\pi} F\left[(2n-1)/2,(2n-1)/2;1;\left((rt+\delta)^2 - 4\delta rt\sin^2(\theta/2)\right)/a^2\right] d\theta,$$

using the generalized hypergeometric series [90], we may deduce

$$S_n = \sum_{m=0}^{\infty}\left[\left(\frac{2n-1}{2}\right)_m \frac{\mu^m}{m!a^m}\right]^2 \int_{-\pi}^{\pi}\left[1-(\beta/\mu)\sin^2(\theta/2)\right]^m d\theta,$$

and in addition, $\beta = 4\delta rt$ and $\mu = (rt+\delta)^2$. On making the substitution $\tau = \sin^2(\theta/2)$, thus S_n becomes

$$S_n = 2\sum_{m=0}^{\infty}\left[\left(\frac{2n-1}{2}\right)_m \frac{\mu^m}{m!a^m}\right]^2 \int_0^1 \tau^{-1/2}(1-\tau)^{-1/2}[1-(\beta/\mu)\tau]^m\, d\tau,$$

by using the integral definition of the hypergeometric function in [90] (p.59, Eq.10), thus

$$S_n = 2\pi \sum_{m=0}^{\infty} \left[\left(\frac{2n-1}{2} \right)_m \frac{\mu^m}{m! a^m} \right]^2 F(-m, 1/2; 1; \beta/\mu).$$

we now preform the integration with respect to t. Using the generalized hypergeometric series [90] and introducing the integral S_n, we may deduce

$$\begin{aligned} S_n &= 2\pi \sum_{m=0}^{\infty} \sum_{k=0}^{m} (-m)_k (1/2)_k (k!)^{-2} 4^k r^k \delta^k \left[\frac{(2n-1/2)_m}{m! a^m} \right]^2 \\ &\times \int_0^1 t^k (rt+\delta)^{2m-2k} \left[1 + (4r^2\pi^2/c^2) t^2 \right]^{1/2} \, dt. \end{aligned}$$

We now expand the $(rt+\delta)^{2m-2k}$ terms as a binomial expansion to give

$$\begin{aligned} S_n &= 2\pi \sum_{m=0}^{\infty} \sum_{k=0}^{m} \sum_{p=0}^{2(m-k)} 4^k r^{k+p} \delta^{2m-k-p} (-m)_k (1/2)_k (k!)^{-2} \binom{2m-2k}{p} \left[\frac{(2n-1/2)_m}{m! a^m} \right]^2 \\ &\times \int_0^1 t^{k+p} \left[1 + (4r^2\pi^2/c^2) t^2 \right]^{1/2} \, dt. \end{aligned}$$

On making the substitution $y = t^2 \Rightarrow dt = (1/2) y^{-1/2} dy$, when $t = 0 \Rightarrow y = 0$, and when $t = 1 \Rightarrow y = 1$, and by letting $\lambda = (2r\pi/c)^2$. Thus, the integral S_n becomes

$$\begin{aligned} S_n &= \pi \sum_{m=0}^{\infty} \sum_{k=0}^{m} \sum_{p=0}^{2(m-k)} 4^k r^{k+p} \delta^{2m-k-p} (-m)_k (1/2)_k (k!)^{-2} \binom{2m-2k}{p} \left[\frac{(2n-1/2)_m}{m! a^m} \right]^2 \\ &\times \int_0^1 y^{(k+p-1)/2} (1+\lambda y)^{1/2} \, dy, \end{aligned}$$

by using the form in [90] (p.59, Eq.10), thus we find that

$$R_n = 2\pi \sum_{m=0}^{\infty} \sum_{k=0}^{m} \sum_{p=0}^{2(m-k)} 4^k r^{k+p} \delta^{2m-k-p} (-m)_k (1/2)_k (k!)^{-2} \binom{2m-2k}{p} \left[\frac{(2n-1/2)_m}{m! a^m} \right]^2 \times \frac{1}{(k+p+1)} F\left[-1/2, (k+p+1)/2; (k+p+3)/2; -\lambda\right]. \quad \text{(C.1.1)}$$

C.2 Analytical evaluation of J_n appeared in (4.5.4)

In this appendix we evaluate the integrals J_n, which are shown in equation (4.5.4)

$$J_n = \int_{-\pi}^{\pi} \int_{-1}^{1} \left(1 + \Lambda' t^2\right)^{1/2} F\left[\frac{2n-1}{2}, \frac{2n-1}{2}; 1; \left(\frac{\Xi}{a}\right)^2 \right] dt\, d\Theta,$$

where $\Lambda' = (2R\pi \sin(\phi/2)/c)^2$ and we evaluate the integral over t, by introducing the integral H_n as

$$H_n = \int_{-1}^{1} \left(1 + \Lambda' t^2\right)^{1/2} \left[\alpha' + \beta' t^2 + \gamma' t\right]^m dt,$$

where $\alpha' = R^2 \cos^2(\phi/2) + R\Delta \cos\Theta + R\Delta \cos(\Theta - \phi) + \Delta^2$, $\beta' = R \sin^2(\phi/2)$ and $\gamma' = R\Delta \cos\Theta - R\Delta \cos(\Theta - \phi)$, by expanding the $[\alpha' + \beta' t^2 + \gamma' t]^m$ terms as a binomial expansion to give

$$H_n = \sum_{k'=0}^{m} \binom{m}{k'} \gamma'^{k'} \alpha'^{m-k'} \int_{-1}^{1} t^{k'} \left[1 + (\beta'/\alpha')\, t^2\right]^{m-k'} \left(1 + \Lambda' t^2\right)^{1/2} dt,$$

we note that the integral is zero whenever k' is odd. Therefore we can replace $k' \to 2k'$ giving

$$H_n = 2 \sum_{k'=0}^{\lfloor m/2 \rfloor} \binom{m}{2k'} \gamma'^{2k'} \alpha'^{m-2k'} \int_{0}^{1} t^{2k'} \left[1 + (\beta'/\alpha')\, t^2\right]^{m-2k'} \left(1 + \Lambda' t^2\right)^{1/2} dt,$$

where $\lfloor v \rfloor$ signifies the largest integer not greater than v, now by taking $w = t^2$, thus

$$H_n = \sum_{k'=0}^{\lfloor m/2 \rfloor} \binom{m}{2k'} \gamma'^{2k'} \alpha'^{m-2k'} \int_0^1 w^{k'-1/2} \left[1 + (\beta'/\alpha')\, w\right]^{m-2k'} (1 + \Lambda' w)^{1/2}\, dt,$$

from the definition of an Appell hypergeometric function we evaluate H_n as

$$\begin{aligned} H_n &= 2 \sum_{k'=0}^{\lfloor m/2 \rfloor} \sum_{i=0}^{\infty} \binom{m}{2k'} \frac{\gamma'^{2k'} \alpha'^{m-2k'-i} (k' + 1/2)_i (2k' - m)_i (-\beta')^i}{(2k' + 1) i! (k' + 3/2)_i} \\ &\times F\left(k' + i + 1/2, -1/2; k' + i + 3/2; -\Lambda'\right). \end{aligned}$$

Now we evaluate J_n with respect to Θ, by defining the integral W_n as

$$W_n = \int_{-\pi}^{\pi} (\ell \cos\Theta + f \sin\Theta)^{2k'} (p + q\cos\Theta - f\sin\Theta)^{m-2k'-i}\, d\Theta,$$

where $\ell = R\Delta - R\Delta\cos\phi$, $f = R\Delta\sin\phi$, $p = R^2\cos^2(\phi/2) + \Delta^2$ and $q = R\Delta + R\Delta\cos\phi$. Thus

$$W_n = \int_{-\pi}^{\pi} \left[\ell\cos(\Theta - \Omega) + f\sin(\Theta - \Omega)\right]^{2k'} \left(p + \sqrt{q^2 + f^2}\cos\Theta\right)^{m-2k'-i} d\Theta,$$

where $\cos\Omega = q/\sqrt{q^2 + f^2}$ and $\sin\Omega = f/\sqrt{q^2 + f^2}$, thus

$$W_n = \int_{-\pi}^{\pi} (g\cos\Theta + h\sin\Theta)^{2k'} \left(p + \sqrt{q^2 + f^2}\cos\Theta\right)^{m-2k'-i} d\Theta,$$

where $g = \ell\cos\Omega - f\sin\Omega$ and $h = \ell\sin\Omega + f\cos\Omega$, and by expanding the term $(g\cos\Theta + h\sin\Theta)^{2k'}$, thus

$$W_n = \sum_{j=0}^{2k'} \binom{2k'}{j} g^j h^{2k'-j} \int_{-\pi}^{\pi} \cos^j\Theta \sin^{2k'-j}\Theta \left(p + \sqrt{q^2 + f^2}\cos\Theta\right)^{m-2k'-i} d\Theta,$$

we note that the integral is zero whenever j is odd, so we replace the $j \to 2j$, thus

$$\begin{aligned} W_n &= \sum_{j=0}^{\lfloor k' \rfloor} \binom{2k'}{2j} g^{2j} h^{2(k'-j)} 2^{2(k'-j)} \left(p + \sqrt{q^2+f^2}\right)^{m-2k'-i} \\ &\times \int_{-\pi}^{\pi} \left[1 - 2\sin^2(\Theta/2)\right]^{2j} \sin^{2(k'-j)}(\Theta/2) \cos^{2(k'-j)}(\Theta/2) \\ &\times \left\{1 - \left[2\sqrt{q^2+f^2} / \left(p + \sqrt{q^2+f^2}\right)\right] \sin^2(\Theta/2)\right\}^{m-2k'-i} d\Theta, \end{aligned}$$

by making the substitutions $\Psi = sin^2(\Theta/2)$, thus W_n becomes

$$\begin{aligned} W_n &= 2\sum_{j=0}^{\lfloor k' \rfloor} \binom{2k'}{2j} g^{2j} h^{2(k'-j)} 2^{2(k'-j)} \left(p + \sqrt{q^2+f^2}\right)^{m-2k'-i} \\ &\times \int_{0}^{1} \left[1 - 2\Psi\right]^{2j} \Psi^{k'-j-1/2} (1-\Psi)^{k'-j-1/2} \\ &\times \left\{1 - \left[2\sqrt{q^2+f^2} / \left(p + \sqrt{q^2+f^2}\right)\right] \Psi\right\}^{m-2k'-i} d\Psi, \end{aligned}$$

due to the positive power of the $[1-2\Psi]^{2j}$ terms, we may expand this as a binomial expansion to give

$$\begin{aligned} W_n &= 2\sum_{j=0}^{\lfloor k' \rfloor} \sum_{\iota=0}^{2j} \binom{2k'}{2j} \binom{2j}{\iota} (-2)^{\iota} g^{2j} h^{2(k'-j)} 2^{2(k'-j)} \left(p + \sqrt{q^2+f^2}\right)^{m-2k'-i} \\ &\times \int_{0}^{1} \Psi^{\iota+k'-j-1/2} (1-\Psi)^{k'-j-1/2} \\ &\times \left\{1 - \left[2\sqrt{q^2+f^2} / \left(p + \sqrt{q^2+f^2}\right)\right] \Psi\right\}^{m-2k'-i} d\Psi. \end{aligned}$$

We note that this W_n is now in the integral form for the usual hypergeometric function $F(a^*, b^*; c^*; z^*)$, as described and can represented as

$$\begin{aligned} W_n &= 2\sum_{j=0}^{\lfloor k' \rfloor}\sum_{\iota=0}^{2j}\binom{2k'}{2j}\binom{2j}{\iota}(-2)^{\iota} g^{2j} h^{2(k'-j)} 2^{2(k'-j)} \left(p+\sqrt{q^2+f^2}\right)^{m-2k'-i} \\ &\times (k'-j-3/2)!(\iota+k'-j+1/2)!/(\iota+2k'-2j)! \\ &\times F\left(2k'+i-m, \iota+k'-j+1/2; \iota+2k'-2j+1; \frac{2\sqrt{q^2+f^2}}{p+\sqrt{q^2+f^2}}\right). \end{aligned}$$

Appendix D

D.1 Analytical evaluation of I_n^* appeared in (5.5.1)

In this appendix we evaluate the integrals I_n^* which appear in equation (5.5.1). By defining the integrals I_n^* as

$$I_n^* = \int_{-\pi}^{\pi}\int_{-1}^{1} P^{-2n} dt\, d\theta,$$

where P here is defined by

$$P = \frac{r}{2}\Big[\cos\theta + \cos(\theta-\phi) + t\Big(\cos\theta - \cos(\theta-\phi)\Big)\Big] + \Delta,$$

and where r, θ, ϕ and Δ are as given in Section 3. We first evaluate the integral with respect to t, thus

$$\begin{aligned} I_n^*(\theta) &= (r/2)^{-2n}\sum_{k=0}^{\infty}\binom{-2n}{2k}\left[\cos\theta + \cos(\theta-\phi) + \Delta\right]^{-2n-2k}\left[\cos\theta - \cos(\theta-\phi)\right]^{2k} \\ &\times \frac{2}{2k+1}F\left(-\frac{1}{2}, k+\frac{1}{2}; k+\frac{3}{2}; -\frac{4r^2\pi^2\sin^2(\phi/2)}{c^2}\right). \end{aligned}$$

Now we evaluate I_n^* with respect to θ, by introducing the integrals H_n as

$$H_n = \int_{-\pi}^{\pi} (\ell \cos\theta + f \sin\theta)^{2k} \, (p + q\cos\theta - f\sin\theta)^{-2n-2k} \, d\theta,$$

where $\ell = 1 - \cos\phi$, $f = \sin\phi$, $p = 2\Delta/r$ and $q = 1 + \cos\phi$. Thus we obtain

$$H_n = \int_{-\pi}^{\pi} [\ell \cos(\theta - \tau) + f \sin(\theta - \tau)]^{2k} \left(p + \sqrt{q^2 + f^2}\cos\theta\right)^{-2n-2k} \, d\theta,$$

where $\cos\tau = q/\sqrt{q^2 + f^2}$ and $\sin\tau = f/\sqrt{q^2 + f^2}$, and therefore

$$H_n = \int_{-\pi}^{\pi} (g\cos\theta + h\sin\theta)^{2k} \left(p + \sqrt{q^2 + f^2}\cos\theta\right)^{-2n-2k} \, d\theta,$$

where $g = \ell\cos\tau - f\sin\tau$ and $h = \ell\sin\tau + f\cos\tau$. By expanding the term $(g\cos\theta + h\sin\theta)^{2k}$, thus

$$H_n = \sum_{j=0}^{2k} \binom{2k}{j} g^j h^{2k-j} \int_{-\pi}^{\pi} \cos^j\theta \sin^{2k'-j}\theta \left(p + \sqrt{q^2 + f^2}\cos\theta\right)^{-2n-2k} \, d\theta,$$

and we note that the integral is zero whenever j is odd, so we replace the $j \to 2j$, so that

$$\begin{aligned} H_n &= \sum_{j=0}^{\lfloor k \rfloor} \binom{2k}{2j} g^{2j} h^{2(k-j)} 2^{2(k-j)} \left(p + \sqrt{q^2 + f^2}\right)^{-2n-2k} \\ &\times \int_{-\pi}^{\pi} \left[1 - 2\sin^2(\theta/2)\right]^{2j} \sin^{2(k-j)}(\theta/2) \cos^{2(k-j)}(\Theta/2) \\ &\times \left\{1 - \left[2\sqrt{q^2 + f^2}/\left(p + \sqrt{q^2 + f^2}\right)\right] \sin^2(\theta/2)\right\}^{-2n-2k} \, d\theta, \end{aligned}$$

where $\lfloor k \rfloor$ signifies the largest integer not greater than k. By making the substitutions $w = \theta/2$ and $u = \sin^2 w$, H_n becomes

$$\begin{aligned} H_n &= 2\sum_{j=0}^{\lfloor k \rfloor} \binom{2k}{2j} g^{2j} h^{2(k-j)} 2^{2(k-j)} \left(p + \sqrt{q^2+f^2}\right)^{-2n-2k} \\ &\times \int_0^1 [1-2u]^{2j}\, u^{k-j-1/2}(1-u)^{k-j-1/2} \\ &\times \left\{1 - \left[2\sqrt{q^2+f^2}/\left(p+\sqrt{q^2+f^2}\right)\right] u\right\}^{-2n-2k} du, \end{aligned}$$

and the positive power of the $[1-2u]^{2j}$ may be expanded as a binomial expansion to give

$$\begin{aligned} H_n &= 2\sum_{j=0}^{\lfloor k \rfloor} \sum_{s=0}^{2j} \binom{2k}{2j}\binom{2j}{s} (-2)^s g^{2j} h^{2(k-j)} 2^{2(k-j)} \left(p + \sqrt{q^2+f^2}\right)^{m-2k-i} \\ &\times \int_0^1 u^{s+k-j-1/2}(1-u)^{k-j-1/2} \left\{1 - \left[2\sqrt{q^2+f^2}/\left(p+\sqrt{q^2+f^2}\right)\right] u\right\}^{-2n-2k} du, \end{aligned}$$

and we note that H_n is now in the integral form for the usual hypergeometric function $F(a^*, b^*; c^*; z^*)$ [82, §7.5] and H_n can be expressed as

$$\begin{aligned} H_n &= 2\sum_{j=0}^{\lfloor k \rfloor} \sum_{s=0}^{2j} \binom{2k}{2j}\binom{2j}{s} (-2)^s g^{2j} h^{2(k-j)} 2^{2(k-j)} \left(p + \sqrt{q^2+f^2}\right)^{m-2k-i} \\ &\times \Gamma(s+k-j+1/2)\Gamma(k+3j+1/2)/\Gamma(s+2k+2j+1) \\ &\times F\left\{2n+2k, s+k-j+1/2; s+2k+2j+1; \left[2\sqrt{q^2+f^2}/\left(p+\sqrt{q^2+f^2}\right)\right]\right\}. \end{aligned}$$

D.2 Analytical evaluation of Y_n appeared in (5.6.2)

In this appendix we evaluate the integrals Y_n, which are shown in equation (5.6.2), using the integral definition of the hypergeometric function to evaluate the integral

over t, we may deduce

$$\begin{aligned} Y_n &= \int_{-\pi}^{\pi} \frac{\pi}{\left[(c\xi/2\pi)\cos\Omega + Z_0\right]^{2n-1}(n-1)} \sum_{\lambda=0}^{\infty} \binom{-2n+2}{\lambda} \left[\frac{\chi \sin\xi \sin\Omega}{(c\xi/2\pi)\cos\Omega + Z_0}\right]^{\lambda} \\ &\times (\lambda+1)^{-1} F\left(-\frac{1}{2}, \lambda+\frac{1}{2}; \lambda+\frac{3}{2}; -\frac{4\chi^2\pi^2}{c^2}\right) d\xi. \end{aligned}$$

Next we define a new integral U_n by

$$U_n = \chi^{\lambda} Z_0^{1-2n-\lambda} \sin^{\lambda}\Omega \int_{-\pi}^{\pi} \left[1 + (c\xi/2\pi Z_0)\cos\Omega\right]^{1-2n-\lambda} \sin^{\lambda}\xi \, d\xi,$$

and on expanding the term $\left[1 + (c\xi/2\pi Z_0)\cos\Omega\right]^{1-2n-\lambda}$, we obtain

$$U_n = \chi^{\lambda} Z_0^{1-2n-\lambda} \sin^{\lambda}\Omega \sum_{\psi=0}^{\infty} \binom{1-2n-\lambda}{\psi} \left[(c/2\pi Z_0)\cos\Omega\right]^{\psi} \int_{-\pi}^{\pi} \xi^{\psi} \sin^{\lambda}\xi \, d\xi.$$

By evaluating the integral V_n defined by

$$V_n = \int_{-\pi}^{\pi} \xi^{\psi} \sin^{\lambda}\xi \, d\xi,$$

where λ can be either odd or even number, and by using the formulas in [82, §2.63 − 2.65] we may deduce

$$\int \xi^{\psi} \sin^{\lambda}\xi \, d\xi = \begin{cases} \binom{2\alpha}{\alpha} \frac{\xi^{\psi+1}}{2^{2\alpha}(\psi+1)} + \frac{(-1)^{\alpha}}{2^{2\alpha-1}} \sum_{\beta=0}^{\alpha-1} (-1)^{\beta} \binom{2\alpha}{\beta} \int \xi^{\psi} \sin(2\alpha-2\beta)\xi \, d\xi & \text{if } \lambda = 2\alpha, \\ \frac{(-1)^{\alpha}}{2^{2\alpha}} \sum_{\beta=0}^{\alpha} (-1)^{\beta} \binom{2\alpha+1}{\beta} \int \xi^{\psi} \sin(2\alpha-2\beta+1)\xi \, d\xi & \text{if } \lambda = 2\alpha+1. \end{cases}$$

Appendix E

E.1 Analytical evaluation of (6.4.1)

In this appendix we summarise the analytical evaluation of the double integral (6.4.1). By defining the integral R_n as

$$R_n = \int_{-\pi}^{\pi}\int_{-1}^{1}\left(1+\frac{4rR^2\pi^2}{c^2}t^2\right)^{1/2}\left(\rho^2-a^2\right)^{-n}dt\,d\Theta,$$

where n is a certain positive integer, and

$$\rho^2 = (Rt)^2 - 2Rt\Delta\cos(\Theta-\Omega)+\Delta^2+\left(c\Theta/2\pi\right)^2,$$

we may evaluate the integral over t by introducing the integral H_n as

$$H_n = R^{-2n}\int_{-1}^{1}\left(1+\Lambda t^2\right)^{1/2}\left[t^2-2\alpha t+\beta\right]^{-n}dt,$$

where $\Lambda=(2R\pi/c)^2$, $\alpha=\Delta\cos(\Theta-\Omega)/R$ and $\beta=\left[\Delta^2-a^2+\left(c\Theta/2\pi\right)^2\right]/R^2$; thus

$$H_n = R^{-2n}\beta^{-n}\int_{-1}^{1}\left(1+\Lambda t^2\right)^{1/2}\left[1-2\alpha t/\beta+t^2/\beta\right]^{-n}dt.$$

By taking $u = t/\sqrt{\beta}$, we have

$$H_n = R^{-2n}\beta^{-n+1/2}\int_{-1/\sqrt{\beta}}^{1/\sqrt{\beta}}\left(1+\Lambda\beta u^2\right)^{1/2}\left[1-2\alpha u/\beta^{1/2}+u^2\right]^{-n}du,$$

and by expanding the $\left[1-2\alpha u/\beta^{1/2}+u^2\right]^{-n}$ terms we may deduce

$$H_n = R^{-2n}\beta^{-n+1/2}\sum_{k=0}^{\infty}C_k^n(x)\int_{-1/\sqrt{\beta}}^{1/\sqrt{\beta}}u^k\left(1+\Lambda\beta u^2\right)^{1/2}du,$$

where $C_k^n(x)$ is the usual Gegenbauer polynomials [90, §3.15.1] and $x = \alpha/\beta^{1/2}$. By making the substitution $y = \sqrt{\beta}u$, thus H_n becomes

$$H_n = R^{-2n}\sum_{k=0}^{\infty}\beta^{-n-k/2}C_k^n(x)\int_{-1}^{1}y^k\left(1+\Lambda y^2\right)^{1/2}dy,$$

and we note that the integral is zero whenever k is odd. Therefore, we can replace $k \to 2k$ giving

$$H_n = 2R^{-2n}\sum_{k=0}^{\infty}\beta^{-n-k}C_{2k}^n(x)\int_{0}^{1}y^{2k}\left(1+\Lambda y^2\right)^{1/2}dy,$$

and by taking $w = y^2$, we may obtain

$$H_n = R^{-2n}\sum_{k=0}^{\infty}\beta^{-n-k}C_{2k}^n(x)\int_{0}^{1}w^{k-1/2}\left(1+\Lambda w\right)^{1/2}dw.$$

From the definition for the usual hypergeometric function [82, §7.5], we may evaluate H_n as

$$H_n = 2R^{-2n}\sum_{k=0}^{\infty}\beta^{-n-k}C_{2k}^n(x)\,F\left(-1/2,k+1/2;k+3/2;-\Lambda\right)/\left(2k+1\right),$$

and from [90, §3.15.1] we have $C_{2k}^{n}(x)$ in terms of a hypergeometric function, which is given as

$$C_{2k}^{n}(x) = (-1)^{k}\binom{k+n-1}{k} F\left(-k, k+n; 1/2; x^{2}\right),$$

and by using the generalized hypergeometric series [90], we may deduce

$$C_{2k}^{n}(x) \;=\; (-1)^{k}\binom{k+n-1}{k}\sum_{i=0}^{\infty}\frac{(-k)_{i}(k+n)_{i}}{(1/2)_{i}i!}x^{2i}.$$

Now we need to evaluate R_n with respect to Θ, by defining the integral J_n as

$$J_{n} \;=\; \int_{-\pi}^{\pi} x^{2i}\beta^{-n-k}\,d\Theta = R^{2(n+k)}\Delta^{2i}\left(\Delta^{2}-a^{2}\right)^{-n-k-i} J_{n}^{*},$$

where

$$J_{n}^{*} \;=\; \int_{-\pi}^{\pi}\cos^{2i}(\Theta-\Omega)\left[1+\left(c^{2}/4\pi^{2}\left(\Delta^{2}-a^{2}\right)\right)\Theta^{2}\right]^{-n-k-i}\,d\Theta,$$

so that

$$J_{n}^{*} \;=\; \int_{-\pi}^{\pi}\left(\cos\Theta\cos\Omega+\sin\Theta\sin\Omega\right)^{2i}\left[1+\gamma\Theta^{2}\right]^{-n-k-i}\,d\Theta,$$

where $\gamma = c^{2}/\left[4\pi^{2}\left(\Delta^{2}-a^{2}\right)\right]$. By expanding the term $\left(\cos\Theta\cos\Omega+\sin\Theta\sin\Omega\right)^{2i}$, thus

$$J_{n}^{*} \;=\; \sum_{j=0}^{2i}\binom{2i}{j}\cos^{2i-j}\Omega\sin^{j}\Omega\int_{-\pi}^{\pi}\cos^{2i-j}\Theta\sin^{j}\Theta\left[1+\gamma\Theta^{2}\right]^{-n-k-i}\,d\Theta,$$

we note that the integral is zero whenever j is odd, so we replace the $j \to 2j$, and we have

$$J_n^* = \sum_{j=0}^{\lfloor i \rfloor} \binom{2i}{2j} \cos^{2(i-j)} \Omega \sin^{2j} \Omega \int_{-\pi}^{\pi} \cos^{2(i-j)} \Theta \sin^{2j} \Theta \left[1 + \gamma\Theta^2\right]^{-n-k-i} d\Theta,$$

where $\lfloor v \rfloor$ signifies the largest integer not greater than v. Thus,

$$J_n^* = \sum_{j=0}^{\lfloor i \rfloor} \sum_{p=0}^{j} \binom{2i}{2j} \binom{j}{p} (-1)^p \cos^{2(i-j)} \Omega \sin^{2j} \Omega \int_{-\pi}^{\pi} \cos^{2m} \Theta \left[1 + \gamma\Theta^2\right]^{-n-k-i} d\Theta,$$

where $m = i - j + p$, and from [82, §1.32] we may expand $\cos^{2m} \Theta$, which is given in the following form

$$\boxed{\cos^{2m} \Theta = \frac{1}{2^{2m}} \left\{ \sum_{q=0}^{m-1} 2 \binom{2m}{q} \cos 2(m-q)\Theta + \binom{2m}{m} \right\}.}$$

Thus J_n^* becomes

$$\begin{aligned} J_n^* &= (1/2^{2m}) \sum_{j=0}^{\lfloor i \rfloor} \sum_{p=0}^{j} \binom{2i}{2j} \binom{j}{p} (-1)^p \cos^{2(i-j)} \Omega \sin^{2j} \Omega \\ &\times \left\{ \sum_{q=0}^{m-1} 2 \binom{2m}{q} \int_{-\pi}^{\pi} \cos 2(m-q)\Theta \left[1 + \gamma\Theta^2\right]^{-n-k-i} d\Theta \right. \\ &+ \left. \binom{2m}{m} \int_{-\pi}^{\pi} \left[1 + \gamma\Theta^2\right]^{-n-k-i} d\Theta \right\}. \end{aligned}$$

Now we introduce the integrals $J_{n_1}^*$ and $J_{n_2}^*$ as

$$J_{n_1}^* = \int_{-\pi}^{\pi} \cos 2(m-q)\Theta \left[1 + \gamma\Theta^2\right]^{-n-k-i} d\Theta, \text{ and } J_{n_2}^* = \int_{-\pi}^{\pi} \left[1 + \gamma\Theta^2\right]^{-n-k-i} d\Theta.$$

First, we evaluate $J^*_{n_1}$, by expanding $\cos 2\,(m-q)\,\Theta$, thus

$$J^*_{n_1} = \int_{-\pi}^{\pi} \sum_{\ell=0}^{\infty} (-1)^{\ell} \frac{2^{2\ell}\,(m-q)^{2\ell}}{(2\ell)!} \Theta^{2\ell} \left[1+\gamma\Theta^2\right]^{-n-k-i}\, d\Theta,$$

making the substitution $\Xi = \Theta/\pi$, thus $J^*_{n_1}$ becomes

$$J^*_{n_1} = 2\pi \int_{0}^{1} \sum_{\ell=0}^{\infty} (-1)^{\ell} \frac{2^{2\ell}\pi^{2\ell}\,(m-q)^{2\ell}}{(2\ell)!} \Xi^{2\ell} \left[1+\gamma\pi^2\Xi^2\right]^{-n-k-i}\, d\Xi,$$

by taking $\tau = \Xi^2$, thus

$$J^*_{n_1} = \pi \int_{0}^{1} \sum_{\ell=0}^{\infty} (-1)^{\ell} \frac{2^{2\ell}\pi^{2\ell}\,(m-q)^{2\ell}}{(2\ell)!} \tau^{\ell-1/2} \left[1+\gamma\pi^2\tau\right]^{-n-k-i}\, d\tau.$$

From the definition of the usual hypergeometric function [82, §7.5], we obtain

$$J^*_{n_1} = 2\pi \sum_{\ell=0}^{\infty} (-1)^{\ell} \frac{2^{2\ell}\pi^{2\ell}\,(m-q)^{2\ell}}{(2\ell+1)(2\ell)!} F\left(n+k+i, \ell+1/2; \ell+3/2; -\pi^2\gamma\right).$$

Now we evaluate $J^*_{n_2}$, by making the substitution $\psi = \Theta/\pi$, and then taking $\chi = \psi^2$, thus $J^*_{n_2}$ becomes

$$J^*_{n_2} = \pi \int_{0}^{1} \chi^{-1/2} \left[1+\pi^2\gamma\chi\right]^{-n-k-i}\, d\chi,$$

and from the definition of the usual hypergeometric function [82, §7.5], thus

$$J^*_{n_2} = 2\pi F\left(n+k+i, 1/2; 3/2; -\pi^2\gamma\right).$$

Bibliography

[1] S. L. Mayo, B. D. Olafson, and W. A. Goddard. DREIDING: a generic force field for molecular simulations. *The Journal of Physical Chemistry*, 94:8897–8909, 1990.

[2] H. Gao, Y. Kong, D. Cui, and C. S. Ozkan. Spontaneous insertion of DNA oligonucleotides into carbon nanotubes. *Nano Letters*, 3:471–473, 2003.

[3] B. Alberts, A. Johnson, J. Lewis, M. Raff, K. Roberts, and P. Walter. *Molecular Biology of the Cell*. Garland Science, New York, 4th edition, 2002.

[4] L. A. Girifalco, M. Hodak, and R.S. Lee. Carbon nanotubes, buckyballs, ropes, and a universal graphitic potential. *Physical Review B*, 62:104–110, 2000.

[5] A. K. Geim and K. S. Novoselov. The rise of graphene. *Nature Materials*, 6:183–191, 2007.

[6] R. Dahm. Discovering DNA: Friedrich Miescher and the early years of nucleic acid research. *Human Genetics*, 122:565–581, 2008.

[7] N. C. Seeman. DNA engineering and its application to nanotechnology. *Trends in Biotechnology*, 17:437–443, 1999.

[8] R. L. W. Chen and P. Fong. Helical configuration of single-stranded DNA. *Journal of Theoretical Biology*, 22:180–187, 1969.

[9] B. Hingerty and S. Broyde. Helix geometry of single stranded DNA 'A' and 'B' forms from minimum energy conformations of dimeric subunits. *Nucleic Acids Res*, 5:127–137, 1978.

[10] V. Luzzati, A. Mathis, F. Masson, and J. Witz. Structure transitions observed in DNA and poly A in solution as a function of temperature and pH. *Journal of Molecular Biology*, 10:28–41, 1964.

[11] K. E. Duderstadt, K. Chuang, and J. M. Berger. DNA stretching by bacterial initiators promotes replication origin opening. *Nature*, 478:209–213, 2011.

[12] L. Chenxiang, L. Yan, R. Sherri, and Y. Hao. DNA tile based self-assembly: building complex nanoarchitectures. *ChemPhysChem*, 7:1641–1647, 2006.

[13] Z. Mingjun, C. L. Sabharwal, W. Tao, T. Tarn, N. Xi, and G. Li. Interactive DNA sequence and structure design for DNA nanoapplications. *IEEE Transactions on NanoBioscience*, 3:286–292, 2004.

[14] J. D. Watson and F. H. Crick. Molecular structure of nucleic acids; a structure for deoxyribose nucleic acid. *Nature*, 171:737–738, 1953.

[15] E. Drexler. *Nanosystems: Molecular Machinery, Manufacturing, and Computation*. Wiley, 1992.

[16] N. C. Seeman. Structural DNA nanotechnology: growing along with nano netters. *Nano Letters*, 10:1971–1978, 2010.

[17] D. Cui. *Medicinal Chemistry and Pharmacological Potential of Fullerenes and Carbon Nanotubes*, chapter Biomolecules functionalized carbon nanotubes and their applications, pages 181–221. Carbon Materials: Chemistry and Physics. Springer Netherlands, 2008.

[18] J. M. Bonard, N. Weiss, H. Kind, T. Stckli, L. Forr, K. Kern, and A. htelain. Tuning the field Emission properties of patterned carbon nanotube films. *Advanced Materials*, 13:184–188, 2001.

[19] H. Gao and Y. Kong. Simulation of DNA-nanotube interactions. *Annual Review of Materials Research*, 34:123–150, 2004.

[20] T. Odom, J. L. Huang, P. Kim, and C. M. Lieber. Structure and electronic properties of carbon nanotubes. *The Journal of physical Chemistry B*, 104:2794–2809, 2000.

[21] C. M. Niemeyer. Progress in "engineering up" nanotechnology devices utilizing DNA as a construction material. *Applied Physics A Materials Science and Processing Processing*, 68:119–124, 1999.

[22] Y. Benenson, T. Paz-Elizur, R. Adar, E. Keinan, Z. Livneh, and E. Shapiro. Programmable and autonomous computing machine made of biomolecules. *Nature*, 414:430–434, 2001.

[23] N. C. Seeman, F. Liu, C. Mao, X. Yang, L. A. Wenzler, R. Sha, W. Sun, Z. Shen, X. Li, and J. Qi. Two dimensions and two states in DNA nanotechnology. *Journal of Biomolecular Structure and Dynamics*, 17:253–262, 2000.

[24] F. W. Stahl. The Holliday junction on its thirtieth anniversary. *Genetics*, 138:241–246, 1994.

[25] Z. Shen, H. Yan, T. Wang, and N. C. Seeman. Paranemic crossover DNA: a generalized Holliday structure with applications in nanotechnology. *Journal of the American Chemical Society*, 126:1666–1674, 2004.

[26] K. M. Abu-Salah, S. A. Alrokyan, M. N. Khan, and A. A. Ansari. Nanomaterials as analytical tools for genosensors. *Sensors*, 10:963–993, 2010.

[27] M. S. Dresselhaus, G. Dresselhaus, and P. Avouris. *Carbon nanotubes: Synthesis, Structure, Properties and Applications*, volume 80. Springer, Berlin, 2001.

[28] S. Iijima. Helical microtubules of graphitic carbon. *Nature*, 354:56–58, 1991.

[29] S. Iijima and T. Ichihashi. Single-shell carbon nanotubes of 1-nm diameter. *Nature*, 363:603–605, 1993.

[30] W. Marx and A. Barth. Carbon nanotubes a scientometric study. *Physics State Solid. B*, 245:2347–2351, 2008.

[31] J. J. Davis, M. L.H. Green, H. A. O. Hill, Y. C. Leung, P. J. Sadler, J. Sloan, A. V. Xavier, and S. C. Tsang. The immobilisation of proteins in carbon nanotubes. *Inorganica Chimica Acta*, 272:261–266, 1998.

[32] T. Ito, L. Sun, and R. M. Crooks. Observation of DNA transport through a single carbon nanotube channel using fluorescence microscopy. *Chemical Communications*, 13:1482–1483, 2003.

[33] F. Albertorio, M. Hughes, J. Golovchenko, and D. Branton. Base dependent DNA–carbon nanotube interactions: activation enthalpies and assembly–disassembly control. *Nanotechnology*, 20:(9pp), 2009.

[34] K. Kamiya and S. Okada. Energetics and electronic structure of encapsulated single-stranded DNA in carbon nanotubes. *Physical Review B*, 83:(6pp), 2011.

[35] J. Li, H. Ng, A. Cassell, W. Fan, H. Chen, Q. Ye, J. Koehne, J. Han, and M. Meyyappan. Carbon nanotube nanoelectrode array for ultrasensitive DNA detection. *Nano Letters*, 3:597–602, 2003.

[36] Y. Xue and M. Chen. Dynamics of molecules translocating through carbon nanotubes as nanofluidic channels. *Nanotechnology*, 17:5216–5223, 2006.

[37] E. Y. Lau, F. C. Lightstone, and M. E. Colvin. Dynamics of DNA encapsulated in a hydrophobic nanotube. *Chemical Physics Letters*, 412:82–87, 2005.

[38] Y. Xu, X. Mi, and N. R. Aluru. Detection of defective DNA in carbon nanotubes by combined molecular dynamics/tight-binding technique. *Applied Physics Letters*, 95:113–116, 2009.

[39] Q. X. Pei, C. G. Lim, Y. Cheng, and H. Gao. Molecular dynamics study on DNA oligonucleotide translocation through carbon nanotubes. *The Journal of Chemical Physics*, 129:125101–125108.

[40] M. Shim, K. N. W. Shi, R. J. Chen, Y. Li, and H. Dai. Functionalization of carbon nanotubes for biocompatibility and biomolecular recognition. *Nano Letters*, 2:285–288, 2002.

[41] D. Cui, C. S. Ozkan, S. Ravindran, and Y. Kong H. Gao. Encapsulation of Pt-labelled DNA molecules inside carbon nanotubes. *Mechanics and Chemistry of Biosystems*, 1:113–122, 2004.

[42] E. D'yachkov, S. Dolin, and P. D'yachkov. Interaction of single-stranded DNA with carbon nanotubes according to the molecular docking method. *Doklady Physical Chemistry*, 423:297–301, 2008.

[43] J. E. Lennard-Jones. Cohesion. *Proceedings of the Physical Society*, 43:461–482, 1931.

[44] K. S. Novoselov, A. K. Geim, S. V. Morozov, D. Jiang, Y. Zhang, S. V. Dubonos, I. V. Grigorieva, and A. A. Firsov. Electric field effect in atomically thin carbon films. *Science*, 306:666–669, 2004.

[45] C. Lee, X. Wei , J. W. Kysar, and J. Hone. Measurement of the elastic properties and intrinsic strength of monolayer graphene. *Science*, 321:385–388, 2008.

[46] S. Garaj, W. Hubbard, A. Reina, J. Kong, D. Branton, and J. A. Golovchenko. Graphene as a subnanometre trans-electrode membrane. *Nature*, 467:190–193, 2010.

[47] Y. Shao, J. Wang, H. Wu, J. Liu, I. A. Aksay, and Y. Lin. Graphene based electrochemical sensors and biosensors: A review. *Electroanalysis*, 22:1027–1036, 2010.

[48] T. Premkumar and K. E. Geckeler. Graphene-DNA hybrid materials: Assembly, applications, and prospects. *Progress in Polymer Science*, 37:515–529, 2012.

[49] N. Mohanty and V. Berry. Graphene-based single-bacterium resolution biodevice and DNA transistor: interfacing graphene derivatives with nanoscale and microscale biocomponents. *Nano Letters*, 8:4469–4476, 2008.

[50] L. Meng, Z. Qiang, Z. Huimin, C. Shuo, Y. Hongtao, Z. Yaobin, and Q. Xie. Controllable oxidative DNA cleavage-dependent regulation of graphene/DNA interaction. *Chemical Communications*, 47:4084–4086, 2011.

[51] A. M. Oliveira-Brett Oliveira-Brett and A. M. Chiorcea. Atomic force microscopy of DNA immobilized onto a highly oriented pyrolytic graphite electrode surface. *Langmuir*, 19:3830–3839, 2003.

[52] S. Gowtham, R. H. Scheicher, R. Ahuja, R. Pandey, and S. P. Karna. Physisorption of nucleobases on graphene: density-functional calculations. *Physical Review B*, 76:(4pp), 2007.

[53] J. Antony and S. Grimme. Structures and interaction energies of stacked graphene–nucleobase complexes. *Physical Chemistry Chemical Physics*, 10:2722–2729, 2008.

[54] X. Zhao. Self-assembly of DNA segments on graphene and carbon nanotube arrays in aqueous solution: a molecular simulation study. *The Journal of Physical Chemistry C*, 115:6181–6189, 2011.

[55] M. Kabelac, O. Kroutil, M. Predota, F. Lankas, and M. Sip. Influence of a charged graphene surface on the orientation and conformation of covalently attached oligonucleotides: a molecular dynamics study. *Physical Chemistry Chemical Physics*, 14:4217–4229, 2012.

[56] N. Varghese, U. Mogera, A. Govindaraj, A. Das, P. K. Maiti, A. K. Sood, and C. N. R. Rao. Binding of DNA nucleobases and nucleosides with graphene. *ChemPhysChem*, 10:206–210, 2009.

[57] H. W. Kroto, J. R. Heath, S. C. O'Brien, R. F. Curl, and R. E. Smalley. C_{60}: Buckminsterfullerene. *Nature*, 318:162–163, 1985.

[58] M. S. Dresselhaus, G. Dresselhaus, and P. C. Eklund. *Science of Fullerenes and Carbon Nanotubes*. Academic Press, San Diego, 1996.

[59] P. J. F. Harris. *Carbon Nanotubes and Related Structures: New Materials for the Twenty-first Century*. Cambridge University Press, Cambridge, 1st edition, 2003.

[60] D. W. Pang, Y. D. Zhao, P. F. Fang, J. K. Cheng, Y. Y. Chen, Y. P. Qi, and H. D. Abruna. Interactions between DNA and a water-soluble C_{60} derivative studied by surface-based electrochemical methods. *Journal of Electroanalytical Chemistry*, 567:339–349, 2004.

[61] X. Zhao, A. Striolo, and T. Peter. C_{60} binds to and deforms nucleotides. *Biophysical Journal*, 89:3856–3862, 2005.

[62] X. Xu, X. Wang, Y. Li, Y. Wang, , and L. Yang. A large-scale association study for nanoparticle C_{60} uncovers mechanisms of nanotoxicity disrupting the native conformations of DNA/RNA. *Nucleic Acids Res*, 40:7622–7632, 2012.

[63] X. Zhao. Interaction of C_{60} derivatives and ssDNA from simulations. *The Journal of Physical Chemistry C*, 112:8898–8906, 2008.

[64] B. J. Cox, N. Thamwattana, and J. M. Hill. Mechanics of atoms and fullerenes in single-walled carbon nanotubes. I. Acceptance and suction energies. *Proceedings of the Royal Society A*, 463:461–477, 2007.

[65] B. J. Cox, N. Thamwattana, and J. M. Hill. Mechanics of atoms and fullerenes in single-walled carbon nanotubes. II. Oscillatory behaviour. *Proceedings of the Royal Society A*, 463:477–494, 2007.

[66] D. Baowan, N. Thamwattana, and J. M. Hill. Encapsulation of C_{60} fullerenes into single-walled carbon nanotubes: Fundamental mechanical principles and conventional applied mathematical modeling. *Physical Review B*, 76:155411, 2007.

[67] D. Baowan, N. Thamwattana, and J. M. Hill. Zigzag and spiral configurations for fullerenes in carbon nanotubes. *Journal of Physics A: Mathematical and Theoretical*, 40:7543–7556, 2007.

[68] E. Kreyszig. *Advanced Engineering Mathematics*. John Wiley and Sons, 10th edition, 2011.

[69] W. Kaplan. *Advanced Calculus*. Addison-Wesley, Reading MA, 3rd edition, 1984.

[70] G. Lu, P. Maragakis, and E. Kaxiras. Carbon nanotube interaction with DNA. *Nano Letters*, 5:897–900, 2005.

[71] T. A. Hilder and J. M. Hill. Modeling the loading and unloading of drugs into nanotubes. *Small*, 5:300–308, 2009.

[72] N. W. S. Kam, M. O'Connell, J. A.Wisdom, and H. Dai. Carbon nanotubes as multifunctional biological transporters and near-infrared agents for selective cancer cell destruction. *Proceedings of the National Academy of Sciences*, 102:11600–11605, 2005.

[73] S. Kilina, D. A. Yarotski, A. A. Talin, S. Tretiak, A. J. Taylor, and A. V. Balatsky. Unveiling stability criteria of DNA-carbon nanotubes constructs by scanning tunneling microscopy and computational modeling. *Journal of Drug Delivery*, 2011:(9pp), 2011.

[74] K. M. Abu-Salah, Ansari A. A., and Alrokayan S. A. DNA-based applications in nanobiotechnology. *Journal of Biomedicine and Biotechnology*, 2010:1–16, 2010.

[75] M. Zheng et al. Structure-based carbon nanotube sorting by sequence-dependent DNA assembly. *Science*, 302:1545–1548, 2003.

[76] M. Zheng, A. Jagota, E. D. Semke, B. A. Diner, R. S. Mclean, S. R. Lustig, R. E. Richardson, and N. G. Tassi. DNA-assisted dispersion and separation of carbon nanotubes. *Nature Materials*, 2:338–342, 2003.

[77] H. Hart, L. E. Craine, D. J. Hart, and C. M. Hadad. *Organic Chemistry, A Short Course*. Houghton Mifflin Company, Boston, 12th edition, 2007.

[78] H. Lodish, A. Berk, S. L. Zipursky, P. Matsudaira, D. Baltimore, and J. Darnell. *Molecular Cell Biology*. W.H.Freeman and Co Ltd, New York, 2000.

[79] J. C. Wang. Helical repeat of DNA in solution. *Proceedings of the National Academy of Sciences*, 76:200–203, 1979.

[80] J. O. Hirschfelder, C. F. Curtiss, and R. B. Bird. *Molecular Theory of Gases and Liquids*. Wiley, New York, 1954.

[81] B. J. Cox, N. Thamwattana, and J. M. Hill. Orientation of spheroidal fullerenes inside carbon nanotubes with potential applications as memory devices in nano-computing. *Journal of Physics A: Mathematical and Theoretical*, 41:235209(27pp), 2008.

[82] I. S. Gradshteyn and I. M. Ryzhik. *Table of Integrals, Series, and Products*. Academic Press, New York, 7th edition, 2007.

[83] D. Hongjie. Carbon nanotubes: synthesis, integration, and properties. *Account of Chemical Research*, 35:1035–1044, 2002.

[84] W. Huang, S. Taylor, K. Fu, Y. Lin, D. Zhang, T. W. Hanks, A. M. Rao, and Y. Sun. Attaching proteins to carbon nanotubes via diimide-activated amidation. *Nano Letters Lett*, 2:311–314, 2002.

[85] G. I. Dovbeshko, O. P. Repnytska, E. D. Obraztsova, and Y. V. Shtogun. DNA interaction with single-walled carbon nanotubes: a SEIRA study. *Chemical Physics Letters*, 372:432–437, 2003.

[86] Q. Zhao, M. B. Nardelli, and J. Bernholc. Ultimate strength of carbon nanotubes: A theoretical study. *Physical Review B*, 65:(6pp), 2002.

[87] M. S. Dresselhaus, G. Dresselhaus, and R. Satio. Physics of carbon nanotubes. *Carbon*, 33:883–891, 1995.

[88] N. Wu, Q. Wang, and B. Arash. Ejection of DNA molecules from carbon nanotubes. *Carbon*, 50:4945–4952, 2012.

[89] J. E. Jones. On the determination of molecular fields. I. from the variation of the viscosity of a gas with temperature. *Proceedings of the Royal Society of London. Series A, Containing Papers of a Mathematical and Physical Character*, 106:441–462, 1924.

[90] A. Erdelyi, W. Magnus, F. Oberhettinger, and F. G. Tricomi. *Higher Transcendental Functions*, volume 1. McGraw-Hill, USA, 1953.

[91] W.N. Bailey. *Generalized hypergeometric series*. Hafner Publishing Company, New York, 1964.